PHYSICAL REVIEW D VOLUME 9, NUMBER 5 1 MARCH 1974

Light-quark hadron spectroscopy: Experimental systematics and angular momentum systematics*

Malcolm H. Mac Gregor
Lawrence Livermore Laboratory, Livermore, California 94550
(Received 4 August 1971; revised manuscript received 16 November 1973)

Quark-model systematics and experimental hadron systematics both indicate that quarks are light, with small binding energies. The assumption of small binding energies leads to two types of quark: (1) a 330-MeV spin-$\frac{1}{2}$ quark, the spinor S, which is required to reproduce the nucleon; (2) a 70-MeV spinless quark, the quantum M, which is required to reproduce the pion. It is shown that S and M, in suitable combinations, constitute a complete set of hadronic basis states, with quark and antiquark binding energies accurately mirroring nucleon and antinucleon binding energies. An extension of the equations of special relativity to include spinning masses establishes a phenomenological mass relationship between M and S, and it also relates M to the μ meson. With the aid of this light-quark basis set, the total angular momentum $\vec{J}$ of a hadron resonance can be separated into spin $\vec{S}$ and orbital $\vec{L}$ components. This separation is facilitated by the phenomenology of resonance widths: Rotationless resonances ($L=0$) have narrow widths ($\Gamma \ll 50$ MeV), and rotational levels ($L>0$) have broad widths ($\Gamma \sim 100$ MeV). An experimental compilation of about 130 low-mass hadron resonances is presented and documented. These resonances can be grouped into rotational bands, as in nuclear physics, but the rotational bands are severely limited by the requirements of special relativity. The rotational bands give a reasonably complete and accurate mapping of the experimental resonances. Predictive successes of this light-quark model are summarized.

I. INTRODUCTION AND SUMMARY

It is well known that the linear phenomenology of the conventional quark model suggests a system of light quarks held together with small binding energies. It does not seem to be as well known that this same conclusion follows directly from an examination[1-24] of the spectrum of narrow-width hadron resonances.[25-117] Evidence which indicates that quarks are light is summarized in Sec. IV of the present paper. Although faced with the contradictions described in Sec. IV, many particle theorists have tended to regard quarks, from their nonobservability, as being very massive objects, with large and consequently unknown binding energies. However, recent CERN ISR experiments[118] have pushed the lower limit on the quark mass up to a value, 25 GeV/c^2, where this position is no longer tenable, and some theorists[119] and experimentalists[120] have now begun to reconsider seriously the possibility that quarks are light.

The present work (see Refs. 23 and 24) is an exploration of the consequences which follow from the assumption that quarks are light and therefore quark binding energies are small (a few percent). Once this decisive assumption is made,[1] the experimental data[25-117] become remarkably restrictive in delimiting the possible light-quark basis states, and the quest[2-24] becomes one of obtaining the simplest possible set of light quarks that will reproduce the observed spectrum of hadron resonances. The conclusion reached from these studies is that the spinless quantum $M=70$ MeV and the spin-$\frac{1}{2}$ quantum $S=330$ MeV constitute a sufficient basis set of light quarks. Furthermore, the equations of special relativity as applied to rotating masses reveal that S is itself composed of three quanta M in a relativistically spinning configuration, so that M emerges as the ultimate hadronic building block. From the special-relativistic result (Sec. VI) that a spinning sphere, with its equator at the velocity of light (or infinitesimally below that value), is half again as massive as it was at rest, a direct mass relationship is established between the spinless 70-MeV quantum M and the spinning 105-MeV μ meson.

The binding energies of the light quarks M and S follow in direct analogy to the known binding energies of nucleons and antinucleons, a result which adds considerably to the plausibility of this light-quark phenomenology. The spinor S has the same electromagnetic properties as the nucleon quark of Gell-Mann and Zweig,[121] but it has the particle-antiparticle properties of the nucleon quark of Fermi and Yang,[122] namely, $N=S\bar{S}S$ (F-Y) rather than $N=SSS$ (G-Z). The spinless quantum M, which

was discussed many years ago by Nambu,[123] has no counterpart in either the Gell-Mann–Zweig or the Fermi-Yang quark model.

In Ref. 24, which we denote here for simplicity as paper II, quark binding energies, electromagnetic effects, geometries, particle-antiparticle states, and strangeness quantum numbers are explored in detail. It is shown in paper II that with a total of ten physically identifiable parameters, and with small arbitrary adjustments of some of these parameters, the absolute masses of the metastable baryon resonances $p, n, \Lambda, \Sigma, \Xi, \Omega, \bar{p}n$ and the very-narrow-width meson resonances π, K, η, η' can be reproduced by the light-quark basis set M and S to an average over-all accuracy of about ±0.1%, or about ±1 MeV, with charge splittings, spins, magnetic-moment ratios, and strangeness quantum numbers accounted for. In the present paper, we concentrate on the angular momentum characteristics of the hadron resonances, and in particular on the decomposition of the total angular momentum $\vec{J}$ into spin angular momentum $\vec{S}$ and orbital angular momentum $\vec{L}$ components. From the special-relativistic equations discussed in Sec. VI and Appendix B, the spin angular momentum $\vec{S}$ appears as a directly calculated quantity. The orbital angular momentum $\vec{L}$ is also a calculable quantity in the sense that rotational energies can be obtained by estimating hadron moments of inertia I and inserting them into the standard nuclear-physics equation for rotational excitations. Phenomenologically, the distinction between rotationless resonances ($L=0$) and rotational resonances ($L>0$) can be made directly on the basis of resonance widths; rotationless excitations have much narrower widths than do rotational excitations, as in outlined in detail in Secs. VII and VIII. The present use of nuclear physics concepts to treat hadron resonances is reinforced by noting that the systematics of the (nonadiabatic) hadron rotational bands appears to extrapolate smoothly into the systematics of nonadiabatic rotational bands in very light nuclei, as is shown in Sec. IX.

One quantum-mechanical implication of the present light-quark phenomenology, namely the necessity for associating the observed spread in orbital rotational energies with a corresponding spread in orbital angular momentum values, is discussed in Sec. X, with the ρ meson serving as an example.

Section XI summarizes predictive successes of the present light-quark model. In the years subsequent to the first publication[3-6] of this model, quite a few experimental hadron resonances have been identified.[25-27] Hence it is a straightforward matter to ascertain whether or not these new resonances are in agreement with the present systematics. As is shown in Sec. XI, these new resonances not only fit the light-quark excitation and rotational systematics, but they have filled in the missing states in this model in rather complete detail. Of particular importance is the recent Syracuse $\bar{p}n$ bound-state experiment,[38] which has revealed that nucleons and antinucleons exhibit the same binding-energy systematics as the binding-energy systematics which had previously been deduced for light quarks[124] directly from the phenomenology of the experimental resonances.

Section XII gives a brief description of lifetime systematics for the long-lived ($\tau > 10^{-17}$ sec) elementary particles. The lifetime systematics indicate that these metastable elementary particles possess a common substructure. This result, which is of course in agreement with the light-quark results described in Secs. I–XI, appears to stand independently of any other considerations in the present paper.

The sections of the paper are the following.

II. THE EXPERIMENTAL DATA

Perhaps the most important step in formulating theories for elementary particles is to establish an agreed-upon set of experimental data. This data base serves two main purposes: (1) By direct inspection of the data, we can obtain information as to the nature of the theoretical structures of these particles; (2) the data serve as the testing ground for theories once they have been formulated. It is of course necessary that a comprehensive theory be directed at the entire set of data, and not just at a particular subset which seems amenable to treatment. And it is highly desirable that a theory should accurately account for the most fundamental properties of these particles—masses, angular momenta, magnetic moments, widths, and strangeness values. It should also correctly handle the mapping problem; that is, it should, broadly speaking, predict all of the resonances and only the resonances in the agreed-upon data set.

In the past two decades, the field of experimental high-energy physics has been one of almost unparalleled achievement. The first high-energy physics colloquium attended by the present author, more than 20 years ago, centered on the statistical analysis of an experiment in which a total of two V particles (as they were then called) were observed. From this kind of a modest beginning, high-energy physics experiments have now progressed to the point where a collection of data can include several hundred thousand carefully reconstructed events. The experimental data have revealed the existence of a large number of hadron resonances. The present section contains a compilation of these resonances, listed in a series of tables: meson, kaon, N, Δ, Λ, Σ, Ξ, and Ω. The 130 or so resonances contained in these tables include all of the low-mass resonances, and also some higher-mass resonances for which spin identification is possible. References[25-117] are given for resonances which require special discussion.

In order to properly judge the significance of each of these resonances, they have been assigned ratings in accordance with the following notation:

A = listed at the front of RPP73 (Ref. 25) as well-established resonances;

B = reasonably well established in the opinion of the author;

C = reported only in one experiment or weakly in several, and with no associated experimental controversies;

D = reported in the literature as a resonance, but lacking either (1) statistical significance, or (2) apparent reproducibility;

E = small fluctuations noted by the author at energies of current theoretical interest.

The data tables I–VII, which summarize the experimental information about these hadron resonances, contain the following numbers of resonances for each confidence-level rating.

Table I: Meson resonances—$42^+ \simeq$ 20A, 3B, 18C, 3D, and 3E.
Table II: Kaon resonances—16 = 6A, 2B, 7C, and 1D.
Table III: N^* resonances—20 = 11A, 6B, and 3C.
Table IV: Δ resonances—11 = 7A and 4C.
Table V: Λ resonances—17 = 9A, 5B, 2C, and 1D.
Table VI: Σ resonances—21 = 10A, 5B, 5C, and 1D.
Table VII: Narrow-width Ξ and Ω resonances—7 = 5A and 2C.

Total resonances in compilation:
134+ = 68A, 21B, 41C, 6D, and 3E.

The six D-rated resonances and three E-rated resonances that are included here are essentially meaningless from the standpoint of furnishing any tests of spectroscopic models. The reason for the inclusion of these low-rated "resonances" is that they all fit naturally into the systematics of the present light-quark model. If it eventually turns out that few of these low-rated levels actually exist, this does not mean that the present systematics is necessarily incorrect; a theoretical model that can accurately reproduce all of the A, B, and C resonances is on fairly firm ground. And, in fact, selection rules are given in Tables XXI and XXII which indicate that these D-rated and E-rated levels should be weakly produced. However, it is the author's opinion that at least some of the D and E levels will turn out to be reproducibly present in certain kinds of experiments.[125] In fact, this circumstance has already happened. The $\bar{p}p(1925)$ resonance of Table I, which until September 1973 was listed in Table I with a D rating, has

TABLE I. An experimental compilation of meson resonances. The compilation is essentially complete below 1600 MeV; above 1600 MeV, however, only a few resonances are included, since spin information is lacking. The resonances are ordered according to width: (1) very narrow width ($\Gamma \ll 5$ MeV), (2) narrow width ($\Gamma \simeq 10$–20 MeV), and (3) broad width ($\Gamma \geq 50$ MeV). They are also ordered according to their experimental status: (A) listed at the front of RPP73; (B) experimentally well established in the opinion of the author; (C) reported in only one experiment, or weakly in several; (D) reported as resonances, but lacking either statistical significance or reproducibility; (E) fluctuations noted at energies of interest in the present model. Finally, they are grouped into what appear to be alternate $I_z = 0$ and $I_z = 1$ forms of the same basic resonance structure (see Ref. 149). The η' multiplet of very-narrow-width resonances is listed at the end of the table.

No.	Status	Resonance	Width	I_z	J^P	Reference
		Very-narrow-width resonances				
1a	A	$\pi^0(135.0)$	$\Gamma \simeq 0$	0	0^-	RPP73[a]
1b	A	$\pi^{\pm}(139.6)$	$\Gamma \simeq 0$	1	0^-	RPP73
2	A	$\eta(548.8)$	$\Gamma \leq 0.9$	0	0^-	RPP73
3	A	$\eta'(958.1)$	$\Gamma < 0.8$	0	0^-	RPP73, pp
		Narrow-width resonances				
4	A	$\omega(784)$	$\Gamma 9.8$	0	1^-	RPP73
5a	A	$\phi(1019) \rightarrow KK$	$\Gamma 4$	0	1^-	RPP73, b
5b	C	$H, \phi(1009) \rightarrow \pi\pi\pi$		0	1^-	c
6	C	$S^*(1019)$	$\Gamma 24$	0	0^+	d
7	C	$\pi_N(1016)$	$\Gamma \sim 25$	1	0^+	RPP71[e]
8	A	$D(1286)$	$\Gamma 21$	0	1^+	RPP73, f
9	C	$A(1289)$	$\Gamma \leq 40$	1	1^-	g
10	A	$E(1416)$	$\Gamma 60$	0	0^- or 1^+	RPP73
11	C	$KK(1425)$	$\Gamma \leq 20$	1		RPP73, f
12	A	$F_1(1543)$	$\Gamma 16$	1	1^+ or 2^-	RPP73
13a	C	$M^0(941)$	$\Gamma \leq 10.4$	0		RPP73, h
13b	D	$\pi\pi\pi(926)$	$\Gamma < 25$	1		i
14a	C	$M^0(1148)$	$\Gamma 15$	0		RPP73, j
14b	C	$X^-(1153)$	$\Gamma 16$	1		k
15	C	$A_{1.5}(1207)$	$\Gamma 39$	1		RPP73, l
16	C	$\bar{p}n(1794.5)$	$\Gamma \leq 8$	1		m
17	D	$\pi\pi(660)$	$\Gamma \sim 15$	0	1	n
18a	D	A_2dip(1310)	$\Gamma \sim 10$		2^+	o
18b	D	$K_S K_S(1311)$	$\Gamma 21$			o
19	D	$K_S K_S(1439)$	$\Gamma 43$			RPP73, f
20a	B	$\bar{p}p(1925)$	$\Gamma 8$			p
20b	D	$S^-(1930)$	$\Gamma 30$	1		q
21	E	$\pi\pi(870)$	$\Gamma \sim 15$	0	1	r
22	E	$X^-(1079)$	$\Gamma 13$	1	1^+	s
		Broad-width resonances				
23	A	$\rho(770)$	$\Gamma 146$	1	1^-	RPP73
24	A	$\epsilon(\sim 800)$	$\Gamma \sim 150$	0	0^+	t
25	A	$\pi_N(975)$	$\Gamma 60$	1	(1)	u
26	A	$S^*(980)$	$\Gamma \sim 50$	0	0^+	v

TABLE I. *(continued)*

27a	A	$A_1(1115)$	$\Gamma 98$	1	1^+	w
27b		$A_1(1070 \pm 20)$	$\Gamma \sim 125$			RPP71, x
28a	C	ϵ' (1096)	$\Gamma 80$	0	0^+	y
28b		$S^*(1070 \pm 30)$	$\Gamma \sim 225$			RPP71, x
29	A	B (1237)	$\Gamma 120$	1	1^+	RPP73
30	C	ϵ'' (1250)	$\Gamma 300$	0	0^+	z
31	A	$A_2(1310)$	$\Gamma 100$	1	2^+	RPP73
32	A	f (1270)	$\Gamma 163$	0	2^+	RPP73, aa
33	A	f' (1516)	$\Gamma 40$	0	2^+	RPP73
34	A	$A_3(1645)$	$\Gamma 129$	1	2^-	RPP73, bb
35	A	$\omega(1648)$	$\Gamma 139$	0		cc
36	A	g (1680)	$\Gamma 160$	1	3^-	RPP73
37	B	$\eta_N(1076)$	$\Gamma 98$	0	2^+	dd
38	C	DEF (~ 450)	$\Gamma \sim 100$	0	(1)	ee
39a	C	$K_S K_S(1412)$	$\Gamma 100$			RPP73, f
39b	C	$\rho^0\rho^0(1410)$	$\Gamma 90$	0	$(2^+?)$	RPP73, ff
40	C	π/ρ (1490)	$\Gamma 85$	1		gg
41	C	$A_4(1829)$	$\Gamma 127$	1		hh
42	E	$\pi\pi$ (520)	$\Gamma 70$		(1)	ii
...	...	ABC (300)				jj
		The η' multiplet of resonances				
3-0^0	B	$M(953 \pm 2)$	$\Gamma < 10$	0	0^-	kk, ll
3-1^0	A	$\eta'(958.1 \pm 0.4)$	$\Gamma < 2$	0	0^-	RPP73, ll
3-2^0	C	$\delta^0(963.5 \pm 1.7)$	$\Gamma < 5.9$	0		mm, ll
3-2^0+?	C	$M^0(1033.6 \pm 2.3)$	$\Gamma 16.2$	0		RPP73, nn, ll
3-1^-	C	$\delta^-(962 \pm 5)$	$\Gamma < 5$	1	0^-	oo, ll
3-1^+?	C	$\delta^+(966 \pm 8)$	$\Gamma \leq 10$	1		oo, ll

[a]Reference 25. [b]Reference 28. [c]Reference 29. [d]Reference 30. [e]Reference 27. [f]Reference 31. [g]Reference 32. [h]Reference 33. [i]Reference 34. [j]Reference 35. [k]Reference 36. [l]Reference 37. [m]Reference 38. [n]Reference 39. [o]Reference 40. [p]Reference 42. [q]Reference 43. [r]Reference 44. [s]Reference 45. [t]Reference 47. [u]Reference 49. [v]Reference 50. [w]Reference 51. [x]Reference 52. [y]Reference 53. [z]Reference 54. [aa]Reference 55. [bb]Reference 56. [cc]Reference 57. [dd]Reference 58. [ee]Reference 59. [ff]Reference 60. [gg]Reference 61. [hh]Reference 62. [ii]Reference 63. [jj]Reference 64. [kk]Reference 65. [ll]Reference 69. [mm]Reference 66. [nn]Reference 67. [oo]Reference 68. [pp]Reference 182.

now received unambiguous experimental confirmation.[42] Also, the C-rated $X^-(1153)$ $\Gamma 16$ resonance in Table I, which was first identified as a resonance by the present author,[126] and which initially carried no more than a D confidence level, now appears to be confirmed by the $M^0(1148)$ $\Gamma 15$ resonance of Jacobel *et al.*[35] The most famous (or notorious) of the D-rated levels is, of course, the celebrated dip in the A_2 meson. In the present systematics, the *location* of this dip is of considerable phenomenological interest.[127]

III. THE SPECTROSCOPY OF THE NUCLEON

Elementary particle theories have two general aspects—spectroscopy and dynamics. Spectroscopy is the study of the stable or metastable states in a system, and dynamics is the study of the transitions between these states. A theory must eventually embrace both of these aspects. The difficulty in concentrating on dynamics at the expense of spectroscopy, as is sometimes the case, is that an infinite number of parametrizations are

TABLE II. An experimental compilation of kaon resonances. The compilation includes all reported resonances below 2000 MeV. The resonances are grouped according to (1) width, (2) experimental status, and (3) related I-spin resonance structures, in the manner defined in the heading for Table I.

No.	Status	Resonance	Width	I	J^P	Reference
		Very-narrow-width resonances				
1a	A	$K^{\pm}$(493.7)	$\Gamma \simeq 0$	$\frac{1}{2}$	0^-	RPP73
1b		$K^0, \bar{K}^0$(497.7)	$\Gamma \simeq 0$			RPP73
		Narrow-width resonances				
2	A	K_N(1160)	$\Gamma \sim 90$	$\frac{1}{2}$	0^+	a
3	C	K_A(1175)	$\Gamma \sim 25$	$\frac{3}{2}$		RPP73, b
4	C	Q(1272)	$\Gamma 18$	$\frac{1}{2}$		c
5	C	K_N(1368)	$\Gamma 19$	$\frac{1}{2}$	0^+	d
6	D	κ(725)	$\Gamma 15$	$\frac{1}{2}$		e
		Broad-width resonances				
7	A	K^*(892)	$\Gamma 50$	$\frac{1}{2}$	1^-	RPP73
8	A	C(1242)	$\Gamma 127$	$\frac{1}{2}$	1^+	RPP73
9	C	K_A(1265)	$\Gamma 50$	$\frac{3}{2}$	(1)	RPP73, f
10	B	Q(1344)	$\Gamma \leq 60$	$\frac{1}{2}$	1^+	g
11	B	Q(1417)	$\Gamma 89$	$\frac{1}{2}$	1^+	h
12	A	K_N(1421)	$\Gamma 100$	$\frac{1}{2}$	2^+	RPP73
13	C	K_N(1660)	$\Gamma 60$	$\frac{1}{2}$		RPP73
14	C	K_N(1753)	$\Gamma 60$	$\frac{1}{2}$	3^-	RPP73
15	A	L(1765)	$\Gamma 140$	$\frac{1}{2}$	2^-	RPP73
16	C	K_N(~1850)	$\Gamma \sim 300$	$\frac{1}{2}$	3^-	RPP73

[a] Reference 70.
[b] Reference 71.
[c] Reference 72.
[d] Reference 73.
[e] Reference 74.
[f] Reference 75.
[g] Reference 76.
[h] Reference 77.

possible for describing dynamical processes. It seems intuitively correct that the theory which gives the best spectroscopic results will probably also give the most meaningful dynamics.

The present status of elementary-particle spectroscopy is perhaps best illustrated by the nucleon. Nucleons—protons and neutrons—are the stable particles upon which all of nuclear physics and ultimately all of hadron physics is based. A spectroscopic theory for the nucleon must include the calculation of several fundamental quantitative properties: mass, spin angular momentum, magnetic moment, and charge and magnetic-moment radii. As a way of arriving at a spectroscopic theory for the nucleon, it has often been assumed that the nucleon is a field-theoretic object—a core region surrounded by a virtual pion cloud. However, neither this approach nor any other of which the author is aware has led to the direct calculation of any of these fundamental properties of nucleons. It would seem that elementary-particle theorists should be directing their main research efforts at the most fundamental unsolved spectroscopic questions, such as, for example, the calculation of the mass of the nucleon.

If we examine the known properties of the nucleon,[25] it does not appear to be a particularly mysterious object. In particular, the nucleon is the *only* subatomic particle for which a size has been measured, and this size is consistent with the other known properties of the nucleon, as we now demonstrate. If the nucleon were a single Dirac particle, it would logically have a radius $R = \hbar/mc \simeq 0.2$ fermi, where $m = 939$ MeV$/c^2$. Since the measured rms charge and magnetic-moment radii of the nucleon are about 0.8 fermi, it is apparent that the nucleon is not a single Dirac particle, a fact that is also demonstrated by the anomalous magnetic moments of the proton and neutron. The nucleon must be a composite structure. Once we reach this conclusion, there are a number of phenomenological arguments which suggest that the nucleon is in fact composed of three subunits of approximately equal mass. As a simple and very general model for a nucleon subunit, we can take a spherical quantum with a mass roughly equal to $\frac{1}{3}$ the nucleon mass, or 313 MeV. If we assume that these nucleon subunits are Dirac-like quark states, then each subunit will have a radius $R = \hbar/mc \simeq 0.6$ fermi. A cluster of three such subunits, each with radius $R = 0.6$ fermi, gives a nucleon with a total rms radius that is about equal to the measured value of 0.8 fermi. Furthermore, if we set a 313-MeV spherical subunit spinning with its equator at the velocity of light, and if we assume that its moment of inertia is about $\frac{2}{5}mR^2$, the classical value, then its calculated angular momentum is roughly $J = \frac{1}{2}\hbar$ (in Sec. VI we use a relativistic moment of inertia and make this result precise). Electromagnetically, if an electric charge e is placed on the spinning subunit and allowed to move freely, it will be forced to the equator of the spinning sphere by the action of the electromagnetic forces. An equatorial current loop with a radius $R = 0.6$ fermi has a calculated magnetic moment (for a unit charge e moving at the velocity of light) equal to 2.8 nuclear magnetons, which is the same magnetic moment that is conventionally associated with a singly charged quark.[128] Thus, this simple model for a nucleon subunit has the angular momentum and magnetic-moment properties that are conventionally attributed to a (singly charged) quark, and three of these subunits form a nucleon that has the proper mass and "size." In addition, an equatorial current distribution on a quark has a number of other interesting properties, as follows. (1) The charge and magnetic-moment radii are

TABLE III. An experimental compilation of N baryon resonances. All resonances up to 2250 MeV are included. The resonances are grouped according to experimental status: A = **** or *** rating in RPP73; B = ** or * rating in RPP73; C = * or no rating in RPP73; D = doubtful status. The $L_{2I,2J}$ notation denotes orbital angular momentum (L), isotopic spin (I), and total angular momentum (J).

No.	Status	Resonance	Width	$L_{2I,2J}$	Reference
1a	A ****	p(938.3)	$\Gamma 0$	S_{11}	RPP73[a]
1b	A ****	n(939.6)	$\Gamma \simeq 0$	S_{11}	RPP73
2	A ****	N(1419)	$\Gamma 148$	P_{11}	AYED,[b] c
3	A ****	N(1508)	$\Gamma 55$	S_{11}	AL,[d] AYED, e
4	A ****	N(1520)	$\Gamma 121$	D_{13}	B-G[f]
5	A ****	N(1672)	$\Gamma 143$	D_{15}	B-G
6	A ****	N(1687)	$\Gamma 128$	F_{15}	B-G
7	A ****	N(1684)	$\Gamma 116$	S_{11}	g
8	A ***	N(1738)	$\Gamma 172$	P_{11}	AL, AYED
9	A ***	$N(\sim 1770)$	$\Gamma \sim 200$	P_{13}	AL, AYED, h
10	A ***	N(2204)	$\Gamma 247$	G_{17}	i
11	A ***	N(2241)	$\Gamma 289$	H_{19}	AYED
12	B **	N(1730)	$\Gamma 130$	D_{13}	AYED, j
13	B **	N(2024)	$\Gamma 191$	F_{17}	AL, AYED
14	B **	N(2075)	$\Gamma 150$	D_{13}	AL
15	B *	N(2078)	$\Gamma 160$	D_{15}	AL, AYED
16	B *	$N(\sim 2088)$	$\Gamma 103$	F_{15}	AL, AYED, k
17	B *	N(2148)	$\Gamma 240$	S_{11}	AL, AYED
18	C	$N(\sim 1300)$		P_{11}	l
19	C	N(1530)	$\Gamma 65$	P_{11}	AYED, m
20	C	N(2130)	$\Gamma 250$	G_{19}	AYED

[a]Ref. 25. [b]Ref. 78. [c]Ref. 79. [d]Ref. 80. [e]Ref. 81. [f]Ref. 82. [g]Ref. 83. [h]Ref. 85. [i]Ref. 87. [j]Also see Ref. 86. [k]Ref. 88. [l]Ref. 89. [m]Ref. 90.

TABLE IV. An experimental compilation of Δ baryon resonances. All resonances up to 2500 MeV are included. The resonances are grouped according to experimental status, as described in the heading for Table III.

No.	Status	Resonance	Width	$L_{2I,2J}$	Reference
1	A ****	Δ(1233)	$\Gamma 115$	P_{33}	B-G[a]
2	A ****	Δ(1618)	$\Gamma 147$	S_{31}	b
3	A ***	Δ(1694)	$\Gamma 216$	D_{33}	b
4	A ***	$\Delta(\sim 1850)$	$\Gamma 215$	P_{31}	AL, [c]AYED, [d]e
5	A ***	Δ(1877)	$\Gamma 255$	F_{35}	AL, AYED
6	A ****	Δ(1923)	$\Gamma 215$	F_{37}	AL, AYED
7	A ***	Δ(2390)	$\Gamma 292$	$H_{3,11}$	AYED
8	C *	Δ(1680)	$\Gamma 220$	P_{33}	AL, f
9	C *	Δ(1824)	$\Gamma 138$	D_{35}	g
10	C *	Δ(2160)	$\Gamma 230$	P_{33}	RPP73
11	C	Δ(2160)		G_{37}	h

[a]Reference 82.
[b]An average value from AL, AYED, and Davies 70 (Ref. 25).
[c]Reference 80.
[d]Reference 78.
[e]AL and AYED do not agree on the position of this resonance. The P_{31} and P_{33} AL and AYED phases appear to constitute a P-wave criss-cross (see Table XI).
[f]See footnote e. The AL value fits the present systematics. AL also report a resonance at 2150 MeV, which is too high to classify accurately.
[g]The value quoted here is from Mehtani (Ref. 91). AYED see this resonance about 50 MeV higher in energy.
[h]Von Schlippe 72 (Ref. 25).

TABLE V. An experimental compilation of Λ hyperon resonances. All resonances up to 2500 MeV are included. The resonances are grouped according to experimental status (see Table III). The standard $L_{2I,2J}$ notation is used, as in Table III; however, since we interpret L as an actual orbital angular momentum in the present paper, the Λ(1115.6) resonance is denoted as S_{01}, and not as the P_{01} assignment of RPP73. The Λ(1518) D_{03} resonance is discussed in Appendix A, Eq. (48).

No.	Status	Resonance	Width	$L_{2I,2J}$	Reference
1	A ****	Λ(1115.6)	$\Gamma \simeq 0$	S_{01}	RPP73[a]
2	A ****	Λ(1402)	Γ38	S_{01}	RPP73
3	A ****	Λ(1518)	Γ16	D_{03}	RPP73
4	A ****	Λ(1673)	Γ30	S_{01}	B-G[b]
5	A ****	Λ(1688)	Γ53	D_{03}	B-G
6	A ****	Λ(1819)	Γ80	F_{05}	B-G
7	A ***	Λ(1827)	Γ89	D_{05}	B-G
8	A ****	Λ(2100)	Γ121	G_{07}	RPP73, c
9	A ****	Λ(2350)	Γ177	H_{09}	RPP73, d
10	B **	Λ(~1737)	Γ~115	P_{01}	RPP73, e
11	B **	Λ(~1827)	Γ~68	S_{01}	RPP73, f
12	B **	Λ(1870)	Γ81	P_{03}	RPP73, g
13	B **	Λ(1990)	Γ155	D_{03}	RPP73, h
14	B **	Λ(2020)	Γ160	F_{07}	RPP73
15	C *	Λ(2110)	Γ185	F_{05}	RPP73, i
16	C	Λ(1570)	Γ50	P_{01}	RPP73, j
17	D "dead"	Λ(1327)	Γ<25		RPP73, k

[a]Reference 25. [b]Reference 82. [c]Reference 92. [d]Reference 93. [e]Reference 94. [f]Reference 96. [g]Reference 98. [h]Reference 100. [i]Reference 102. [j]Reference 101. [k]Reference 103.

equal; (2) low-energy electron scattering off a current loop, where the wavelength is large as compared to the dimensions of the loop, appears as a dipole interaction; (3) high-energy electron scattering off a current loop, where the wavelength is small as compared to the dimensions of the loop, appears as a pointlike (parton) interaction. All three of these properties have been verified experimentally for the nucleon.

In summary, straightforward estimates show that the known first-order properties of the nucleon seem to be expressible in terms of very simple, self-consistent, and in fact almost classical concepts. Thus, the nucleon has none of the mystery of the (assumed) point electron, which continues to defy all attempts at providing a calculable spectroscopic explanation.[129] The fact that the nucleon admits an essentially classical explanation suggests that nucleon subunits (quarks) have well-defined geometries, and that these subunits keep their essential integrity when bound together in the nucleon. Hence nucleon quark binding energies must be small in comparison to nucleon quark masses, which is the crucial point we seek to establish here with respect to the present light-quark systematics.

The present work[23,24] is centered on one main idea: to produce a simple and yet accurate model for spectroscopically reproducing the resonances listed in Tables I–VII. In particular, we show by direct calculation that such a model is possible.

IV. EVIDENCE FOR LIGHT QUARKS AND SMALL BINDING ENERGIES

Evidence from five facets of hadron phenomenology is cited to establish the conclusion that hadrons must be composed of a set of light quarks held together with small (a few percent) binding energies:

(1) The spectroscopy of the nucleon indicates, as discussed in Sec. III, that the nucleon admits an essentially classical explanation for all of its first-order properties.

(2) The narrow-width experimental hadron resonances, both meson and baryon, show very accurate linear mass spacings, which are indicative of a fundamental set of hadronic mass quanta held together with small binding energies.

(3) The phenomenological successes of the conventional quark model of Gell-Mann and Zweig[121] have always suggested that quarks must be light.

(4) The masses of the nucleon[25] and the $\bar{p}n$ bound state[38] can be accurately reproduced by a straightforward extension of the Fermi-Yang model of the nucleon,[122] using the known (small) binding energies of nucleons and antinucleons to serve also as the binding energies of nucleon quarks and anti-

TABLE VI. An experimental compilation of Σ hyperon resonances. All resonances up to 2500 MeV are included. The resonances are grouped and labeled in the same manner as the Λ resonances of Table V. The Σ(1385) resonance is discussed in Appendix A, Eq. (48).

No.	Status	Resonance	Width	$L_{2I,2J}$	Reference
1a	A ****	$\Sigma^+(1189.4)$	$\Gamma \simeq 0$	S_{11}	RPP73[a]
1b	A ****	$\Sigma^0(1192.5)$	$\Gamma \simeq 0$	S_{11}	RPP73
1c	A ****	$\Sigma^-(1197.3)$	$\Gamma \simeq 0$	S_{11}	RPP73
2	A ****	Σ(1385)	Γ36	P_{13}	RPP73
3	A ****	Σ(1669)	Γ50	D_{13}	B-G[b]
4	A ***	Σ(1756)	Γ65	S_{11}	B-G
5	A ****	Σ(1765)	Γ108	D_{15}	B-G,c
6	A ****	Σ(1910)	Γ70	F_{15}	RPP73,d
7	A ****	Σ(2030)	Γ151	F_{17}	RPP73,e
8	A ****	Σ(2250)	Γ165	G_{17}	RPP73,f
9	A ***	Σ(2455)	Γ120	H?	RPP73,g
10	A ***	Σ(~1900)	Γ~200	D_{13}	RPP73,h
11	B **	Σ(1620)	Γ40	S_{11}	RPP73,i
12	B **	Σ(1669)	Γ140	P_{11}	RPP73,j
13	B **	Σ(1926)	Γ185	P_{11}	RPP73
14	B **	Σ(2080)	Γ170	P_{13}	RPP73
15	B **	Σ(2090)	Γ103	G_{17}	RPP73
16	C *	Σ(1472)	Γ30		RPP73,k
17	C *	Σ(~1840)	Γ120	P_{13}	l
18	C *	Σ(~1900)		S_{11}	m
19	C *	Σ(2070)	Γ140	F_{15}	RPP73,n
20	C	Σ(1682)	Γ25	S_{11}	o
21	D	Σ(~1550)	Γ50	P_{11}	p

[a]Reference 25. [e]Reference 106. [i]Reference 110. [m]Reference 115.
[b]Reference 82. [f]Reference 107. [j]Reference 111. [n]Reference 116.
[c]Reference 104. [g]Reference 108. [k]Reference 112. [o]Reference 113.
[d]Reference 105. [h]Reference 109. [l]Reference 114. [p]Reference 117.

quarks.

(5) The lifetimes of supposedly dissimilar and independent metastable elementary particles exhibit numerical relationships[19] which suggest that these particles must possess a common substructure.

Facet (1), the spectroscopy of the nucleon, has already been summarized in Sec. III. Facet (2), the linear hadronic mass intervals, can be directly illustrated in a series of three figures. Figure 1 shows *very-narrow-width* meson resonances (taken from Table I) plotted against a mass scale that is in units of 137 MeV. As can be seen in Fig. 1, the mass intervals are very accurate. Figure 2 shows a series of *narrow-width* meson resonances (also taken from Table I) plotted against this same 137-MeV mass scale. Again the intervals are very accurate. The linear mass spacings observed in Figs. 1 and 2 suggest two conclusions: (a) Binding energies are weak; (b) a basic resonance structure $\pi \sim 137$ MeV is a constituent of these resonances. Since the resonances of Figs. 1 and 2 are nonstrange, that is, have balanced particle-antiparticle symmetry, we can draw a further tentative conclusion that $\pi = M\overline{M}$, where M and $\overline{M}$ are ~70-MeV light-quark mass quanta. This last conclusion is reinforced by noting that the one *very-narrow-width* boson resonance not included in Fig. 1, namely the K meson of Table II, can be constructed from seven 70-MeV quanta M. Since the kaon is spinless, the quantum M must also be spinless.

The results of Figs. 1 and 2 can be carried over directly to the *narrow-width and S-state* baryon and hyperon resonances. Figure 3 shows the narrow-width and S-state resonances of Tables III–VII plotted against 70-MeV mass grids that are erected above the basic "ground states" $N(939)$, $\Lambda(1116)$, $\Sigma(1193)$, and $\Xi(1321)$. From the observed level spacings in Fig. 3, it appears that these excitations also occur in units of $M = 70$ MeV, as was the case for the levels of Figs. 1 and 2. However, whereas the meson excitations of Figs. 1 and 2 occurred in quantum steps of $\pi \sim 137$ MeV, the baryon excitations of Fig. 3 occur in quantum steps of $3 \equiv 3M = 210$ MeV and $4 \equiv 4M = 280$ MeV, as is indicated in the far left column in Fig. 3. Thus we should consider the mass groupings 3 and 4 as in some manner constituting a part of the hadronic basis set of light quarks.

TABLE VII. An experimental compilation of narrow-width Ξ and Ω resonances. Although several broad-width Ξ resonances have been reported, they have no spin identification, and they are not included in the present compilation. The narrow widths of the resonances listed here serve to identify them as S-state excitations. The $\Xi(1535)$ resonance is discussed in Appendix A, Eq. (48).

No.	Status	Resonance	Width	Reference
1a	A	$\Xi^0(1314.9)$	$\Gamma \simeq 0$	RPP73[a]
1b	A	$\Xi^-(1321.3)$	$\Gamma \simeq 0$	RPP73
2a	A	$\Xi^0(1531.6)$	$\Gamma 9$	RPP73
2b	A	$\Xi^-(1535.0)$	$\Gamma 13$	RPP73
3	C	$\Xi^0(1606)$	$\Gamma 21$	RPP73, b
4	A	$\Xi(1814)$	$\Gamma 12$	RPP73, c
5	A	$\Xi(1956)$	$\Gamma 35$	RPP73, d
6	C	$\Xi(2295)$	$\Gamma < 30$	RPP73, e
7	A	$\Omega^-(1672.5)$	$\Gamma \simeq 0$	RPP73

[a]Reference 25.

[b]This is Ross 72 in RPP73, who do not observe a broader $\Xi(1635)$ peak.

[c]This is Badier 65 in RPP73, which may be confirmed by Smith 65, but which is otherwise unconfirmed; hence the A rating denotes the existence of a resonance, but not necessarily with the width quoted here.

[d]Several experiments report Ξ resonances at about 1955 MeV; the one quoted here is Badier 72, the one with the narrowest width.

[e]This is Goldwasser 70 in RPP73.

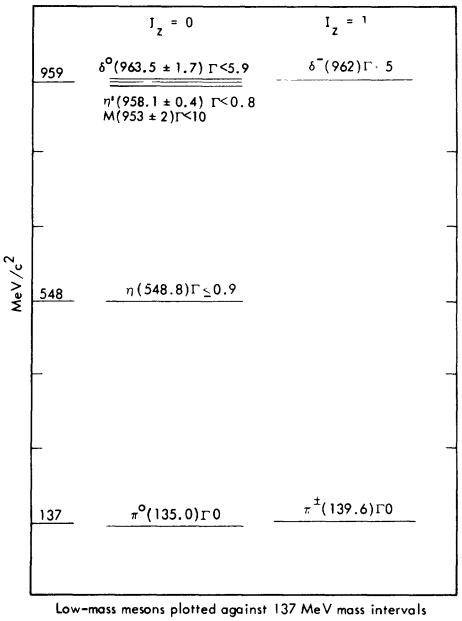

FIG. 1. Low-mass very-narrow-width meson resonances plotted against a mass grid $M = 137$ MeV/c^2. The accurate mass interval spacings suggest a linear system of weakly bound mass quanta. Data on these resonances are summarized in Table I. These resonances are probably all spinless excitations, and they all appear to have widths $\Gamma \ll 5$ MeV. The observed 5-MeV fine-structure spacing of the triplet (M, η', δ^0) is accounted for in paper II. The isospin headings are discussed in Ref. 149.

The over-all conclusion to be drawn from Figs. 1–3 is that all of these resonance intervals suggest excitations which occur in quantum units of about 70 MeV, and which thus indicate collections of 70-MeV basis states held together with small binding energies. The reason for specifying narrow-width and S-state resonances in Figs. 1–3 is that these are all rotationless ($L = 0$) excitations, so that the very large hadron rotational energies do not add to the S-state energies to obscure the mass quantization of the levels. The excitation bands shown in Figs. 1–3 are roughly analogous to vibrational excitations in nuclear physics. In assessing the phenomenological significance of Figs. 1–3, the completeness of the mapping is as important as the accuracy of the mass intervals. This completeness is discussed in detail in Secs. VII–IX.

Facet (3), the phenomenological quark-model arguments that favor light quarks, is well known. For example, quark magnetic moments are assumed to be additive. This additivity implies that *anomalous* magnetic moments must be small. But according to conventional notions, small anomalous magnetic moments are associated with small virtual-pion fields and hence with small quark binding energies. For strongly-interacting quarks that have large binding energies, anomalous magnetic moments are expected to be large. It can be argued that quark *charges* retain accurate ratios under strong interactions because the charge is related to a conserved vector current, but this mechanism is not available for the *magnetic moments*.[130] Thus the assumption of additivity for quark magnetic moments can only be interpreted as meaning that quarks have small binding energies and therefore small quark masses.

The same logical connection between additivity and small binding energies occurs with respect to high-energy quark scattering amplitudes, as was noted by Feld[131]: "The success of the factorizability model (of quarks) seems to imply that, at least for scatterings involving appreciable momentum transfer, the individual quark-rearrangement probabilities (amplitudes) may be thought of as being statistically independent, so that a given reaction requires the coincidence of independent quark deflections through the appropriate angle for all of the quarks involved. In a very crude sense, this model would seem to imply relatively weak quark binding energies and, correspondingly, relatively small quark masses."

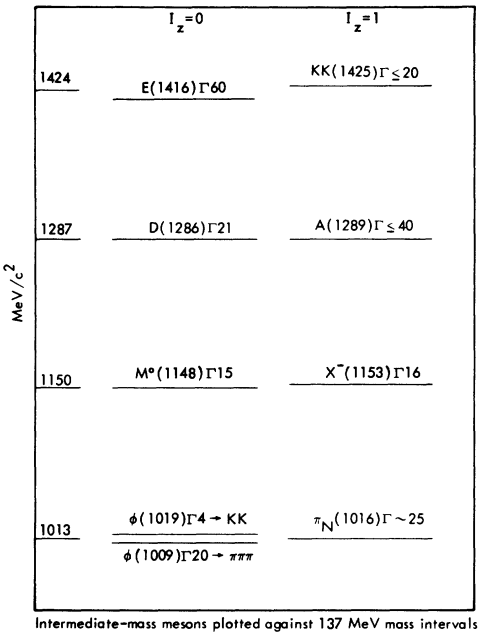

FIG. 2. Intermediate-mass narrow-width meson resonances plotted against a 137-MeV/c^2 mass grid. The accurate interval spacings that were observed in Fig. 1 are also seen here. Data on these resonances are summarized in Table I. In contrast to the spinless resonances of Fig. 1, some of the resonances of this figure are known to be spin-1 excitations. In Fig. 6 these resonances are shown as part of a "meson excitation tower" based on a 658-MeV spin-1 "ground state." The natural widths for these spin-1 resonances are $\Gamma \simeq 10$–20 MeV, in contrast to the widths $\Gamma << 5$ MeV for the spinless excitations of Fig. 1.

In recent work, both Vinciarelli[132] and Drell and Johnson[119] have been led to the concept of light nucleon quarks [$M<500$ MeV (Ref. 132) and $M\sim300$ MeV (Ref. 119)] to explain the early onset of the electromagnetic scaling laws ("precocious scaling").

Franklin has summarized the implications of the quark model with respect to quark masses and quark binding energies in a very succinct manner[133]: "The agreement of quark predictions with experiment could be described as spectacular, and yet virtually every prediction really makes sense only if quarks are not too heavy or if the binding is not too strong."

The only real argument for believing that quarks are very massive has been one based on their nonobservability. However, now that the CERN ISR experiments[118] have pushed the lower limit on the quark mass, from this line of reasoning, up to 25 GeV/c^2, it is apparent that this argument is no longer tenable in view of the linear systematics that are known to obtain for the quark model. A review of recent ideas about light quarks is contained in an article by Jones,[120] who comments: "... it is my understanding that theorists now favor quarks of rest mass of about 0.3 GeV/c^2 (about a third of a nucleon mass or twice a pion mass), and in fact they would be somewhat embarrassed if 10-GeV/c^2 quarks were now discovered and had to be built into their models."

Facet (4), the fourth argument presented here in favor of light quarks, is one that is obtained by phenomenologically reproducing the observed masses of the nucleon, $N=939$ MeV (Ref. 25), and the $\bar{p}n$ bound state, $N\bar{N}=1795$ MeV (Ref. 38). This argument proceeds as follows. Many phenomenological results (see Sec. III) indicate that the nucleon is composed of three subunits of approximately equal mass. In particular, detailed electromagnetic properties of nucleon quarks, which are summarized in Table VIII (see Refs. 132, 134–136, 38, 12, 119), pinpoint the average mass of the nucleon quark at just about 330 MeV. If we denote this 330-MeV nucleon quark, for generality, as the spinor S, then there are two ways in which the nucleon can be constructed:

$$\text{(F-Y):}\quad N=S\bar{S}S \text{ and } \bar{N}=\bar{S}S\bar{S},\quad \text{Fermi and Yang}[122]; \tag{1a}$$

$$\text{(G-Z):}\quad N=SSS \text{ and } \bar{N}=\bar{S}\bar{S}\bar{S},\quad \text{Gell-Mann and Zweig.}[121] \tag{1b}$$

The G-Z formulation is the conventional quark model that has been widely discussed in the literature for the past decade. The F-Y formulation is an earlier model that appeared prior to the introduction of the name "quark." Both the G-Z and F-Y models reproduce the quantum numbers of the nucleon. In the F-Y model, the quark states S are assigned the same quantum numbers as the nucleon states N. Thus the F-Y model has an advantage over the G-Z model in that unobserved[120] fractional quantum numbers are avoided. We can use a straightforward extension of the F-Y model to reproduce the N and $N\bar{N}$ masses by attributing to the spinor S not only the same *quantum numbers* as the nucleon N but also the same *binding energies* (B.E.). Experimentally, the nucleon ($N\equiv p, n$) has the following binding energies:

$$pp=nn=0,\quad pn\simeq 0.1\%,\quad \bar{p}n=4.4\%.[38] \tag{2}$$

These binding energies can be extrapolated to nucleon states N as follows:

$$NN=\bar{N}\bar{N}\simeq 0,\quad N\bar{N}\simeq 4\%\,. \tag{3}$$

If we extend these same binding energies to the 330-MeV spinor S, we obtain

$$SS=\bar{S}\bar{S}\simeq 0,\quad S\bar{S}\simeq 4\%\simeq 26\text{ MeV}. \tag{4}$$

Since this 4% (hadronic) binding energy is much

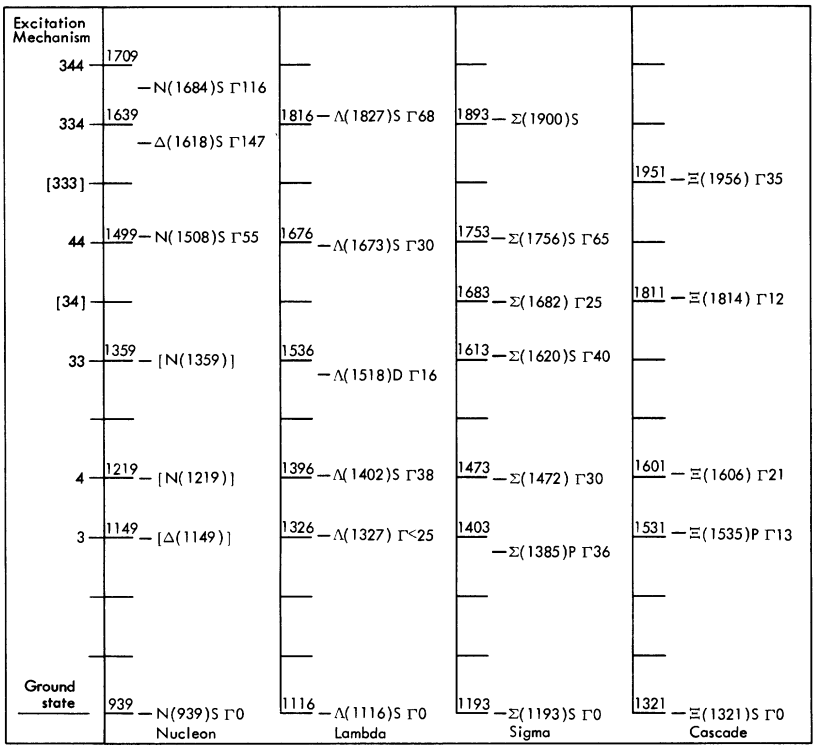

FIG. 3. The narrow-width baryon and hyperon resonances plotted against 70-MeV mass grids based on the "ground states" $N(939)$, $\Lambda(1116)$, $\Sigma(1193)$, and $\Xi(1321)$. The accurate level spacings suggest that these levels are formed by adding $M \equiv 70$ MeV "excitation quanta," with essentially zero binding energy, to these fundamental ground states. The observed gaps in the level spacings can be accounted for by assuming that the excitations occur as the combinations $3 \equiv 3M = 210$ MeV and $4 \equiv 4M = 280$ MeV [see Eq. (29)]. Data on these resonances are summarized in Tables III–VII.

TABLE VIII. Calculations that point to the existence of a fundamental 330-MeV spin-$\frac{1}{2}$ hadronic mass quantum, which is denoted here as the spinor S. S has the same mechanical and electromagnetic properties as the conventional nucleon quark, but it has different particle-antiparticle properties; as discussed in the text, S resembles the Fermi-Yang nucleon quark rather than that of Gell-Mann and Zweig.

Type of calculation	Mass indicated	Footnote
Inelastic scattering ("precocious scaling")	$M \sim 500$ MeV	a
Range of quark, magnetic mass splitting	$M = 322$ MeV	b
Intrinsic quark magnetic moment	$M = 336$ MeV	c
Dirac moments for quarks: proton	$M_p = 339$ MeV	d
neutron	$M_n = 323$ MeV	d
Given the $\bar{p}n$ binding energy of 4.4%, suppose the nucleon is $N = QQQ$ with B. E. = 4.4%; then $M_Q = (939 \times 1.044)/3 = 327$ MeV.	$M = 327$ MeV	e f
Dynamical quark model	$M \sim 300$ MeV	g
Average value for this mass quantum	$M \simeq 330$ MeV	

[a] Vinciarelli (1972), Ref.132.
[b] Feld (1969), Ref. 134.
[c] Feld (1969), Ref. 135.
[d] Franklin (1968), Ref. 136.
[e] Gray (1971), Ref. 38.
[f] Mac Gregor (1972), Ref. 12.
[g] Drell (1972), Ref. 119.

larger than nuclear binding energies, which are always less than 1%, the hadronic $S\bar{S}$ force is more short-ranged than nuclear forces, and only *adjacent* $S\bar{S}$ spinor pairs in a cluster of spinors will bind together hadronically. The nucleon appears as the spinor cluster

$$N = S\bar{S}S \text{ or } \bar{S}^{S}_{S}, \tag{5}$$

with a calculated mass of $3\times330 - 2\times26 = 938$ MeV, as compared to the experimental nucleon mass of 939 MeV. The $\bar{p}n$ bound state appears as the spinor cluster

$$N\bar{N} = \bar{S}^{S}_{S\bar{S}S} \text{ or } \bar{S}\bar{S}\bar{S}_{S\bar{S}S}, \tag{6}$$

with a calculated mass of $6\times330 - 7\times26 = 1798$ MeV, as compared to the experimental $\bar{p}n$ mass of 1795 MeV.[38] Furthermore, it is shown in paper II that the addition of electromagnetic effects does not destroy this accurate agreement between the Fermi-Yang nucleon quark model and experiment. Of course, the Gell-Mann–Zweig quark model for the nucleon, Eq. (1b), can also be made to reproduce the N and $N\bar{N}$ masses, since there are two masses to reproduce and two adjustable binding energies available (B_{SS} and $B_{S\bar{S}}$). However, in the G-Z formulation the interesting binding-energy analogy given by Eqs. (3) and (4) is lost, so that we have a model with two arbitrary parameters. The decisive point to be made in favor of the F-Y formulation of the nucleon, though, is the following: The F-Y formulation of the nucleon can be extended, as shown in the present studies,[23,24] to include all of the hadron resonances in a consistent weak-binding-energy formalism, whereas this extension does not appear to be possible if the G-Z formulation is used. From the standpoint of the present section, the significant results of the above calculations are that nucleon quarks appear to be light (Table VIII), and that quark binding energies appear to be small [Eq. (4)]. As one additional result, we note that in both the F-Y and G-Z quark models the pion is constructed as

$$\pi = S\bar{S}, \tag{7}$$

with the nucleon quark states S and $\bar{S}$ used also for the pion. Since we cannot reproduce the 140-MeV pion as a pair of 330-MeV spinors bound together with 4% binding energies, it is clear that in this weak-binding-energy context both the F-Y and G-Z quark models are incomplete: The spinless quantum $M = 70$ MeV, deduced from Figs. 1–3, must be added to the spinor $S = 330$ MeV in order to complete the light-quark basis set. This gives the π meson as

$$\pi = M\bar{M}, \tag{8}$$

with, as will be shown in detail in paper II, a 4% binding energy, the same binding energy as for the nucleon.

It should be noted here that the coplanarity of the six spinors in the $N\bar{N}$ clusters of Eq. (6) results from the essentially cylindrical configuration of the spinor S with respect to binding energies (paper II). From this coplanarity, the N and $N\bar{N}$ spinor clusters of Eqs. (5) and (6) uniquely have two and seven $S\bar{S}$ bonds, respectively.

Facet (5), the lifetime systematics of the metastable ($\tau > 10^{-17}$ sec) elementary particles, is presented in Sec. XII, since it is a result that is phenomenologically independent of the rest of the paper. A key point in this lifetime systematics is that the $K^{\pm}$, $\pi^{\pm}$, and K^{0}_{L} mesons, which are supposedly independent particles, and which have completely different decay modes,[19] have lifetimes that occur in the ratios 1:2:4 (see Fig. 20). An examination of the other metastable particles[19] indicates that this result is not accidental. Statistically, the 1:2:4 lifetime ratios suggest the existence of 4:2:1 independent decay triggers (70-MeV mass quanta), whose spontaneous annihilations trigger the particle decay process. The lifetime systematics of Fig. 21 reveals a second scaling of lifetimes, as powers of $\alpha = e^2/\hbar c$, and this scaling in α establishes a common link between the weakly interacting μ meson and the strongly interacting metastable hadron resonances. The evidence for a well-defined particle substructure, which is indicated by the lifetime systematics of Sec. XII, carries with it the implication that binding energies must be small, since strong binding energies would tend to obscure this substructure.

The main conclusion to be drawn from the arguments of facets (1)–(5) in the present section is that both the experimental hadron data and the phenomenological hadron analyses point to the facts that quarks are light and quark binding energies are small. In order to establish the validity of this light-quark approach to hadron structure, it must be demonstrated that a light-quark model can be devised which accurately reproduces the spectrum of hadron resonances listed in Tables I–VII. This is the problem that is treated in the remainder of the present paper and in paper II.

V. A LIGHT-QUARK BASIS SET

In the present paper, we do not consider binding-energy systematics, electromagnetic effects, particle-antiparticle states, strangeness quantum numbers, or quark-state geometries in any detail; these topics are dealt with in paper II. However, in order to provide a background for the system-

atic results mentioned in the present paper, we outline here the salient features of the light-quark hadronic basis set obtained from the present phenomenology.

The phenomenological arguments which delineate the fundamental light-quark basis states were presented in Sec. IV: (a) Evidence summarized in Table VIII points to the existence of a $J=\frac{1}{2}\hbar$ nucleon quark, the spinor S, with a mass of about 330 MeV. It was shown in Eqs. (2)–(6) of Sec. IV that the spinor S correctly reproduces the masses of the nucleon and the $N\bar{N}$ bound state. (b) From the observed 137-MeV level spacings of Figs. 1 and 2, the existence of a spinless 70-MeV mass quantum M was deduced ($\pi = M\bar{M} \sim 137$ MeV). (c) Figure 3 demonstrated that a series of S-state baryon excitations are produced by adding the spinless excitation groups $3 \equiv 3M = 210$ MeV and $4 \equiv 4M = 280$ MeV to the fundamental "ground states" N, Λ, Σ, and Ξ. (d) If we add the kaon, $K = 7M \equiv 7$, to this set of states, and if we define $1 \equiv M$, then the set

$$1, 3, 4, 7, S \rightarrow 1 \equiv M,\ 3 \equiv 3M,\ 4 \equiv 4M,\ 7 \equiv 7M,\ S \equiv (3M)_{\text{spinning}} \tag{9}$$

is obtained as a sufficient set of light-quark basis states for reproducing the observed spectrum of hadron resonances. In addition to the basis set $1, 3, 4, 7, S$, the (π meson) excitation

$$\pi = 1\bar{1} \equiv M\bar{M} \tag{8'}$$

appears as a prominent structural component of meson excitations (but not baryon excitations).

In detailed calculations of binding energies and electromagnetic effects, the basis states 3, 4, 7, and S interact phenomenologically as if they are constructed in the form of *linear arrays* of subquanta M (literally, aligned arrays of 70-MeV oblate spheroids). These linear arrays of quanta M are denoted here as "cabers." From the special-relativistic equations of Appendix B, it can be concluded, as is indicated in Eq. (9) (and is shown in detail in paper II), that the spinor S is a relativistically spinning form of the spinless caber 3. Thus the quantum M emerges as the fundamental building block for the light-quark set of basis states listed in (9). The masses of the basis states 3, 4, and 7 are obtained as the simple sums of the masses of the constituent subquanta M, with small Coulomb corrections required in cases where multiple charges are present.

The mass quantum M appears to have the same quantum numbers as the K meson. In particular, corresponding to its isotopic spin $I=\frac{1}{2}$, M occurs in the forms

$$M^+ = 74.6 \text{ MeV},\quad M^0 = 70.0 \text{ MeV},\qquad \bar{M}^0 = 70.0 \text{ MeV},\quad M^- = 74.6 \text{ MeV}, \tag{10}$$

with (M^+, M^0) = particle states and $(M^-, \bar{M}^0)$ = antiparticle states. The cabers 3, 4, and S have more complicated particle-antiparticle configurations than the quantum M. Phenomenologically, they occur in resonances in three general forms:

$$\begin{aligned} &3, 4, S \equiv \text{strange (ST) all quanta } M \\ &\qquad \rightarrow \text{strangeness } S = +1, \\ &\bar{3}, \bar{4}, \bar{S} \equiv \text{antistrange } (\overline{\text{ST}}) \text{ all quanta } \bar{M} \\ &\qquad \rightarrow \text{strangeness } S = -1; \\ &\dot{3}, \dot{4}, \dot{S} \equiv \text{nonstrange (NS) mixed quanta } M \text{ and } \bar{M} \\ &\qquad \rightarrow \text{strangeness } S = 0. \end{aligned} \tag{11}$$

The strangeness quantum numbers shown in (11) for the spinless cabers $3, \bar{3}$ and $4, \bar{4}$ are the conventional strangeness quantum numbers of Gell-Mann and Nishijima. The strange spinors $S, \bar{S}$ are different in that they occur only in the form of invariant spinor triplets $S\bar{S}S$ and $\bar{S}S\bar{S}$ [see Eq. (15) below], and the conservation of baryon number is precisely equivalent to the conservation of these triplets. Thus the strangeness quantum numbers carried by the triplets $S\bar{S}S$ and $\bar{S}S\bar{S}$ are invariants with respect to associated production processes, so that the strangeness of the spinor S does not enter into the conventional strangeness formalism. However, from the binding energy systematics cited just below, the spinors S and $\bar{S}$ are "strange," and this "invariant strangeness" has observable consequences with respect to the production of Y^* resonances and the nonproduction of Z^* resonances (Y^* and Z^* production is summarized in Ref. 25).

A striking aspect of the particle-antiparticle configurations shown in (11), and the reason that the cabers 3, 4 and S are all denoted as "strange," is the phenomenological connection that occurs between strangeness quantum numbers and hadronic binding energies (H.B.E.). This connection is as follows:

$$\begin{aligned} &\text{ST-}\overline{\text{ST}} \text{ adjacent caber pairs have H.B.E.} \simeq 4\%; \\ &\text{NS-ST, NS-}\overline{\text{ST}}\text{, and NS-NS caber pairs have H.B.E.} \simeq 0\%; \\ &\text{ST-ST and } \overline{\text{ST}}\text{-}\overline{\text{ST}} \text{ caber pairs do not bind hadronically.} \end{aligned} \tag{12}$$

The binding-energy systematics given in Eq. (4) for the spinor S is thus a part of the general binding-energy systematics of Eq. (12).

The long-lived, very-narrow-width hadron res-

onances are composed entirely of strange and antistrange cabers. Examples of these resonances are as follows.

$$\text{Resonance: } \pi = 1\bar{1},\ \eta = 4\bar{4},\ \eta' = 7\bar{7},\ K = 7,\ \bar{K} = \bar{7} \qquad (13)$$

$$\text{strangeness: } 0 \quad 0 \quad 0 \quad +1 \quad -1$$

and

$$\text{resonance: } N = S\bar{S}S,\ \Lambda = S\bar{S}S\bar{3},\ \Sigma = S\bar{S}S\bar{4},\ \Xi = S\bar{S}S\bar{3}\bar{3},\ \Omega = S\bar{S}S\bar{3}\bar{4}\bar{4} \qquad (14)$$

$$\text{strangeness: } 0 \quad -1 \quad -1 \quad -2 \quad -3$$

From the strangeness quantum numbers of these configurations, it is clear that the strangeness is carried by the spinless cabers 3, 4, and 7. Empirically, the antistrange cabers $\bar{3}$ and $\bar{4}$ will bind to the spinor core $S\bar{S}S$ to produce Y^* resonances, but the strange cabers 3 and 4 will not bind to this same spinor core to produce Z^* resonances. Thus the particle-antiparticle asymmetry of the spinor core $S\bar{S}S$ does have observable consequences, even though we formally assign a strangeness value of zero to S to be in agreement with standard terminology.

The spinor S occurs in meson and baryon resonances in a very characteristic manner:

$$S \text{ appears pairwise as } \dot{S}\dot{S} \text{ in meson resonances,} \qquad (15)$$

$$S \text{ appears tripletwise as } S\bar{S}S \text{ or } \bar{S}S\bar{S} \text{ in baryon resonances.}$$

To illustrate Eq. (15), we give some examples of meson and baryon resonances. In meson resonances, the excitations $\dot{S}\dot{S}\pi$, $3\dot{S}\dot{S}\pi$, $3\dot{S}\dot{S}3\dot{3}$, and $3\dot{S}\dot{S}4\dot{4}$ correspond to the rotationless resonances, ω, ϕ, D, and E, respectively. The spinor pair $\dot{S}\dot{S}$ by itself is the bandhead (see Fig. 4) for the dominant $\rho(770)$ $\Gamma 146$ and $\epsilon(\sim 800)$ $\Gamma \sim 150$ rotational resonances, which are $^{2S+1}L_J = {}^1P_1$ and $^3P_0$ spectroscopic states, respectively. Spinors pairs $\dot{S}\dot{S}$ that are produced with no accompanying spinless quanta attached are very difficult to observe as S states: The spinor pair $\dot{S}\dot{S}$ is the ground state of the meson excitation tower of Fig. 6, and a slight experimental indication for its appearance as an S state is shown in Fig. 18 (also see Ref. 39); the spinor quartet $\dot{S}\dot{S}\dot{S}\dot{S}$ has a mass of about 1310 MeV and a spin-parity $J^P = 2^+$, so that it matches the elusive dip in the A_2 meson.[40]

Examples of $S\bar{S}S$ spinor baryon excitations were given in the baryon excitations of Eq. (14). Other prominent S-state baryon excitations are $(S\bar{S}S)\dot{4}\dot{4} = N(1508)S$, $(S\bar{S}S\bar{3})\dot{4}\dot{4} = \Lambda(1673)S$, and $(S\bar{S}S\bar{4})\dot{4}\dot{4} = \Sigma(1756)S$, in which these dominant S states appear at intervals of 560 MeV above the corresponding ground states (see Fig. 3). The $\Lambda(1518)$ $D_{03}\Gamma 16$ resonance, which from its very narrow width cannot be a rotational level, is the excitation $S_\uparrow\bar{S}_\uparrow S_\uparrow\bar{3}\dot{3}\dot{3}$, with the angular momentum $J = \frac{3}{2}\hbar$ arising from the alignment of the three $J = \frac{1}{2}\hbar$ spins in the $S\bar{S}S$ spinor core (note that no narrow-width $J = \frac{5}{2}, \frac{7}{2}, \ldots$ resonances have ever been observed). The famous $\Delta(1233)$ $P_{33}\Gamma 115$ resonance is the excitation $S\bar{S}S\dot{3}$ in a $^{2S+1}L_J = {}^2P_{3/2}$ rotational mode (see Refs. 82 and 137). The $\Lambda(1518)D$ is a $^4S_{3/2}$ excitation.

The distinction between rotationless and rotational hadron resonances can be made directly on the basis of resonance widths, as follows.

Meson resonances:

$$S \text{ states } (L = 0) \text{ have widths } \Gamma \leq 20 \text{ MeV},$$
$$\text{rotational levels } (L > 0) \text{ have widths } \Gamma \geq 50 \text{ MeV}; \qquad (16)$$

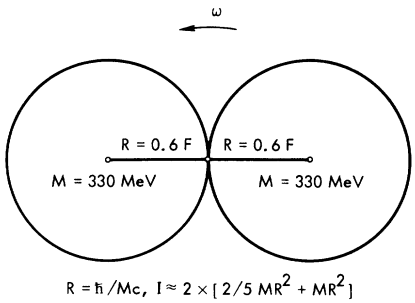

FIG. 4. A model for the ρ meson. Table VIII suggests the existence of a fundamental spinning mass quantum $S = 330$ MeV. If we give the spinor S a radius $R = \hbar/mc$ equal to its Compton wavelength, and if we place an SS spinor pair into an $L = 1$ rotational mode as shown, then the classical estimate for the moment of inertia I shown in this figure results in a rotational energy which combines with the 660-MeV bandhead energy to give the correct total energy for the peak of the ρ resonance (see the discussion in the text).

baryon resonances:

$$S \text{ states } (L=0) \text{ have widths } \Gamma \leq 50 \text{ MeV}, \quad \text{rotational levels } (L>0) \text{ have widths } \Gamma \sim 100 \text{ MeV}. \tag{17}$$

For the meson resonances, this distinction is particularly clear-cut. Sections VII and VIII contain detailed compilations of these resonance widths.

As one immediate result of this light-quark phenomenology, we note that the excitations $3, \bar{3}, \dot{3}$, which contain an odd number of subquanta M, can have different symmetry properties from excitations $4, \bar{4}, \dot{4}$, which contain an even number of subquanta M. These differences in symmetry properties do seem to occur, and they can be identified in the characteristics of the experimental resonances. A summary of these symmetry differences is given in Appendix A.

VI. SPIN ANGULAR MOMENTUM AND ORBITAL ANGULAR MOMENTUM

A. Spin angular momentum

We know empirically that the spin angular momentum $\vec{S}$ of a particle is a true angular momentum in the same sense that the orbital angular momentum $\vec{L}$ is a true angular momentum, because $\vec{L}$ and $\vec{S}$ couple together in a very direct manner. From the spectroscopy of the nucleon discussed in Sec. III, it seems natural to attribute the spin angular momentum of the nucleon substate (the spinor S) to the rotation of an extended mass. In order to attain the required angular momentum value $J=\frac{1}{2}\hbar$ for this substate, the rotation must be rapid, so that special-relativistic effects will be important. We ordinarily think of special relativity as applying to linear velocities, but a perusal of the textbooks and papers on special relativity makes it clear that special relativity is equally relevant for angular velocities (see the references in Appendix B).

The equations of special relativity as applied to rotating masses are derived and discussed in Appendix B. The special-relativistic results that are important for the present phenomenology, and which in fact led to the investigation of these relativistic equations,[3] are the following:

(a) If a uniform sphere of matter is rotated until the equation reaches the velocity of light (or remains infinitesimally below that value), the relativistically-spinning sphere becomes *half again as massive* as it was at rest.

(b) If the radius of the spinning sphere is set equal to its Compton wavelength, $R=\hbar/mc$, where m is the spinning mass, then the calculated angular momentum of the sphere about the spin axis is $J=\frac{1}{2}\hbar$.

(c) If a unit charge e is placed on the spinning sphere and allowed to move freely, it will be forced to the equator of the sphere, where it will give rise to a calculated magnetic moment $\mu=e\hbar/2mc$.

(d) Changing from a spherical geometry to a spheroidal geometry produces only small changes in the above calculated quantities.

As a first application of results (a)–(d), we can denote the spinless 70-MeV quark state of the present model as the (spherical or spheroidal) quantum M, and a relativistically spinning form of this same quark state as the quantum M_s. Then result (a) leads to the result that

$$M = 70 \text{ MeV} \rightarrow M_s = \tfrac{3}{2}M = 105 \text{ MeV}, \tag{18}$$

and the phenomenological association between the spinning quantum M_s and the 105-MeV μ meson seems unmistakable.[138] However, in the present hadron phenomenology, the utility of the special-relativistic results (a)–(d) lies not in their application to single quanta M, but rather in their application to combinations of three quanta M as they occur in the spinless caber $3 \equiv 3M$ and in the spinor $S \equiv 3M_s$ [see Eq. (9)]. The mass of a caber $3^{\pm}$ is 214.6 MeV [see Eq. (10) and the accompanying discussion], and the mass of a spinor $S^{\pm}$ is about 330 MeV (Table VIII), so that the ratio of these masses is $330/214.6 = 1.54$, or just slightly larger than the ratio of 1.50 given in result (a) and Eq. (18). Thus the spinor S appears as a relativistically spinning form of the caber 3, and the mass increase of 1.54 instead of 1.50 can be attributed to the need for using an oblate spheroidal geometry [result (d)] rather than a spherical geometry (a spherical geometry would give to the nucleon too large a volume to be consistent with optical-model calculations, as is discussed in paper II). In detail, the spinor S is constructed as an aligned array of three oblate spheroids M, each having radii $R_{\max} \simeq \frac{1}{3}\sqrt{3}$ fermi and $R_{\min} \simeq \frac{1}{3}$ fermi. Since the value for $R_{\max}$ quoted here is $R_{\max} \simeq \hbar/mc$, with $m = 330$ MeV, the radius $R_{\max}$ for each subquantum M_s in the spinor S reflects the *total mass* of the spinor S. With this construction for the spinor S, result (b) gives $J=\frac{1}{2}\hbar$ as the calculated spin angular momentum, and result (c) gives $\mu = 2.8$ nuclear magnetons as the calculated magnetic moment for a unit equatorial charge distribution. Thus the spinor S has *calculated* spin angular momentum and magnetic moment values that are the same as the *assumed* spin and (intrinsic) magnetic moment values for

the conventional nucleon quark.[128] If the spinor S is given the geometry described here, then the known first-order properties of the nucleon, which is constructed as $N = S\bar{S}S$, are reproduced.[139]

The special-relativistic result (a) leads to another important phenomenological result, namely, the mechanism for producing spinor pairs SS. From the structures of meson resonances (in which spinors always appear in pairs), and from the conservation of baryon number (which requires spinor triplets to be produced in pairs), it seems that spinors are always created (and destroyed) in a pairwise manner. The mechanism for producing spinor pairs appears to be the isoergic transition

$$333 \rightarrow SS \ . \tag{19}$$

In the mapping of the meson resonances, which is described in Sec. VIII, this transition is seen to be of central importance. From the observed meson decay mode $\phi \rightarrow KK$, which from the present viewpoint is the transition $3SS\pi \rightarrow 3333\pi = 77 = KK$, we can unequivocally establish that the inverse transition also occurs:

$$SS \rightarrow 333 \ . \tag{20}$$

The transition $333 \rightarrow SS$, in addition to forming an integral part of the meson excitation scheme of Sec. VIII, has two other consequences that are important in the present light-quark hadron spectroscopy. (1) By its isoergic nature, Eq. (19) furnished an immediate explanation for the quantization of spin angular momentum, in which the spinors S always spin at the full relativistic limit (with their equators at the velocity of light); spin angular momentum quantization emerges as a consequence of energy conservation. (2) The production transition $333 \rightarrow SS$ leads to a fundamental spin and isotopic-spin selection rule for meson resonances:

$$\begin{aligned} &\text{spin-1 spinor pairs } \dot{S}\dot{S} \text{ have isotopic spin } I = 0, \\ &\qquad\qquad\qquad\qquad\qquad\qquad\qquad\qquad (21) \\ &\text{spin-0 spinor pairs } \dot{S}\dot{S} \text{ have isotopic spin } I = 1 \ . \end{aligned}$$

The workings of rule (21) can be clearly observed in the experimental meson resonances of Sec. VIII. Rule (21) can be "derived" by thinking of the transition $333 \rightarrow \dot{S}\dot{S}$ as a two-step process: (1) One of the 3's in the cluster 333 annihilates, and the tangential forces set the other two 3's spinning in opposite directions, so that the total angular momentum is $J = 0$ for the spinor pair $\dot{S}\dot{S}$ that is produced, and angular momentum is conserved locally; (2) if and only if the spinor pair is in an isotropic spin $I = 0$ charge mode, $\dot{S}\dot{S} = S^+S^-$, the spinor pair couples externally via a virtual spin-1 photon process to produce a $J = 0$ to $J = 1$ spinor-flip transition.

In Sec. VI B, we extend the present considerations to include hadron orbital angular momenta.

B. Orbital angular momentum

In the standard classification of meson resonances,[25] each resonance is assigned a total angular momentum $\vec{J}$, and no distinction is made as to whether this angular momentum reflects an intrinsic spin or an orbital rotation or both. The *heavy-quark* models of Fermi and Yang[122] and Gell-Mann and Zweig[121] both picture mesons as being constructed from a pair of nucleon quarks,

$$\text{meson} = S\bar{S} \ , \tag{7'}$$

and the $J = 1$ mesons ρ and ω are assumed to have intrinsic spins $S = 1$ and orbital angular momenta $L = 0$. However, we have already seen that in the present *light-quark* context, Eq. (7) cannot be used for the π meson and must be replaced by Eq. (8). Similarly, if S and $\bar{S}$ are 330-MeV light quarks, as indicated in Table VIII, then it is clear that Eq. (7) cannot be used to reproduce the masses $\rho(770)$ and $\omega(784)$ if no energy is to be attributed to orbital rotations, since the spin energy is already included in the masses of the spinors S and $\bar{S}$. Moreover, as another complication for the ρ and ω mesons, these appear experimentally to be quite different types of resonance, as is illustrated in Table IX. Table IX shows three *narrow-width* $J = 1$ meson resonances—ω, ϕ, D—and three *broad-width* $J = 1$ meson resonances which occur with roughly the same mass values—ρ, A_1, B. In addition to the striking differences in the widths, these resonances also differ characteristically in their isotopic spins. As was mentioned in Sec. V and is shown in detail in Sec. VIII, the ω, ϕ, and D resonances in a light-quark model are the *rotationless* excitations $\dot{S}\dot{S}\pi$, $3\dot{S}\dot{S}\pi$, and $3\dot{S}\dot{S}33$, respectively, and their $S = 1$, $I = 0$ spin, isotopic spin modes are examples of rule (21) as applied to the $\dot{S}\dot{S}$ spinor pair contained in each of these resonances; these resonances are ${}^{2S+1}L_J = {}^3S_1$ configurations. If we also apply rule (21) to the ρ, A_1, and B resonances, then the isotopic spins $I = 1$ of these resonances indicate that they must have spins $S = 0$ and hence must be $L = J = 1$ *rotational* resonances; as shown in Sec. VIII, these resonances are ${}^{2S+1}L_J = {}^3P_1$ configurations, with the rotational bandheads $\dot{S}\dot{S}$, $3\dot{S}\dot{S}\pi$, and $3\dot{S}\dot{S}4$, respectively. The ρ bandhead $\dot{S}\dot{S}$ is shown in Fig. 4. Later on in the present section it is shown that the calculated rotational energy of the ρ adds to the 660-MeV $\dot{S}\dot{S}$ bandhead energy to accurately reproduce the peak energy of the ρ.

TABLE IX. A comparison of three narrow-width $I=0$, $J=1$ meson resonances with three broad-width $I=1$, $J=1$ meson resonances in the same general mass region. The angular momentum $J=1$ of the narrow-width resonances ($\Gamma \simeq 10$ MeV) appears to arise from the intrinsic spin $\vec{S}$ of the resonance structure, whereas the angular momentum $J=1$ of the broad-width resonances ($\Gamma \simeq 100$ MeV) appears to arise from a less precisely quantized orbital angular momentum $\vec{L}$ (see Sec. X). The spin–isotopic-spin relationship $\vec{S}=1$, $I=0$ or $\vec{S}=0$, $I=1$ illustrated by these resonances is a very general result for all meson resonances [see Eq. (21)].

Resonance	Energy (MeV)	Width (MeV)	Ang. mom.	I spin	Spect. state [e]
ω	784	$\Gamma = 9.8 \pm 0.5$ [a]	$J=1$	$I=0$	$^3S_{01}$
ϕ	1019	$\Gamma = 4.2 \pm 0.2$ [a,b]	$J=1$	$I=0$	$^3S_{01}$
D	1283	$\Gamma = 10 \pm 10$ [c]	$J=1$	$I=0$	$^3S_{01}$
ρ	770	$\Gamma = 146 \pm 10$ [a]	$J=1$	$I=1$	$^1P_{11}$
A_1	1115	$\Gamma = 98 \pm 45$ [d]	$J=1$	$I=1$	$^1P_{11}$
B	1237	$\Gamma = 120 \pm 20$ [a]	$J=1$	$I=1$	$^1P_{11}$

[a] RPP73, Ref. 25.
[b] This width is anomalously narrow (see Refs. 28 and 29).
[c] This narrow width for the D is from Boesebeck 71 in Ref. 25.
[d] This is the nondiffractive measurement of Anderson 69 in Ref. 25.
[e] Rule (7) of Table XII.

The heavy-quark meson configurations typified by Eq. (7) illustrate one version of the quark model. This model can of course have both spin angular momenta $\vec{S}$ and orbital angular momenta $\vec{L}$, although the $\vec{L}$ and $\vec{S}$ assignments,[140] as we have just seen, are not the same as the ones obtained in the light-quark model. As another approach to this problem, studies have been carried out to investigate the use of the group SL(3, R) as a generator of orbital excitations in nucleons.[141] The noncompact group SL(3, R) is the special linear group of rotations and deformations at constant volume in three-dimensional space, and this group has been successfully applied to E_2 transitions in nuclear physics.[142] Although the introduction of orbital angular momentum raises problems with respect to relativistic (Lorentz) invariance,[143] recent investigations suggest[144] that rotational excitations are in fact quite consistent with the requirement of relativity.

The concept of light quarks and small binding energies indicates that quarks have well-defined geometries, and that clusters of quarks will also have well-defined and in general nonspherical geometries. Since nonspherical geometries are associated with rotational excitations in all other branches of molecular and submolecular physics, it is to be expected that nonspherical hadron resonances will show similar characteristics. As we have indicated above, this is in fact the case, and we outline here the systematics of hadron rotational excitations.

If we assume that the theory of hadron rotational bands is similar to the theory of nuclear physics rotational bands, as is suggested for example by the SL(3, R) applications mentioned above, then there is one overriding consequence for hadron rotational levels that emerges from nuclear physics theory: *The energies of hadron rotational levels depend on the orbital angular momentum* $\vec{L}$ *and not on the total angular momentum* $\vec{J}$; hadron rotational energies are given by the equation

$$E_{\text{total}} = E_0 + E(L) = E_0 + (\hbar^2/2I)\, L(L+1)\,, \tag{22}$$

where L is the orbital angular momentum, I is the moment of inertia, and E_0 is the bandhead (S-state) energy. The reason for this L dependence of hadron rotational energies is that in hadrons the moment of inertia I is very small, so that rotational energies are very large, and in fact comparable to the rest-mass energy E_0. Hence hadron rotations are, by nuclear physics standards, highly nonadiabatic,[7] and this nonadiabaticity effectively decouples spins and orbital angular momenta, at least as far as rotational energies $E(L)$ are concerned. In nuclear physics, if the bandhead has spin $\vec{S}$ we can set $\vec{L}^2 = (\vec{J}-\vec{S})^2 = \vec{J}^2 - 2\vec{J}\cdot\vec{S} + \vec{S}^2$. The "Coriolis" cross-product term $\vec{J}\cdot\vec{S}$ vanishes[7] if three conditions are satisfied: (1) The system is markedly unspherical, so that rotational axes are clearly defined; (2) the rotational velocity is "slow" (the adiabatic approximation), so that the rotation does not appreciably affect the intrinsic spin $\vec{S}$; (3) the intrinsic spin $\vec{S}$ does not have the value $\frac{1}{2}$. If the Coriolis term vanishes, then a $J(J+1)$ interval rule is obtained for the rotational energies. However, in the meson resonances,

rotational excitations are highly nonadiabatic; and in baryon and hyperon rotations, all three of these conditions are violated. Hence we have no theoretical reason to expect hadron rotational bands to follow the $J(J+1)$ energy interval rule that occurs for some rotational bands in nuclear physics. Instead, rotational energies will follow Eq. (22), which is a very general equation that applies in all cases where the more specialized conditions just described do not apply.

Phenomenologically, it is quite clear from the results of the present paper that an $L(L+1)$ energy interval rule, and not a $J(J+1)$ energy interval rule, governs the rotational levels in the baryon and hyperon resonances. For example, it is shown in Table X (discussed below) that some rotational bands contain both $J=L-\frac{1}{2}$ and $J=L+\frac{1}{2}$ resonances, and these mixed rotational bands occur with $L(L+1)$ energy intervals.

Although baryon and hyperon rotational energies follow an $E(L)$ energy dependence [Eq. (22)], this does not necessarily mean that the amplitudes $J=L-\frac{1}{2}$ and $J=L+\frac{1}{2}$ in πN and KN phase-shift analyses will both resonate at the same energy. In fact, from observed πN and KN polarizations, it is clear that they do not. Let us define $L_-\equiv J=L-\frac{1}{2}$ and $L_+\equiv J=L+\frac{1}{2}$. If we assume that the intrinsic spin $S=\frac{1}{2}\hbar$ of a baryon or hyperon resonance arises from the rotations of spinors whose equators are already moving at the velocity of light (Sec. VI A), then $J=L-\frac{1}{2}$ amplitudes will be relativistically favored, and we expect L_- resonances to appear in phase-shift analyses at lower energies that L_+ resonances. That this is actually the case is demonstrated in Table X. Table X is a compilation of the L_- and L_+ resonant amplitudes as obtained from the rotational systematics of Sec. VII and from the data compilation of Tables III–VI. In πN and KN phase-shift analyses, the most clearly defined phase shifts seem to be the D waves and F waves, and Table X shows that these resonate as a function of increasing energy in a very clear pattern: L_-, L_+, L_- (how much this reflects the actual physics of the scattering and how much it reflects the continuity contraints imposed on the energy-dependent amplitudes is an interesting point to consider). As is shown in Table X, the lowest-lying rotational bands (except for the Δ resonances) are composed entirely of L_- amplitudes. At the high energies, and in phase-shift analyses in which very weak resonances are identified, these is some tendency for L_- and L_+ amplitudes to show resonances at the same energy.

In baryon and hyperon phase-shift analyses, P-wave resonances seem characteristically difficult to pin down. Most of the C-rated resonances in Table X are P waves. As an example of a P-wave ambiguity that has appeared recently in πN phase-shift analyses, we show in Table XI two sets of (P_{11}, P_{13}) and (P_{31}, P_{33}) resonances in the

TABLE X. $L_-\equiv J=L-\frac{1}{2}$ and $L_+\equiv J=L+\frac{1}{2}$ partial-wave resonant amplitudes for the hyperon and baryon rotational bands of Tables XV–XX. The A–D labels are the confidence values assigned to these resonances in Tables III–VI. The D and F waves, which have high confidence values, show a clear ordering of the resonances with increasing energy: L_-, L_+, L_-. The P waves, which have generally lower confidence values than D and F waves, have resonances that appear mainly in the L_- amplitude, as do the G waves. An illustration of a P-wave L_-, L_+ ambiguity in the amplitudes—a P-wave "criss-cross"—is shown in Table XI.

Bandhead [a]	S	P	D	F	G	H
$N4$	···	L_- C				
$N33$	···	L_- A	L_- A	L_- A	···	L_- A
$N44$	L A	L_- C	L_+ A	···	L_+ C	
$N344$	L A	L_- A L_+ A	L_- B	L_+ B L_- B	L_- A	
$\Delta 3$	···	L_+ A				
$\Delta 44$	···	···	L_- A	L_- A		
$\Delta 334$	L A	L_+ C	L_+ C	L_+ A	L_+ C	L_+ A
$\Lambda 33$	L A	L_- C	L_- A	L_- A	L_- A	L_- A
$\Lambda 44$	L A	L_- B	L_+ A	L_+ B		
$\Lambda 334$	L B	L_+ B	L_- B	L_- C		
$\Sigma 4$	L C	L_- D	L_- A			
$\Sigma 33$	L B	L_- B	L_+ A	L_- A	L_- B	
$\Sigma 44$	L A	L_+ C	L_- A	L_+ A	L_- A	$L_?$ A
$\Sigma 334$	L C	L_- B				

[a] See Fig. 3 and Table XIV.

TABLE XI. Examples of P-wave "criss-cross" amplitude ambiguities. The recent phase shift analyses of AYED (Ref. 78) and AL (Ref. 80) point to the need for both $L_-\equiv J=L-\frac{1}{2}$ and $L_+\equiv J=L+\frac{1}{2}$ P-wave resonances in the $I=\frac{1}{2}$ (P_{11}, P_{13}) and $I=\frac{3}{2}$ (P_{31}, P_{33}) baryon amplitudes in the energy region from about 1700 MeV to 1900 MeV, but they differ in the L_-, L_+ ordering of the resonances. In particular, the AYED solution, which features two P_{11} resonances below 1700 MeV (a split Roper resonance), selects the P_{13} resonance at 1700 MeV, whereas the AL solution, which features an unsplit Roper resonance, selects the P_{11} resonance at 1700 MeV.

AYED	AL
$N(1691)\ P_{13}\ L_+$	$N(1720)\ P_{11}\ L_-$
$N(1755)\ P_{11}\ L_-$	$N(1850)\ P_{13}\ L_+$
$\Delta(1795)\ P_{31}\ L_-$	$\Delta(1680)\ P_{33}\ L_+$
$\Delta(1890)\ P_{33}\ L_+$	$\Delta(1900)\ P_{31}\ L_-$

1700–1900 MeV energy region, taken from the phase-shift analyses of AYED (Ref. 78) and of AL (Ref. 80) (P_{11} and $P_{13} = L_-$ and L_+ for N resonances; P_{31} and $P_{33} = L_-$ and L_+ for Δ resonances). As can be seen in Table XI, the two sets AYED and AL show a "P-wave criss-cross": Where one solution selects the L_- amplitude to resonate, the other solution selects the L_+ amplitude. Both AYED and AL agree on the need for two P-wave resonances in each isospin state in this energy region, one L_- and one L_+, and they agree approximately on the positions of these resonances, but they reverse the order of the L_- and L_+ assignments. These ambiguities in the amplitudes arise at least in part from the incomplete nature of the πN experimental data, a circumstance that is discussed at the beginning of Sec. VII.

By estimating the moment of inertia I of a hadron resonance structure, we can deduce the magnitude of the rotational energies to be expected in hadron orbital rotations. As a typical example, consider a rigid body with a rest mass of 1500 MeV and a radius $R \sim 1$ fermi. A rough estimate for the moment of inertia is $I \sim \frac{2}{5} MR^2 \sim 600$ MeV fermi^2. Defining

$$E_{\text{rot}} \equiv \hbar^2/2I \tag{23}$$

as a useful rotational energy parameter, and inserting $I = 600$ MeV fermi^2, we obtain $E_{\text{rot}} \sim 32$ MeV. Hence P, D, and F rotational levels ($L = 1$, 2, and 3) for this case will have rotational energies,

$$E(L) = E_{\text{rot}} L(L+1) , \tag{24}$$

of about 65 MeV, 200 MeV, and 400 MeV, respectively. As we show in Sec. VII, these are about the energies that are observed experimentally for a bandhead mass in the neighborhood of 1500 MeV. An example of a rotational resonance at a lower energy is provided by the ρ meson. The ρ-meson bandhead is the 660-MeV $\dot{S}\dot{S}$ spinor pair. A representation for this $\dot{S}\dot{S}$ spinor pair is shown in Fig. 4. The classical estimate for the moment of inertia I shown in Fig. 4 gives the value $I = 333$ MeV fermi^2. Inserting this value into Eqs. (23) and (24) and setting $L = 1$ yields a rotational energy $E(L) = 117$ MeV. Adding this to the 660-MeV bandhead energy gives 777 MeV as the calculated energy for the peak of the ρ resonance, which compares to the experimental value[25] of 770 MeV.

A feature that is unique to hadron rotational bands is the cutoff $L_{\max}$ imposed by special relativity. As postulated at the beginning of this section, resonance structures have well-defined geometries. Hence in rotational excitations, the periphery of the resonance cannot exceed the velocity of light; the limiting angular velocity $\omega_{\max}$ is given by the equation

$$\omega_{\max} = c/R , \tag{25}$$

where R is the peripheral radius of the rotating structure. In estimating a moment of inertia I for Eq. (23), we used the example of a 1500-MeV bandhead with a radius $R \sim 1$ fermi, which gave a moment of inertia $I \sim 600$ MeV fermi^2. Inserting $R \sim 1$ fermi into Eq. (25) gives $\omega_{\max} \sim 1$ fermi^{-1}, which leads to $[L_{\max}(L_{\max}+1)]^{1/2}\hbar = I\omega_{\max} \sim 600$ MeV $\times$fermi, and $L_{\max} \sim 2.5$, as an order-of-magnitude estimate. Empirically, the following special-relativistic limits seem to apply to meson and baryon rotational bands.

Bandhead energy	$L_{\max}$ observed
< 700 MeV	1
< 1100 MeV	2
< 1300 MeV	3

(26)

Although the geometries of hadron resonances about their rotational axes are not clearly defined in the present work, the relativistic limits shown in (26) and the experimental values for E_{rot} [Eq. (23)] obtained in Sec. VII both suggest that there is a tendency for over-all hadron geometries to scale inversely with the masses of the resonance structures (see Fig. 12).

Rules for meson and baryon rotational bands are summarized in Table XII. The phenomenological arguments which were used to obtain these rules are given in Appendix C. In Secs. VII and VIII, we use the rules of Table XII to sort the experimental resonances of Tables I–VI into rotational bands.

As one final task in this section, we write down a suitable spectroscopic notation to describe meson and baryon resonances whose total angular momentum $\vec{J}$ has been decomposed into spin $\vec{S}$ and orbital angular momentum $\vec{L}$ components. The standard elementary-particle spectroscopic notation for baryons and hyperons is[25]

$$L_{(I,2I)\,(J,2J)} , \tag{27}$$

where L, I, and J are the orbital angular momentum, isotopic spin, and total angular momentum, respectively; where the choices $(I, 2I)$ and $(J, 2J)$ are made so as to give integral values; and where S, P, D, F, G, H indicate $L = 0, 1, 2, 3, 4, 5$. Although both L and J labels appear in (27), the L value is conventionally used, for example, to indicate the parity of a resonance, and it is not generally interpreted as specifying an actual rotational excitation. From the present results, it appears meaningful to give a literal interpretation to the quantum number L, and to extend the notation of (27) by appending the usual $2S+1$ superscript of nuclear physics, so that

$$^{2S+1}L_{(I,2I)(J,2J)} \quad (28)$$

becomes a complete spectroscopic labeling system for spins and isotopic spins. Comparing spectroscopic assignments in the notations of Eq. (27) and (28), we find the following illustrative examples.

Old notation [Eq. (27)]	New notation [Eq. (28)]
$\Sigma(1385)\ P_{13}\Gamma 36$	$\Sigma(1385)\ ^4S_{13}$
$\Lambda(1518)\ D_{03}\Gamma 16$	$\Lambda(1518)\ ^4S_{03}$
$\Xi(1535)\ P_{13}\Gamma 13$	$\Xi(1535)\ ^4S_{13}$
$\Lambda(1688)\ D_{03}\Gamma 53$	$\Lambda(1688)\ ^2D_{03}$
$\Lambda(1116)\ P_{01}\Gamma \simeq 0$	$\Lambda(1116)\ ^2S_{01}$

As is shown by these examples, the notation (28) and the distinction between rotationless and rotational levels changes the L assignments of the *narrow-width* $J=\frac{3}{2}$ resonances. It does not change the L assignment for a true rotational level such as $\Lambda(1688)$, but it changes the L assignment for a level such as $\Lambda(1116)$. The $\Lambda(1116)$ is clearly not a rotational excitation, and the P_{01} label was conventionally attached in order to indicate the positive parity of the Λ. Thus in going over from the notation of (27) to that of (28), we are in fact doing much more than just attaching a $2S+1$ spin superscript. We are now using the L quantum number to represent the actual orbital angular momentum of the resonance structure. In the older notation, the L quantum number was somewhat ambiguous, and the L value and the parity of a resonance sometimes represented redundant information. In Table XIII the experimental resonances of Tables I–VII are shown catalogued in terms of the notation of Eq. (28).

VII. MAPPING THE BARYON AND HYPERON RESONANCES

A. Incompleteness of the experimental data

In this section we map first the hyperon resonances and then the baryon resonances. This is because the observed hyperon resonances, from a phenomenological point of view, appear to be more complete than the observed baryon resonances. One fact that needs to be considered at the outset is that the experimental data for both KN and πN interactions are manifestly incomplete. In spin-0–spin-$\frac{1}{2}$ scattering processes, four different types of experiment are required in order to define the scattering matrix—σ, P, R, and A. However, the KN and πN phase-shift analyses whose results are discussed here have been based only on σ and P data, and the addition of R and A data is just now becoming a possibility.[145]

Analyses of nucleon-nucleon scattering, which bear some relationship to analyses of pion-nucleon and kaon-nucleon scattering, furnish a useful example of the effect of data incompleteness. In elastic N-N scattering analyses, it was found[146] that energy-independent solutions are ambiguous unless a complete set of measurements is included—in this case σ, P, D, R, and A. Furthermore, any ambiguities that are present in energy-independent analyses carry over more or less directly to the corresponding energy-dependent analyses.[146] In the case of πN and KN scattering, single-energy analyses based only on σ and P data give ambiguous results.[147] Hence in analogy to N-N scattering, some of this ambiguity in the single-energy analyses must carry over into the corresponding energy-dependent analyses. In particular, if a theoretical model is invoked in order to obtain energy-dependent forms for the amplitudes, any ambiguities due to the incompleteness of the experimental data will have the effect in phase-shift searches of yielding solutions which remain near their starting points and hence favor the theoretical model; in this event the procedure reduces to a tautology. However, there is one major difference between the elastic NN analyses and the πN and KN analyses: Whereas elastic NN amplitudes exhibit no resonant structure, πN and KN amplitudes do contain resonances, and these resonances influence the scattering over a considerable span of energies. Hence the continuity constraints on the amplitudes have a physical significance in πN and KN scattering that they do not have in elastic NN scattering. But if the πN and KN experimental data are not complete, the benefits of continuity may be obtained at a price: The dominant resonances may obscure the presence of other nearby, but much weaker, resonances. Thus, given the incompleteness of the existing experimental data, the πN and KN resonances which have been identified to date (Tables III–VII) should be considered as a minimum set of resonances.

From the systematics of the present paper, S-wave resonances are expected to have narrow widths, $\Gamma \leq 50$ MeV, and rotational levels are expected to have moderately broad widths, $\Gamma \sim 100$ MeV. When resonances are observed with very broad widths, $\Gamma > 200$ MeV, as is the case particularly in the Δ resonances, these very broad widths seem to reflect either a lack of flexibility in the amplitudes (which is necessary in order to obtain unique solutions with an incomplete data set) or else averages over more than one resonance. An interesting case in point in the N resonances is the split Roper P_{11} resonance. The splitting in the Roper resonance was predicted several years ago on the basis of the present sys-

TABLE XII. Summary of rules for meson and baryon rotational bands. These rules are discussed in detail in Appendix C.

Meson and baryon resonances

(1). The narrow-width S-state resonances form the bandheads for the broad-width rotational levels.

(2). Rotational levels follow an $L(L+1)$ energy interval rule because of the nonadiabatic nature of the rotations: $E_{\text{total}} = E_0 + (\hbar^2/2I)L(L+1)$, where L is the orbital angular momentum quantum number, E_0 is the bandhead energy, and I is the moment of inertia.

(3). Moments of inertia I are well approximated by rigid-body estimates.

(4). The experiment values for the moments of inertia from meson, kaon, baryon, and hyperon rotational bands show a uniform functional dependence on the rest mass of the bandhead, and this dependence extrapolates smoothly to match moments of inertia from what appear to be nonadiabatic rotational levels in very light nuclei (see Figs. 10–12 and Table XXX).

(5). All levels in a rotational band have the same isotopic spin.

(6). Special relativity—the requirement that the periphery of the rotating resonance not exceed the velocity of light—limits meson and baryon rotational levels roughly as follows.

Mass of bandhead	$L_{\max}$
<700 MeV	1
<1100 MeV	2
<1300 MeV	3

(7). The angular momentum states and isotopic spins of hadron resonances can be specified by using the spectroscopic notation $^{2S+1}L_{(I,2I)(J,2J)}$, where S is the intrinsic spin angular momentum, L is the orbital angular momentum, $(I, 2I)$ is the isotopic spin, and $(J, 2J)$ is the total angular momentum, and where the labels for I and J are chosen so as to yield integral subscripts. In order to denote spinless resonances which have no intrinsic spins (π, K, η, η'), the S and J labels are omitted (see Table XIII); and to complete the spectroscopic labeling of the states, a right superscript can be added to specify the strangeness quantum number (see Table XXI).

Baryon resonances

(8). The narrow-width S-state resonances are created by adding spinless excitation quanta $\dot{3} = 210$ MeV and $\dot{4} = 280$ MeV to basic N, Λ, Σ, and Ξ "ground states," as shown in Fig. 3 and Table XIV.

(9). The $J = L - \frac{1}{2} \equiv L_-$ and $J = L + \frac{1}{2} \equiv L_+$ resonant amplitudes for D through H waves occur in a fairly regular pattern with increasing energy: L_-, L_+, L_-. However, P waves, except in the Δ amplitudes, tend to show a predominance of low-mass L_- resonances.

Meson resonances

(10). The narrow-width S-state resonances are formed from spinless quanta 1, 3, 4, 7 and spinor pairs $\dot{S}\dot{S}$ in accordance with the symmetry scheme of Tables XXII and XXIII.

(11a). Isotopic-spin $I = 0$ boson resonances have spin-$(S = 1)$ bandheads, and isotopic-spin $I = \frac{1}{2}$ and $I = 1$ boson resonances have spin-$(S = 0)$ bandheads [Eq. (21)].

(11b). $I = \frac{1}{2}$ and $I = 1$ boson bandheads, which from (11a) have spins $S = 0$, occur in rotational bands with all successive L values up to the relativistic limit of rule (6): $^1S_{10}$, $^1P_{11}$, $^1D_{12}$, $^1F_{13}$, using the notation of rule (7).

(11c). $I = 0$ boson bandheads, which from (11a) have spins $S = 1$, occur in rotational bands with only the following states: $^3S_{01}$, $^3P_{00}$, $^3D_{02}$, using the notation of rule (7) (see the discussion of this result in Appendix C).

(12). All rotational levels in a meson rotational band have the same G parity, but negative-parity rotationless bandheads have the opposite G parity (see Appendix C).

(13). The spinless meson and kaon resonances π, K, η, η' have no associated rotational levels (see Appendix C).

(14). Boson resonances which are formed from excitations that contain an odd number of (asymmetric) 3's are not allowed to appear as $^1S_{10}$ states (see Appendix C); hence the ρ and K^* bandheads cannot be observed directly (the 660-MeV effect of Fig. 18 and Ref. 39 is observed only in the $I = 0$ channel).

(15). If we attribute the large spread in energies of the broad-width rotational resonances to a spread in rotational energies (as opposed to a spread in bandhead energies), then this implies a corresponding spread in orbital angular momentum L values [see Eqs. (40) and (41), and the examples shown in Figs. 14–17 in Sec. X].

TABLE XIII. Angular momentum classification of meson and baryon resonances in terms of the spectroscopic notation of Eq. (28) in the text, $^{2S+1}L_{(I,2I)(J,2J)}$, where (S,L,I,J) denote (spin angular momentum, orbital angular momentum, isotopic spin, total angular momentum), and where the choices $(I,2I)(J,2J)$ are made so as to give integral subscripts. Resonances with the S and J labels omitted are states that contain no spinors S. A meson and kaon selection rule, Eq. (21), requires $S+(I,2I)=1$ for $I=0$, $\frac{1}{2}$, and 1 resonances which contain spinor pairs SS.

Notation	Meson resonances	Kaon resonances
S_1	π,δ^-	K
S_0	$\eta,(M,\eta',\delta^0)$	
P_0	$DEF,\pi\pi(520)$	
$^1S_{10}$	$\pi_N(1016),X^-(1153),A(1289)?,KK(1425)$	$\kappa(725),K_N(1160),Q(1272),K_N(1368)$
$^1S_{30}$		$K_A(1175)?$
$^3S_{01}$	$\pi\pi(660),\omega,\pi\pi(870),\phi,M^0(1148),D,E$	
$^1P_{11}$	$\rho,\pi_N(975),A_1,B,\pi/\rho(1490)$	$K^*(892),C(1242),Q(1344),Q(1417)$
$^1P_{31}$		$K_A(1265)?$
$^3P_{00}$	$\epsilon,S^*,\epsilon',\epsilon''$	
$^1D_{12}$	$A_2,K_SK_S(1412)?,A_3$	$K_N(1421),L(1765)$
$^3D_{02}$	$\eta_N(1076),f,\rho^0\rho^0(1410)?,f',\omega(1648)$	
$^1F_{13}$	g	$K_N(1753),K_N(1850)$
$^5S_{22}$	$A_2\text{dip},K_SK_S(1439)$	

Notation	Baryon resonances	Notation	Hyperon resonances
$^2S_{11}$	$N(939),N(1508),N(1684),N(2148)$	$^2S_{01}$	$\Lambda(1116),\Lambda(1402),\Lambda(1673),\Lambda(1827)$
$^2S_{31}$	$\Delta(1618)$	$^2S_{11}$	$\Sigma(1193),\Sigma(1472),\Sigma(1620),\Sigma(1682),$ $\Sigma(1756),\Xi(1315),\Xi(1606),\Xi(1814),$ $\Xi(1956),\Xi(2295)$
		$^4S_{03}$	$\Lambda(1327)?,\Lambda(1518),\Omega(1672)?$
		$^4S_{13}$	$\Sigma(1385),\Xi(1532)$
$^2P_{11}$	$N(1300),N(1419),N(1530),N(1738)$	$^2P_{01}$	$\Lambda(1570),\Lambda(1737)$
$^2P_{31}$	$\Delta(1850)$	$^2P_{11}$	$\Sigma(1669),\Sigma(1926)$
$^2P_{13}$	$N(1770)$	$^2P_{03}$	$\Lambda(1870)$
$^2P_{33}$	$\Delta(1233),\Delta(1680),\Delta(2160)$	$^2P_{13}$	$\Sigma(2080)$
$^2D_{13}$	$N(1520),N(1730),N(2075)$	$^2D_{03}$	$\Lambda(1688),\Lambda(1990)$
$^2D_{33}$	$\Delta(1694)$	$^2D_{13}$	$\Sigma(1669),\Sigma(1900)$
$^2D_{15}$	$N(1672),N(2078)$	$^2D_{05}$	$\Lambda(1827)$
$^2D_{35}$	$\Delta(1824)$	$^2D_{15}$	$\Sigma(1765)$
$^2F_{15}$	$N(1687),N(2088)$	$^2F_{05}$	$\Lambda(1819),\Lambda(2110)$
$^2F_{35}$	$\Delta(1877)$	$^2F_{15}$	$\Sigma(1910),\Sigma(2070)$
$^2F_{17}$	$N(2024)$	$^2F_{07}$	$\Lambda(2020)$
$^2F_{37}$	$\Delta(1923)$	$^2F_{17}$	$\Sigma(2030)$
$^2G_{17}$	$N(2204)$	$^2G_{07}$	$\Lambda(2100)$
$^2G_{39}$	$\Delta(2160)$	$^2G_{17}$	$\Sigma(2090),\Sigma(2250)$
$^2H_{19}$	$N(2241)$	$^2H_{09}$	$\Lambda(2350)$
$^2H_{3,11}$	$\Delta(2390)$	$^2H_{19}$	$\Sigma(2455)?$

tematics,[60] but in πN phase-shift analyses the splitting has appeared only recently, in the latest AYED (Ref. 46) analysis (see Table XXXII).

B. Mapping the narrow-width and S-state resonances

The narrow-width and S-state resonances constitute the rotationless ($L=0$) baryon and hyperon levels. On the basis of the present systematics, we expect that all S states should have narrow widths ($\Gamma \leq 50$ MeV). However, probably for reasons stated in Sec. VII A, some of the S-states are reported with broad widths. Hence we require both the S-state classifications of phase-shift analyses and, in some cases, the narrow widths in order to identify all of the rotationless levels.

The rotationless baryon and hyperon resonances were catalogued graphically in Fig. 3. As indicated in the column at the far left in Fig. 3, these excitations are formed by adding combinations of the spinless cabers $\dot{3}$ and $\dot{4}$ to the basic metastable ground states $N=S\bar{S}S$, $\Lambda=S\bar{S}S\dot{3}$, $\Sigma=S\bar{S}S\dot{4}$, and $\Xi=S\bar{S}S\dot{3}\dot{3}$ of Eq. (14). Of the resonances shown in Fig. 3, the identified S states clearly correspond to rotationless excitations. In addition, the three *narrow-width* $J=\frac{3}{2}$ resonances $\Lambda(1518)D$,

TABLE XIV. The narrow-width and S-state N, Δ, Λ, and Σ resonances. States marked with an asterisk (*) have identifiable overlying rotational levels; these states constitute an essentially complete mapping of all of the observed baryon and hyperon rotational bands. States enclosed in brackets have not been observed directly. The channel numbers refer to the 70-MeV mass intervals that are shown graphically in Fig. 3.

Channel no.	Excitation	N, Δ	Λ	Σ
0	$\cdots$	$N(939)S\Gamma 0$	$\Lambda(1116)S\Gamma \simeq 0$	$\Sigma(1193)S\Gamma \simeq 0$
1				
2				
3	$\dot{3}$	$[\Delta(1149)]^{*\,a,b}$	$\Lambda(1327)\,\Gamma < 25$	$\Sigma(1385)P\,\Gamma 36$
4	$\dot{4}$	$[N(1219)]^{*\,b}$	$\Lambda(1402)S\Gamma 38$	$\Sigma(1472)\Gamma 30^*$
5				
6	$\dot{3}\dot{3}$	$[N(1359)]^{*\,b}$	$\Lambda(1518)D\,\Gamma 16^*$	$\Sigma(1620)S\,\Gamma 40^*$
7	$\dot{3}\dot{4}$			$\Sigma(1682)S\Gamma 25$
8	$\dot{4}\dot{4}$	$N(1508)S\Gamma 55^*$	$\Lambda(1673)S\Gamma 30^*$	$\Sigma(1756)S\Gamma 65^*$
9	$\dot{3}\dot{3}\dot{3}$	(ruled out by competition with the $\dot{3}\dot{3}\dot{3} \rightarrow \dot{S}\dot{S}$ transition) [c]		
10	$\dot{3}\dot{3}\dot{4}$	$\Delta(1618)S\Gamma 147^*$	$\Lambda(\sim 1827)S\Gamma \sim 68^*$	$\Sigma(\sim 1900)S^*$
11	$\dot{3}\dot{4}\dot{4}$	$N(1684)S\Gamma 116^*$		
12	$\dot{3}\dot{3}\dot{3}\dot{3}$	(ruled out by competition with the $\dot{3}\dot{3}\dot{3} \rightarrow \dot{S}\dot{S}$ transition) [c]		

[a] See Ref. 137.
[b] See Eq. (43).
[c] See Eq. (29) and the rules of Sec. VIIIA.

$\Sigma(1385)P$, and $\Xi(1535)P$ are also classified as rotationless levels [see the examples after Eq. (28)]. Similarly, the $\Lambda(1327)$, $\Sigma(1472)$, $\Sigma(1682)$, $\Xi(1606)$, $\Xi(1814)$, and $\Xi(1956)$ resonances have no spin identification, but their narrow widths single them out as rotationless excitations. The $\Delta(1149)$, $N(1219)$, and $N(1359)$ levels in Fig. 3, which are enclosed in brackets, have not been observed directly (but see Ref. 137), and their existence is deduced from the presence of overlying rotational levels [see Eq. (43)].

The rotationless N, Δ, Λ, and Σ resonances from Fig. 3 are shown in Table XIV. From the systematics of Table XIV, we can write down a set of rules for generating these rotationless baryon and hyperon excitations:

> Rotationless baryon and hyperon excitations are formed by attaching combinations of the nonstrange spinless cabers $\dot{3} \equiv 210$ MeV and $\dot{4} \equiv 280$ MeV to the "ground states" $N(939)$, $\Lambda(1116)$, $\Sigma(1193)$, and $\Xi(1321)$, with essentially zero binding energy [Eq. (12)]. (29a)
>
> The mixed excitation $\dot{3}\dot{4}$ is weak. (29b)
>
> The excitations $\dot{3}\dot{3}\dot{3}$ and $\dot{3}\dot{3}\dot{3}\dot{3}$ are weak because of competition with the transition $\dot{3}\dot{3}\dot{3} \rightarrow \dot{S}\dot{S}$ (Eq. 20). (29c)
>
> The presence in Tables III–VI of high-energy (>2000 MeV) S–D resonances shows that the systematics of Table XIV must extend up beyond the eleven 70-MeV excitation channels included in the table. (29d)

As can be seen in Table XIV, rule (29a) together with the qualifying remarks of (29b) and (29c) gives an accurate mapping of the observed spectrum of S-state baryon and hyperon resonances. As discussed in Sec. XI, Fig. 3 and Table XIV have led to some predictive successes; for example, in the identification of the $\Sigma(1620)$ peak as an S-state resonance, and also in the recent appearance of the narrow-width $\Xi(1606)$ resonance. From the experimental incompleteness discussed in Sec. VII A and from (29d), it is apparent that in Fig. 3 and Table XIV we have plotted only the low-ener-

TABLE XV. Λ rotational bands. The seventeen Λ resonances of Table V are shown grouped into rotational bands. Table XVII gives a quantitative evaluation of these rotational bands, and also a comparison to the Σ rotational bands. Section IX contains a summary of all of the hadron rotational bands.

Excitation	E_{calc}	S	P	D	F	G	H
Λ	(1116)	1116 S_{01}					
$\Lambda 3$	1326	1327					
$\Lambda 4$	1396	1402 S_{01}					
$\Lambda 33$	1536	1518 D_{03}	1570 P_{01}	1688 D_{03}	1819 F_{05}	2100 G_{07}	2350 H_{09}
$\Lambda 44$	1676	1673 S_{01}	~1737 P_{01}	1827 D_{05}	2020 F_{07}		
$\Lambda 334$	1816	~1827 S_{01}	1870 P_{03}	1990 D_{03}	2110 F_{05}		

gy portion of the baryon and hyperon S-state spectrum. The levels in Table XIV that are labeled with asterisks are the levels for which overlying rotational bands have been identified. These rotational bands are discussed in Sec. VII C.

C. Mapping the Λ and Σ rotational bands

The mapping of the baryon and hyperon rotational bands follows from a straightforward application of the rules summarized in Table XII. In particular, the phenomenology proceeds according to the following steps:

Rotational bandheads are selected from the levels listed in Table XIV. (30a)

The rotational levels follow an $L(L+1)$ energy interval rule [Eq. (22)]. (30b)

Rotational energies correspond to $E_{\rm rot} \equiv \hbar^2/2I$ ~30 MeV [Eq. (23)]. (30c)

The number of levels in each rotational band is limited by the requirements of special relativity [Eq. (26)]. (30d)

The L_+ and L_- ordering of the levels follows the systematics of Table X. (30e)

TABLE XVI. Σ rotational bands. Nineteen of the twenty-one Σ resonances of Table VI are shown grouped into rotational bands [the $\Sigma(2080)P_{13}$ resonance of Table VI is at too high an energy to classify accurately, and the C-rated $\Sigma(2070)F_{15}$ resonance appears at almost the same energy as the A-rated $\Sigma(2030)F_{17}$ resonance]. Table XVII gives a quantitative evaluation of these rotational bands, and also a comparison to the Λ rotational bands.

Excitation	$E_{\rm calc}$	S	P	D	F	G	H
Σ	(1193)	1193 S_{11}					
Σ3	1403	1385 P_{13}					
Σ4	1473	1472	~1550 P_{11}	1669 D_{13}			
Σ33	1613	1620 S_{11}	1669 P_{11}	1765 D_{15}	1910 F_{15}	2090 G_{17}	
Σ34	1683	1682 S_{11}					
Σ44	1753	1756 S_{11}	~1840 P_{13}	~1900 D_{13}	2030 F_{17}	2250 G_{17}	2455 H?
Σ334	1893	~1900 S_{11}	1926 P_{11}				

TABLE XVII. Quantitative values for the Λ and Σ rotational bands. The confidence-level ratings A–D, the widths Γ, and the values for $E_{\rm rot} \equiv \hbar^2/2I$ in MeV [Eq. (23)] are shown. An average width Γ is given at the bottom of each partial-wave column (S, P, D, F, G, H); as can be seen from these average widths, S states have much narrower widths than rotational P–H states. The values for $E_{\rm rot}$ are shown graphically in Fig. 10, where they are compared to values for $E_{\rm rot}$ obtained from all of the other hadron rotational bands. Rotational bands are shown in Fig. 5.

Excitation	S	P	D	F	G	H	S	P	D	F	G	H
	Λ resonances						Σ resonances					
3	1327						1385					
Rating	D						A					
Width	Γ<25						Γ36					
4	1402						1472	~1550	1669			
Rating	A						C	D	A			
Width	Γ38						Γ30	Γ50	Γ50			
$E_{\rm rot}$								~39	33			
33	1518	1570	1688	1819	2100	2350	1620	1669	1765	1910	2090	
Rating	A	C	A	A	A	A	B	B	A	A	B	
Width	Γ16	Γ50	Γ53	Γ80	Γ121	Γ177	Γ40	Γ140	Γ108	Γ70	Γ103	
$E_{\rm rot}$		26	28	25	29	28		25	24	24	24	
44	1673	~1737	1827	2020			1756	~1840	~1900	2030	2250	2455
Rating	A	B	A	B			A	C	A	A	A	A
Width	Γ30	Γ~115	Γ89	Γ160			Γ65	Γ120	Γ~200	Γ151	Γ165	Γ120
$E_{\rm rot}$		~32	26	29				~42	~24	23	25	23
334	~1827	1870	1990	2110			~1900	1926				
Rating	B	B	B	C			C	B				
Width	Γ~68	Γ81	Γ155	Γ185				Γ185				
$E_{\rm rot}$		22	27	24								
$\Gamma_{\rm ave}$	Γ35	Γ82	Γ99	Γ142	Γ121	Γ177	Γ43	Γ124	Γ119	Γ111	Γ134	Γ120

When the procedure outlined in (30a)–(30e) is applied to the Λ resonances of Table V, three well-defined rotational bands appear. These Λ rotational bands are shown in Table XV. The Σ resonances of Table VI similarly fall into clear-cut rotational bands. The Σ rotational bands are shown in Table XVI.

The quantitative aspects of the Λ and Σ rotational bands are summarized in Table XVII. These include the measured widths of the resonances, the confidence-level ratings of the resonances, and the experimental values of the rotational energy parameter $E_{\rm rot}$ [Eq. (23)] that are obtained by fitting the experimental levels to Eq. (22). The average widths Γ for resonances of each L value are shown at the bottom of Table XVII for both the Λ and Σ resonances. From these average widths, we see that the rotationless S states have widths $\Gamma < 50$ MeV, whereas the rotational P–H states have widths $\Gamma \sim 100$ MeV, in agreement with our phenomenological expectations [Eq. (17)]. In Table XVII, most of the A-rated rotational levels correspond to the bandheads $\Lambda\dot{3}\dot{3}$, $\Lambda\dot{4}\dot{4}$, $\Sigma\dot{3}\dot{3}$, and $\Sigma\dot{4}\dot{4}$. The values for $E_{\rm rot}$ shown in Table XVII are in general agreement with the estimate $E_{\rm rot} \sim 30$ MeV [Eq. (30c)]. Figure 10 shows a comparison of the experimental values of $E_{\rm rot}$ from Table XVII, with the values of $E_{\rm rot}$ obtained from the N and Δ rotational bands and from meson and kaon rotational bands. All of these different resonances obey the same rotational systematics, in which the values for $E_{\rm rot}$ (or for the moment of inertia I) vary in a smooth and continuous manner as a function of the mass of the bandhead. In Sec. IX these results are extended to encompass nonadiabatic rotational levels in very light nuclei.

Since the Λ and Σ partial-wave amplitudes, as determined in various phase-shift analyses, still contain ambiguities, each worker who attempts to fit these amplitudes to theory is faced with a number of rather arbitrary decisions. In order to ascertain how these decisions were reached in the present case, it is useful to discuss the available experimental information as it applies directly to each individual partial-wave amplitude. This discussion is given in Appendix D.

D. Mapping the N and Δ rotational bands

The observed N and Δ resonances do not appear to be as complete as the Λ and Σ resonances discussed above. However, if we use the Λ and Σ rotational bands of Tables XV–XVII as a guide, it seems clear that the N and Δ resonances occur with the same basic rotational systematics. Table XVIII lists the N rotational bands, and Table XIX lists the Δ rotational bands. Table XX gives the measured widths, confidence-level ratings, and experimental values of $E_{\rm rot}$ for these N and Δ rotational bands.

A comparison of Tables XVII and XX reveals many similarities. This is shown in more detail in Sec. IX. The average widths for the N and Δ S-state resonances are narrower than the widths for the P–H resonances, as is shown at the bottom of Table XX, although the difference in widths between rotationless and rotational levels is not as pronounced in Table XX as it was in Table XVII. In general, all of the resonance widths of Table XX are broader than the corresponding resonance widths of Table XVII. Phenomenologically, resonance formation in the Λ and Σ resonances, which is accompanied by a 4% hadronic binding energy [see Eq. (12)], seems to be more distinctive than resonance formation in the N and Δ resonances, which is accomplished via ~0% hadronic binding. Table XI illustrated one ambiguity, the P-wave criss-cross, that occurs in the N and Δ amplitudes. The addition of R and A data[145] to the πN and KN data sets should considerably improve all of these analyses. The individual N and Δ partial-wave amplitudes are discussed in Appendix D.

E. Discussion of the over-all mapping efficiency

It is difficult to judge the completeness of the N, Δ, Λ, and Σ data compilation shown in Tables III–VI. There are probably some low-energy resonances ($E < 1500$ MeV) that have not yet been identified, and there appear to be many high-energy resonances ($E > 2000$ MeV) that are still awaiting discovery. However, if we confine our remarks to the region of intermediate energies spanned by Tables III–VI, we can make some general remarks as to the efficiency of the present mapping procedure.

Examination of Fig. 3 and Table XIV shows that the narrow-width and S-state resonances form a reasonably complete pattern, although some of the N and Δ S states are missing. Tables III–VI include a total of 69 experimentally identified N, Δ, Λ, and Σ resonances. Of these, 60 are mapped in the rotational bands of Tables XV–XX and the S-state levels of Table XIV, 8 are too high in energy to map accurately, and one [$\Sigma(2070)F_{15}$] does not fit the rotational assignments. The A-rated resonances, in general, fit accurately into the $L(L+1)$ splitting of the rotational bands. As another way of looking at the mapping efficiency, Tables XIV and XV–XX show that 60 resonances are mapped, and that (at least) 7 levels are missing, as evidenced by holes in the identified rotational bands. A further discussion of the mapping problem is given in Sec. XI.

TABLE XVIII. N rotational bands. Fifteen of the twenty N resonances of Table III are shown grouped into rotational bands [the $N(2075)$ D_{13}, $N(2078)$ D_{15}, $N(\sim 2088)$ F_{15}, and $N(2148)$ S_{11} resonances are at too high an energy to classify accurately, and the $N(\sim 1770)$ P_{13} resonance is part of a P_{11}-P_{13} "criss-cross" ambiguity shown in Table XI]. Table XX gives a quantitative evaluation of these rotational bands, and also a comparison to the Δ rotational bands. Levels enclosed in brackets are unobserved S states.

Excitation	E_{calc}	S	P	D	F	G	H
N	(939)	939 S_{11}					
$N4$	1219	[1219]	~1300 P_{11}				
$N33$	1359	[1359]	1419 P_{11}	1520 D_{13}	1687 F_{15}	···	2241 H_{19}
$N44$	1499	1508 S_{11}	1530 P_{11}	1672 D_{15}	···	2130 G_{19}	
$N344$	1709	1684 S_{11}	1738 P_{11}	1730? D_{13}	2024 F_{17}	2204 G_{17}	

When we examine the rotational bands of Tables XV–XX, it is not immediately clear why some bands extend to H waves and others only to D waves or F waves. In particular, the broad widths of the higher levels in the N and Δ resonances indicate that they are probably averages over more than one level. Thus numerical estimates of the mapping efficiency are not very meaningful. However, the important point to notice is that there is a reasonable correspondence between the number of observed resonances (Tables III–VI) and the number of available rotational levels (Tables XV–XX). We are not faced with order-of-magnitude discrepancies between theory and experiment, as is the case for example with SU(6). Furthermore, the present rotational baryon systematics has already exhibited some predictive power in dealing with phase-shift ambiguities (see Table XXXII); as the phase-shift analyses have been extended and refined, the results have tended to agree more closely with the present rotational systematics. A comparison of calculated rotational mass values with experiment is given in Table XXXIV.

TABLE XIX. Δ rotational bands. Nine of the eleven Δ resonances of Table IV are shown grouped into rotational bands [the $\Delta(\sim 1850)$ P_{31} resonance is part of a P_{31}-P_{33} "criss-cross" ambiguity shown in Table XI, and the $\Delta(2160)$ P_{33} resonance is too high in energy to be included here]. Table XX gives a quantitative evaluation of these rotational bands, and also a comparison to the N rotational bands. Levels enclosed in brackets are unobserved S states.

Excitation	E_{calc}	S	P	D	F	G	H
Δ	(939)						
$\Delta 3$	1149	[1149]	1233 P_{33}				
$\Delta 44$	1499	[1508]	···	1694 D_{33}	1877 F_{35}		
$\Delta 334$	1639	1618 S_{31}	1680 P_{33}	1824 D_{35}	1923 F_{37}	2160 G_{39}	2390 $H_{3,11}$

Figure 5 gives a graphical display of the hyperon and baryon rotational levels, which are shown in the form of an energy-level diagram, and it illustrates both the observed $L(L+1)$ energy intervals of the rotational bands and the completeness of the mapping of the rotational bands. From Fig. 5, it is clear that strange (Λ, Σ) and nonstrange (N, Δ) rotational bands both follow the same rotational systematics. Thus strangeness is an internal particle-antiparticle symmetry property which does not directly affect the over-all geometric configuration of a resonance.

It should be stressed here that the theory of hadron rotational bands set forth in this paper was not invented just to fit the resonances of Tables I–VII. The rules for these rotational bands [Table XII and Eq. (30)] follow, insofar as the author has been able to determine, the results we should logically expect by extending the known systematics of rotational bands in nuclear physics. The order-of-magnitude estimates given in this section show that the relationships between masses, moments of inertia, angular momenta, and rotational energies are reasonable and self-consistent. The features that appear uniquely in the hadron rotational bands, such as the $E(L)$ energy dependence for spin-$\frac{1}{2}$ bandheads and the special relativistic cutoff L_{max}, are natural consequences of limiting conditions that do not occur in nuclear rotations, except possibly in very light nuclei.

TABLE XX. Quantitative values for the N and Δ rotational bands. The confidence-level ratings (A, B, C), the widths Γ, and the values for $E_{\text{rot}} \equiv \hbar^2/2I$ in MeV [Eq. (23)] are shown. An average width Γ is given at the bottom of each partial-wave column (S, P, D, F, G, H); as can be seen from these average widths, S states have narrower widths than rotational P–H states. The values for E_{rot} are shown graphically in Fig. 10, where they are compared to values for E_{rot} obtained from all of the other hadron rotational bands. Rotational bands are shown in Fig. 5.

	N resonances						Δ resonances					
Excitation	S	P	D	F	G	H	S	P	D	F	G	H
4,3	[1219]	~1300					[1149]	1233				
Rating		C						A				
Width								Γ115				
E_{rot}		~41						42				
33	[1359]	1419	1520	1687	···	2241						
Rating		A	A	A		A						
Width		Γ148	Γ121	Γ128		Γ289						
E_{rot}		30	27	27		29						
44	1508	1530	1672	···	2130		[1508]	···	1694	1877		
Rating	A	C	A		C				A	A		
Width	Γ55	Γ65	Γ143		Γ250				Γ216	Γ255		
E_{rot}		···	27		31				31	31		
334							1618	1680	1824	1923	2160	2390
Rating							A	C	C	A	C	A
Width							Γ147	Γ220	Γ138	Γ215		Γ292
E_{rot}								31	34	25	27	26
344	1684	1738	1730?	2024	2204							
Rating	A	A	B	B	A							
Width	Γ116	Γ172	Γ130	Γ191	Γ247							
E_{rot}		27	···	28	26							
Γ_{ave}	Γ86	Γ128	Γ131	Γ160	Γ249	Γ289	Γ147	Γ168	Γ177	Γ235		Γ292

As a final comment in this section, we note that there appears to be nothing in the present results to indicate that the squares of resonance masses have any particular phenomenological significance.

VIII. MAPPING THE MESON AND KAON RESONANCES

A. A theory for meson excitations

The baryon and hyperon resonances studied above have a simple excitation structure: Combinations of the spinless excitation quanta 3 and 4 cluster with an existing SSS spinor core and appear either as narrow-width S-state excitations or else as broad-width rotational levels. Meson resonances, on the other hand, are formed as independent structures, and they have a more involved excitation pattern in that both spinless and spinning quanta can be simultaneously produced. Since meson resonances represent the direct conversion of kinetic energy into hadronic matter without the constraints imposed by the existing SSS spinor core, they provide the best examples for studying the basic symmetries of the hadron production process.

In the baryon and hyperon resonances, we have already seen that one basic excitation (bandhead) can appear in a number of different modes. If it is the bandheads which carry the excitation symmetries, then this suggests that we must look at a deeper level than the observed resonances in order to ascertain the symmetries. Or, we must at least sort out all of the rotationless S-state levels from among the totality of observed resonances. In the meson resonances this procedure is even more important. One basic meson excitation can give rise to as many as thirteen observed meson and kaon resonances, as is shown in Table XXI. Since it is the basic excitation structures which appear to exhibit the fundamental symmetries, we cannot use the observed meson resonances *per se* to obtain meaningful symmetry relationships. It is first necessary to combine the observed meson resonances into excitation-related groupings. At that point, the underlying excitation patterns which lead to these groupings can then be ascertained. To express the situation metaphorically, the observed meson resonances are just the tips of the proverbial icebergs, with each iceberg having several exposed tips; in order to obtain the proper symmetry relationships, we must study the spectrum of icebergs and not the spectrum of tips of ice-

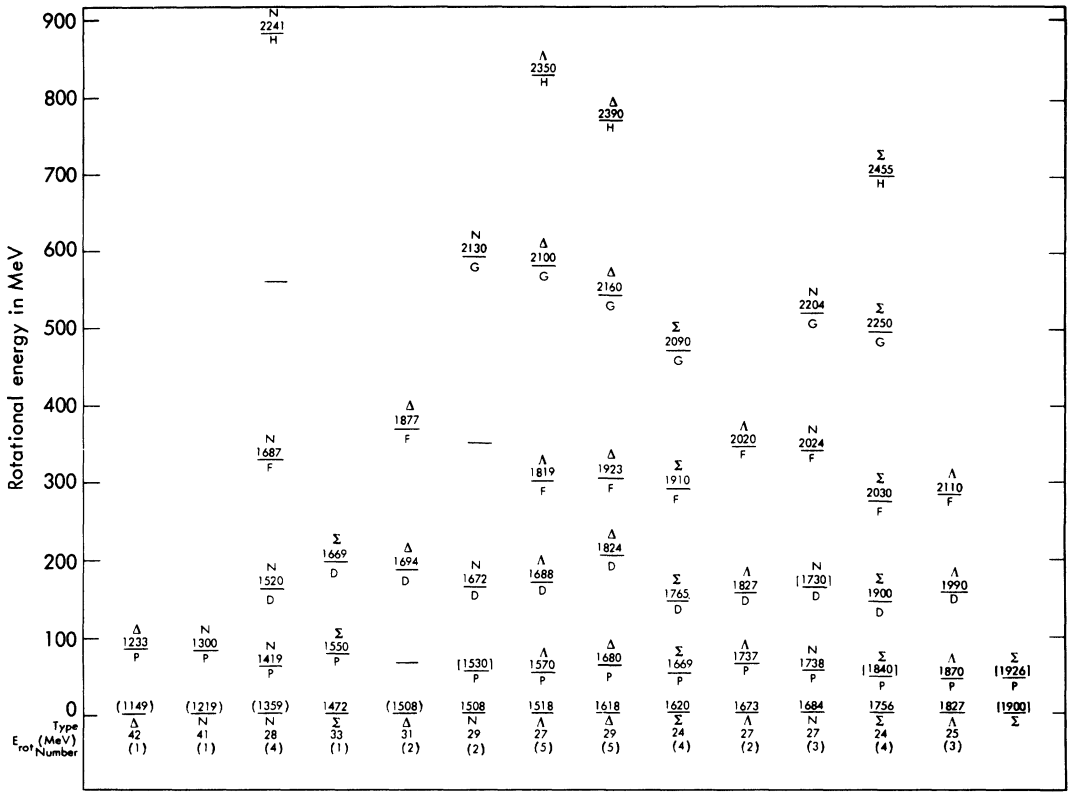

FIG. 5. An energy-level diagram for the N, Δ, Λ, and Σ rotational bands of Tables XV–XX. The levels labeled P, D, F, G, H have the identified L values 1, 2, 3, 4, 5, respectively. Values for $E_{\rm rot} = \hbar^2/2I$ in MeV are listed at the bottom of each rotational band, together with the number of rotational levels used to determine $E_{\rm rot}$ experimentally. The $L(L+1)$ splitting of the rotational bands is apparent in the diagram. S states enclosed in parentheses are unobserved levels, and rotational levels enclosed in brackets have been shifted graphically to match the $E_{\rm rot}$ values for their rotational bands.

bergs.

In Figs. 1 and 2 we saw that 137-MeV mass intervals play an important role in meson excitations. This suggests that the symmetric mass quantum

$$\pi = M\bar{M} \tag{8}$$

is an important excitation unit for meson resonances (this quantum was not of importance for the baryon and hyperon excitations discussed above, although it may be implicitly contained in some of the excitation structures of Fig. 3). Similarly, from the existence of narrow-width spin-1 meson resonances, which contain SS spinor pairs produced in the transition $333 \to SS$ (Sec. VI), we know that the asymmetric mass quantum

$$3 = MMM \text{ or } M\bar{M}M \text{ or } \bar{M}M\bar{M} \text{ or } \bar{M}\bar{M}\bar{M} \tag{31}$$

is another important excitation unit for meson resonances. At the deepest interaction level, where kinetic energy is converted directly into hadronic matter, it seems phenomenologically useful to consider excitations as consisting entirely of symmetric quanta π and asymmetric quanta 3, which are created in six basic excitation units:

$$\begin{aligned} &E_1 = \pi, \quad E_{1'} = 3\pi, \\ &E_2 = 33, \quad E_{2'} = 33\pi, \\ &E_3 = 333, \quad E_{3'} = 333\pi. \end{aligned} \tag{32}$$

The 3's are the "gluons" which hold the excitations together, and it is the 3's which determine the excitation symmetries. The basic excitation symmetry is obtained by separating the excitation units E_1, $E_{1'}$, E_2, $E_{2'}$, E_3, and $E_{3'}$ into three groups:

$S \equiv$ singlet group—combinations of E_1 and $E_{1'}$, excitations containing zero or one 3;

$D \equiv$ doublet group—combinations of E_2 and $E_{2'}$, excitations containing 3's produced in pairs;

$T \equiv$ triplet group—combinations of E_3 and $E_{3'}$, excitations containing 3's produced in triplets. (33)

TABLE XXI. Examples showing that one basic boson excitation structure can give rise to several (as many as thirteen) different resonances. This suggests that we must look at a deeper level than the observed resonances in order to ascertain the fundamental boson symmetries.

Excitation [a]	Geometric form [b]	Observed resonances [b]	Spectroscopic states [c]
333	SS	$\pi\pi(660)$, $\rho(770)$, $\epsilon(800)$ (three observed resonances)	${}^3S_{01}, {}^1P_{11}, {}^3P_{00}$
333π	$SS\pi$	$\omega(784), K^*(892), \eta_N(1076)$ (three observed resonances)	${}^3S_{01}, {}^1P^1_{11}, {}^3D_{02}$
3333π	77	$M(953)$, $\eta'(958)$, $\delta^0(963)$, $\delta^-(962)$	S_0, S_0, S_0, S_1
	$3SS\pi$	$\phi(1019)$, $\epsilon'(1096)$, $f(1270)$	${}^3S_{01}, {}^3P_{00}, {}^3D_{02}$
	$3SS\pi$	$\pi_N(1016), A_1(1115), A_2(1310)$ (ten observed resonances)	${}^1S_{10}, {}^1P_{11}, {}^1D_{12}$
$33\pi \cdot 33\pi$	$3SS4$	$X^0(1148)$, $\epsilon''(1250)$, $\rho\rho(1410)$	${}^3S_{01}, {}^3P_{00}, {}^3D_{02}$
	$3SS4$	$X^-(1153), B(1237), K_SK_S(1412), g(1680)$	${}^1S_{10}, {}^1P_{11}, {}^1D_{12}, {}^1F_{13}$
	SSK	$K_N(1160)$, $C(1242), K_N(1421), K_N(1660)$	${}^1S^1_{10}, {}^1P^1_{11}, {}^1D^1_{12}, {}^1F^1_{13}$
	SSK	$K_A(1175), K_A(1265)$ (thirteen observed resonances)	${}^1S^1_{30}, {}^1P^1_{31}$

[a] See Table XXII.

[b] See Tables XXIII, XXIV, and XXVII.

[c] The spectroscopic notation of rule (7) in Table XII is used, and a right superscript has been added for strange resonances to indicate the absolute value of the strangeness quantum number.

With the notation that $E_{11'} = E_1 E_{1'}$, etc., the actual combinations which are required in these groups in order to reproduce the observed spectrum of meson resonances are the following.

$$\begin{aligned} &S\colon\ E_1, E_{1'};\\ &D\colon\ E_2, E_{2'}, E_{22}, E_{22'}, E_{2'2'};\\ &T\colon\ E_3, E_{3'}, E_{33}, E_{33'}, E_{3'3'}, E_{333}, E_{333'}, \ldots \end{aligned} \tag{34}$$

The singlet group S has only the two first-rank members E_1 and $E_{1'}$. The doublet group D includes the first-rank members E_2 and $E_{2'}$ and the second-rank members E_{22}, $E_{22'}$, and $E_{2'2'}$. Since the excitation $333 \cdot 333$ seems dominant over the excitation $33 \cdot 33 \cdot 33$, the doublet group D terminates at the second rank. The triplet group T has identified members up to at least the third rank.

To complete the specification of the excitation groupings, we need one additional result. The quanta 3 and π are spinless. However, whenever an excitation contains three or more 3's, the transition $333 \rightarrow SS$ can occur [Eq. (19)]. The rule governing this transition is the following.

In an excitation cluster containing three or more 3's, the transition $333 \rightarrow SS$ always occurs, with two exceptions: (a) If the excitation quanta appear in the form of a linear array, the transition does not occur. Examples are

$$E_{22'} = 33 \cdot 33\pi \rightarrow 77 = \eta' \text{ spinless}$$

$$\rightarrow 3SS\pi = \phi \text{ spin } 1.$$

(b) If the excitation contains six or more 3's, the first transition usually blocks the second transition. Examples are

$$E_{33} = 333 \cdot 333 \rightarrow 33SS3 = D \text{ spin } 1 \text{ (dominant)}$$

$$\rightarrow SSSS = A_2 \text{ dip spin } 2 \text{ (weak)}.$$

To denote the number of $333 \rightarrow SS$ transitions that have occurred, excitations are assigned left superscripts:

$$\begin{aligned} &E_{22'} = 77, \quad {}^1E_{33} = 33SS3,\\ &{}^1E_{22'} = 3SS\pi, \quad {}^2E_{33} = SSSS,\\ &{}^1E_3 = SS, \quad {}^3E_{333} = SSSSSS. \end{aligned} \tag{35}$$

Table XXII summarizes the systematics of the meson excitation symmetries.

B. Mapping the narrow-width meson resonances

The mapping of the rotationless meson resonances is accomplished by first writing down the basic excitation states from Table XXII, and then matching them to the observed narrow-width and very-narrow-width meson resonances of Table I (see Figs. 6 and 1). The results of this mapping are shown in Table XXIII. As can be seen, there is a reasonable approximation to a 1:1 correspondence between the theoretical excitation states and the observed meson resonances. The very-narrow-width meson resonances of Table I are formed entirely from spinless excitation quanta (these resonances are described in detail in paper II), and

TABLE XXII. The basic meson-excitation symmetry groups. These symmetry groups give an essentially 1:1 mapping of the 22^+ very-narrow-width and narrow-width meson resonances of Table I, as is shown in Table XXIII.

(1). Fundamental excitation quanta:

$\pi = M\bar{M}$ (symmetric),
$3 = MMM$ or $M\bar{M}M$ or $\bar{M}M\bar{M}$ or $\bar{M}\bar{M}\bar{M}$ (antisymmetric),

where M is the 70-MeV hadronic mass quantum of Secs. IV and V.

(2). Fundamental excitation units:

$E_1 = \pi$, $E_{1'} = 3\pi$,
$E_2 = 33$, $E_{2'} = 33\pi$,
$E_3 = 333$, $E_{3'} = 333\pi$.

(3). Origin of the excitation symmetries:

(a) The 3's are the "gluons" which hold resonances together, and it is the 3's which determine the symmetry characteristics of the groups.

(b1) $S \equiv$ singlet group—the 3's occur singly in the excitation units E_1 and $E_{1'}$.

(b2) $D \equiv$ doublet group—the 3's occur pairwise in the excitation units E_2 and $E_{2'}$.

(b3) $T \equiv$ triplet group—the 3's occur in triplets in the excitation units E_3 and $E_{3'}$.

(c) The dominant excitations occur with no mixing of the S, D, and T excitation units.

(d1) The meson S group has only single excitation units.

(d2) The meson D group has linear (first-rank) and quadratic (second-rank) pairings of the excitation units. Since the excitation $333 \cdot 333$ is dominant over $33 \cdot 33 \cdot 33$, the D group terminates at the second rank.

(d3) The meson T group has observed resonances up to at least the third rank.

(4). Notation:

(a) A multiple subscript denotes the product of several excitations: $E_2 = 33$, $E_{2'} = 33\pi$, $E_{22} = 33 \cdot 33$, $E_{22'} = 33 \cdot 33\pi$, $E_{333} = 333 \cdot 333 \cdot 333$, etc.

(b) A left superscript denotes the number of $333 \rightarrow SS$ transitions which have occurred: $E_{33} = 333 \cdot 333$, ${}^1E_{33} = 33SS3$, ${}^2E_{33} = SSSS$, etc. Whenever three or more 3's are present in an excitation, at least one $333 \rightarrow SS$ transition usually occurs [see Eqs. (27) and (28)].

(5) Basic excitation groups:

Group	Member	Primary excitation	Final excitation	Geometry [a]
S_1	E_1	π	π	11
S_2	$E_{1'}$	3π	3π	3π
D_1	E_2	33	33	33
D_2	$E_{2'}$	33π	33π	44
D_3	${}^1E_{22}$	$33 \cdot 33$	$3SS$	$3SS$
D_4	$E_{22'}$	$33 \cdot 33\pi$	3333π	77
D_5	${}^1E_{22'}$	$33 \cdot 33\pi$	$3SS\pi$	$3SS\pi$
D_6	${}^1E_{2'2'}$	$33\pi \cdot 33\pi$	$3SS\pi\pi$	3SS4
T_1	${}^1E_3$	333	SS	SS
T_2	${}^1E_{3'}$	333π	$SS\pi$	$SS\pi$
T_3	${}^1E_{33}$	$333 \cdot 333$	$33SS3$	$33SS3$
T_4	${}^2E_{33}$	$333 \cdot 333$	$SSSS$	$SSSS$
T_5	${}^1E_{33'}$	$333 \cdot 333\pi$	$33SS3\pi$	$44SS3$
T_6	${}^2E_{33'}$	$333 \cdot 333\pi$	$SSSS\pi$	$SSSS\pi$
T_7	${}^1E_{3'3'}$	$333\pi \cdot 333\pi$	$33SS3\pi\pi$	$33SS34$
T_8	${}^3E_{333}$	$333 \cdot 333 \cdot 333$	$SSSSSS$	$SSSSSS$
T_9	${}^3E_{333'}$	$333 \cdot 333 \cdot 333\pi$	$SSSSSS\pi$	$SSSSSS\pi$
⋮				

[a] The basic states 1, 3, 4, 7, S, and π are illustrated in paper II.[24]

the narrow-width meson resonances of Table I are formed from spinor pairs SS combined with spinless excitation quanta. As Table XXIII shows, the calculated masses of the excitation states accurately match the masses of the observed meson resonances. Also, as is discussed in more detail in paper II, spins and isotopic spins are correctly accounted for [Eq. (21)], and some parity rules can be deduced (paper II).

The "Yes" labels in the right-hand column of Table XXIII indicate the resonances which serve as bandheads for overlying rotational levels. The spinless mesons do not have observed rotational bands, nor do the very weak mixed excitations listed at the bottom of Table XXIII.

The D-rated resonances $K_SK_S(1311)$ and $K_SK_S(1439)$ that are shown in Table XXIII are speculative entries, both because of their low statistical significance or apparent lack of reproducibility, and because spin information is lacking. Since all the low-rated resonances of Table I fit naturally into Table XXIII, it will be interesting to see if future experiments confirm or deny the existence of these resonances. However, whether or not these low-rated resonances really exist, the main points to keep in mind with respect to Table XXIII are the following: (1) All of the well-established narrow-width and very-narrow-width meson resonances are accurately accounted for; (2) the mapping between theory and experiment is reasonably complete.

The rules for meson rotational levels, which are somewhat more complex than the rules for baryon rotational levels, are summarized in Table XII. These rules are discussed in detail in Appendix C. In Sec. VIIIC, we use the rotational systematics of Table XII and the excitation systematics of Table XXIII to carry out the mapping of the meson rotational bands.

C. Mapping the meson rotational bands

Table XXIII gave a mapping of the narrow-width meson resonances, and it also indicated which of these resonances serve as bandheads for rotational bands by the "Yes" labels in the right-hand column. Using the meson rotational rules of Table XII, we give in Table XXIV the mapping of the broad-width meson resonances. A comparison between the experimental meson data of Table I and the resonances mapped in Tables XXIII and XXIV (see rules of Table XII; also Ref. 148) shows that all of the resonances of Table I are accounted for (the η' multiplet is treated in detail in paper II).

In order to assess the physical content of Table XXIV, we show in Table XXV the measured widths for the resonances of Table XXIV, and also the ex-

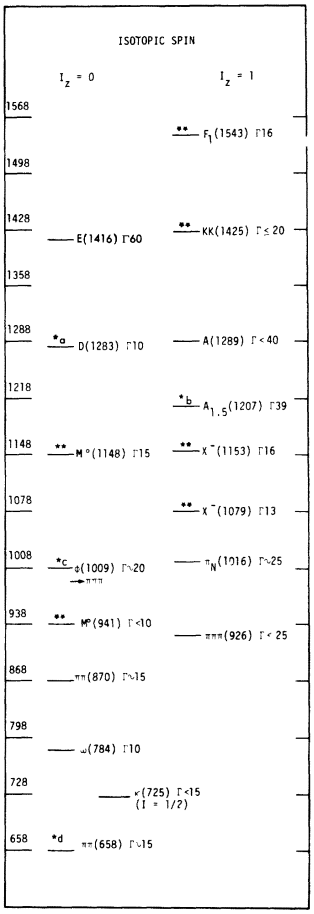

FIG. 6. An energy-level diagram for the narrow-width (spin-1) meson resonances of Table I. These resonances appear at 70-MeV intervals above the basic $\dot{S}\dot{S}$ "ground state" $\pi\pi(658)$ (see Fig. 8 in Ref. 14). This diagram illustrates the predictive power of the present systematics. Levels marked with a double asterisk have appeared since the first publication of this "meson excitation tower" (Ref. 5, Table I). Levels marked with a single asterisk correspond to new experimental results that are along the lines suggested by the excitation tower, as follows: *a is the measurement of Boesebeck 71 in RPP73 (Ref. 25), which gives the narrow width expected for this S-state resonance; *b is a new $A_{1,5}$ measurement by Morse 72 of this very weak level; *c is the first determination of the ϕ parameters from the $\pi\pi\pi$ decay mode (see Refs. 28 and 29), and it suggests relating the $\phi \rightarrow \pi\pi\pi$ decay mode to the H meson of RPP73; *d refers to the 660-MeV anomaly shown in Fig. 18 [it should be noted here that the existence of this fundamental 658-MeV $\dot{S}\dot{S}$ ground state was predicted in Ref. 2(d) prior to the experiment reported in Ref. 39]. The $\kappa(725)$ is a D-rated $I = \frac{1}{2}$ level that fits naturally into the meson excitation tower. Of the 17 levels shown in this figure, six have appeared subsequent to the original publication of this diagram, and four others have appeared with significant additions to the experimental data.

TABLE XXIII. Mapping the narrow-width meson resonances. The excitation groups of Table XXII accurately map the very-narrow-width and narrow-width meson resonances of Table I. The excitations indicated as "Yes" in the right-hand column serve as the bandheads for the meson rotational levels of Table XXIV. The very weak mixed excitations shown at the bottom of the table do not have observed rotational bands.

Group element	Geometry of res. [a]	Approx. mass [b]	Spinless mesons	Single spinor pair $I=0$	Single spinor pair $I=1$	2 spinor pairs	3 spinor pairs	Bandhead
S_1	11	140 [c]	$\pi(140)$					No
S_2	3π	350	...					Yes
D_1	33	420	...					Yes
D_2	44	548 [c]	$\eta(549)$					No
D_4	77	958 [c]	$\eta'(958)$					No
D_3	3SS	870		$\pi\pi(870)$				Yes
D_5	$3SS\pi$	1010		$\phi(1009)$	$\pi_N(1016)$			Yes
D_6	3SS4	1150		$M^0(1148)$	$X^-(1153)$			Yes
T_1	SS	660		$\pi\pi(660)$				Yes
T_2	$SS\pi$	800		$\omega(784)$				Yes
T_3	33SS3	1290		$D(1286)$	$A(1289)$			Yes
T_5	44SS3	1430		$E(1416)$	$KK(1425)$			Yes
T_7	33SS34	1570			$F_1(1543)$			(Yes)
T_4	SSSS	1320				$K_SK_S(1311)$		
T_6	$SSSS\pi$	1460				$K_SK_S(1439)$		
T_8	SSSSSS	1795 [c]					$\bar{p}n(1795)$	
T_9	$SSSSSS\pi$	d					$\bar{p}p(1925)$	
	Resonances formed as mixed combinations of the excitations S_1, S_2, D_1, D_2, T_1, and T_2.							
S_1T_2	SS4	940			$M(941)$			No
D_1T_1	3SS3	1080			$X^-(1079)$			No
D_1T_2	4SS4	1220			$A_{1.5}(1207)$			No
	The combinations S_1D_2 and D_2T_2 are not observed; all other combinations are redundant.							

[a] See Table XXII.
[b] These values are from $SS=660$, $\pi=140$, $3=210$, $4=280$, B.E.$=0$.
[c] See paper II.
[d] See Fig. 8 and Ref. 42.

perimental values for the rotational energy parameter $E_{\rm rot}$ [Eq. (23)] obtained by fitting to Eq. (22). As can be seen in Table XXV, the width distinction between rotationless and rotational levels in the meson resonances is very clear-cut: The S states have widths $\Gamma \simeq 20$ MeV, and the rotational levels have widths $\Gamma \sim 100$ MeV. This is the same trend that was noted for hyperon resonances in Table XVII and for baryon resonances in Table XX. The experimental values for $E_{\rm rot}$ shown in Table XXV are of the same order of magnitude as the values for $E_{\rm rot}$ shown in Tables XVII and XX. In Fig. 10 a graphical comparison is made between the $E_{\rm rot}$ values for the meson resonances and the $E_{\rm rot}$ values for the baryon resonances.

Table XXVI summarizes the spin values that have been determined experimentally for the meson resonances of Table XXIV, and it also shows the principal decay modes. Although not all meson spins have been determined, the ones that have been determined fit the present rotational assignments. In Table XXIX we show how spin values measured for the kaon resonances can be used to augment the spin values given in Table XXVI.

The G-parity rule for meson rotational bands [rule (12) of Table XII] is illustrated by the decay modes shown in Table XXVI. As can be seen in Table XXVI, the negative-spatial-parity bandheads have G parities that are opposite in sign to those of the overlying rotational levels.

D. Mapping the kaon resonances

If we did not have the systematics of the meson resonances as a guide, it would be very difficult to sort out the kaon resonances. By comparison with the meson resonances, the kaon resonances appear fragmentary, and a complete excitation mapping of the kaon resonances along the lines shown for the meson resonances in Table XXII is not possible. However, the kaon resonances which have been observed clearly fit into the framework that was erected for the mson resonances. Table XXVII shows the mapping of the kaon resonances listed in Table II.

The best way to evaluate the mapping of the kaon

TABLE XXIV. Mapping the broad-width meson resonances into rotational bands. All of the broad-width resonances of Table I are included here. Narrow-width resonances from Table XXIII serve as bandheads for the rotational bands. The only rotational levels included are those allowed by the rules of Table XII.

Group element	Spinless bandheads S	P					
S_2	*** [a]	$DEF(450)$					
D_1	...	$\pi\pi(520)$					
		Bandheads which contain SS spinor pairs					
		$I=0$			$I=1$		
Group element	$^3S_{01}$	$^3P_{00}$	$^3D_{02}$	$^1S_{10}$	$^1P_{11}$	$^1D_{12}$	$^1F_{13}$
D_3	$\pi\pi(870)$	$S^*(980)$ [b]	*** [c]	...	$\pi_N(975)$	*** [c]	*** [c]
D_5	$H,\phi(1009)$	$\epsilon'(1096)$	$f(1270)$	$\pi_N(1016)$	$A_1(1115)$	$A_2(1310)$	*** [c]
D_6	$M^0(1148)$	$\epsilon''(1250)$	$\rho\rho(1410)$	$X^-(1153)$	$B(1237)$	$K_SK_S(1412)$	$g(1680)$
T_1	$\pi\pi(660)$	$\epsilon(800)$	*** [c]	*** [a]	$\rho(770)$	*** [c]	*** [c]
T_2	$\omega(784)$	... [b]	$\eta_N(1076)$				
T_3	$D(1286)$	... [b]	$f'(1516)$				
T_5	$E(1416)$	... [b]	$\omega(1648)$	$KK(1425)$	$\pi/\rho(1490)$	$A_3(1645)$	$A_4(1829)$
T_7				$F_1(1543)$	$\rho'(\sim1600)$ [d]?		

[a] Not allowed by rule (14) of Table XII.
[b] The $\pi\pi$ S-wave phase shift stays near 90° in this whole energy region.
[c] Not allowed by rule (6) of Table XII.
[d] See Ref. 148.

resonances is to compare this mapping with the mapping of the meson resonances. This is the subject of Sec. VIII E.

E. Intercomparison of the meson and kaon resonances

Although the kaon resonances as shown in Table XXVII seem rather incomplete, a comparison between the meson resonances of Table XXIV and the kaon resonances of Table XXVII shows a very orderly structure. This comparison is given in Table XXVIII. As shown in Table XXVIII, both the dominant $K(494)$ meson and the mysterious D-rated $\kappa(725)$ meson fit in naturally with the low-mass meson excitations. The spin-1 $K^*(892)$ resonance, whose bandhead cannot be observed directly because of rule (14) in Table XII, fits in accurately as a P-state counterpart of the ω rotational band. At a higher mass value, the related bandheads $3SS4$ and SSK (Ref. 149) ($K \equiv 34$) give rise to rotational bands in four isotopic spin states: $I=0$, $\frac{1}{2}$, 1, and $\frac{3}{2}$. The observed kaon complexity in the spin-1 Q region[25] seems attributable to P-wave contributions from three rotational bands in this energy region.

As a further illustration of the usefulness of the meson-kaon intercomparison, we show in Table XXIX the measured spin values for the meson and kaon rotational bands of Table XXVIII. As can be seen, measured kaon spin values are complementary to the measured meson spin values. Experimental values for $E_{\rm rot}$ are also given in Table XXIX, and it can be seen that the values of $E_{\rm rot}$ for the meson and kaon resonances are comparable, although the experimental kaon uncertainties, especially in the P waves, are rather large.

Tables XXVIII and XXIX are useful for more than just showing how the kaon data augment the meson data. They are useful in a deeper sense by illustrating that kaon resonances are of the same general types as meson resonances. Although meson and kaon resonances differ in their particle-antiparticle symmetries (and hence in their strangeness values), these internal particle-antiparticle differences evidently do not affect the over-all geometrical features of the resonances. This same conclusion was reached with respect to the baryon and hyperon resonances in Sec. VII. An intercomparison of the meson and kaon resonances is illustrated graphically in Fig. 7, which is an energy-level diagram for the meson and kaon rotational bands. A corresponding baryon and hyperon energy level diagram was given in Fig. 5. In both Figs. 5 and 7, the strange and nonstrange rotational bands show a uniform and slowly varying dependence of the energy levels on the mass of the bandhead. Below, Figs. 5 and 7 are combined together as Fig. 9 to give one over-all hadron rotational energy-level diagram.

TABLE XXV. Quantitative values for the meson rotational bands. The observed widths Γ and the experimental values of the rotational energy parameter $E_{\rm rot} \equiv \hbar^2/2I$ are given for the meson rotational bands of Table XXIV. As can be seen, S states have much narrower widths on the average ($\Gamma \simeq 21$ MeV) than do P–F states ($\Gamma \simeq 115$ MeV). The experimental values for $E_{\rm rot}$ shown here are compared graphically in Fig. 10 with values for $E_{\rm rot}$ obtained from baryon and hyperon rotational bands.

Group element	Meson rotational levels (see Table XXVI) S	P	$^3S_{01}$	$^3P_{00}$	$^3D_{02}$	$^1S_{10}$	$^1P_{11}$	$^1D_{12}$	$^1F_{13}$
				Observed resonance widths					
S_2	···	$\Gamma\sim100$							
D_1	···	$\Gamma70$							
D_3			$\Gamma\sim15$	$\Gamma\sim50$		···	$\Gamma60$		
D_5			$\Gamma\sim20$	$\Gamma80$	$\Gamma163$	$\Gamma\sim25$	$\Gamma98$	$\Gamma100$	
D_6			$\Gamma15$	$\Gamma300$	$\Gamma90$	$\Gamma16$	$\Gamma120$	$\Gamma100$	$\Gamma160$
T_1			$\Gamma\sim15$	$\Gamma\sim150$			$\Gamma146$		
T_2			$\Gamma10$	···	$\Gamma98$				
T_3			$\Gamma21$	···	$\Gamma40$				
T_5			$\Gamma60$	···	$\Gamma139$	$\Gamma\leq20$	$\Gamma85$	$\Gamma129$	$\Gamma127$
Rotational state	S	P	S	P	D	S	P	D	F
Average width	···	$\Gamma85$	$\Gamma22$	$\Gamma145$	$\Gamma106$	$\Gamma20$	$\Gamma102$	$\Gamma110$	$\Gamma144$
				Experimental values in MeV for $E_{\rm rot} \equiv \hbar^2/2I$					
S_2	···	~50							
D_1	···	~50							
D_3			···	~55		···	53		
D_5			···	44	44	···	50	49	
D_6			···	~51	44	···	42	43	44
T_1			···	~70		···	53		
T_2			···		49				
T_3			···		38				
T_5			···		39	···	33	37	34

IX. HADRON ROTATIONAL SUMMARY AND AN EXTENSION TO LIGHT NUCLEI

Although the above discussion of the mapping of meson and baryon resonances was rather lengthy, we can combine these results in a very succinct manner. The mapping problem reduces to two aspects: (1) mapping the narrow-width S-state resonances, and (2) mapping the overlying rotational levels. Graphical displays of these two aspects portray the systematics much more clearly than verbal or tabular descriptions. Figure 8 shows an energy-level diagram for the narrow-width and S-state resonances of Tables I–VII, using a 70-MeV mass grid superimposed on the fundamental vacuum, SS, $SSSS$, $SSSSSS$, $SSS \equiv N$, $SSS3 \equiv \Lambda$, $SSS4 \equiv \Sigma$, and $SSS33 \equiv \Xi$ "ground states." The mass quantization of these levels is evident from the observed interval spacings. The levels labeled with a letter R serve as bandheads for identified overlying rotational levels. In the meson resonances based on the SS spinor-pair ground state, an alternation of dominant (R) and weak (no R) levels can be noted. This alternation, which appears here as a phenomenological result, follows from the meson excitation systematics of Table XXIII.

The rotational levels which correspond to the bandheads (R) of Fig. 8 are shown in Fig. 9. The $L(L+1)$ interval rule of Eq. (22) is evident in the level spacings of Fig. 9. The fact that all types of hadron resonances appear in Fig. 9 with uniform rotational characteristics indicates that these resonances have a common geometrical structure which is independent of isotopic spins or strangeness quantum numbers. It should be stressed that the energy spacings observed in Fig. 9 are in accord with first-order estimates for the moments of inertia of these resonances, where we use the known rotational systematics of nuclear physics to provide a mathematical framework [Eq. (22)] for describing these resonances.

Figures 8 and 9, when taken together, provide an essentially complete mapping of the 130 or so hadron resonances of Tables I–VII.

One remaining task in this section is to make a quantitative comparison of the experimental moments of inertia of these resonances as deduced from the experimental rotational mass intervals,

TABLE XXVI. Measured spin values and principal decay modes for the meson rotational bands of Table XXIV. The spins, where measured, are in agreement with the present assignments; measurements of kaon spins, shown in Table XXIX, complement the values shown here. The decay modes show that P–F levels in a rotational band have the same G parities, but negative-parity S-state bandheads have opposite G parities (see the discussion of this point in Appendix C).

Group element	Meson rotational levels (see Table XXVI)							
	S	P	$^3S_{01}$	$^3P_{00}$	$^3D_{02}$	$^1S_{10}$	$^1P_{11}$	$^1D_{12}$	$^1F_{13}$
			Measured spin values						
S_2	•••	(1?)[a]							
D_1	•••	(1?)[b]							
D_3			(1)[c]	0		•••	(1)[d]		
D_5			1	0	2	0	1	2	
D_6			?	0	(2?)[e]	?	1	?	3
T_1			(1)[f]	0					
T_2			1	•••	2				
T_3			1	•••	2				
T_5			0, 1	•••	?	?	?	2	?
			Principal decay modes						
S_2	•••	$\pi\pi$							
D_1	•••	$\pi\pi$							
D_3			$\pi\pi$	$\pi\pi$		•••	$\eta\pi$		
D_5			$\pi\pi\pi$	$\pi\pi$	$\pi\pi$	KK	$\pi\pi\pi$	$\pi\pi\pi$	
D_6			?	$\pi\pi$	$\pi\pi\pi\pi$	?	$\pi\pi\pi\pi$	$\pi\pi\pi\pi$	$\pi\pi\pi\pi$
T_1			$\pi\pi$	$\pi\pi$			$\pi\pi$		
T_2			$\pi\pi\pi$	•••	$\pi\pi$				
T_3			$\pi\pi\pi\pi$	•••	$\pi\pi$				
T_5			$\pi\pi\pi\pi$	•••	$\pi\pi\pi$	KK	$KK\pi$	$\pi\pi\pi$	$\pi\pi\pi$

[a] See Ref. 59.
[b] See Ref. 63.
[c] See Ref. 44.
[d] See Ref. 49.
[e] See Ref. 60.
[f] See Ref. 39.

and to see what conclusions can be drawn as to the over-all geometries of these resonances. Experimental values of the rotational energy parameter $E_{\text{rot}} \equiv \hbar^2/2I$ [Eq. (23)] for the meson (M), kaon (K), baryon (N, Δ), and hyperon (Λ, Σ) resonances are listed at the bottom of Fig. 9, and are shown graphically in Fig. 10. As can be seen in Fig. 10, these values for E_{rot} exhibit a smooth dependence on the rest mass of the bandhead, and they seem to be independent of isotopic spins and strangeness quantum numbers.

The bandhead masses shown in Fig. 10 extend up almost to the range of very light nuclei. Hence it is of interest to ascertain if evidence for nonadiabatic rotations of the type considered here can be found in these light nuclei. Table XXX gives a summary of identified rotational levels in very light nuclei extending from Be^8 to Si^{28}. Also included in Table XXX are some levels in He^3, He^5, and Li^5 that, at least from the present viewpoint, can possibly be considered to be nonadiabatic rotational levels. Experimental values of E_{rot} for these levels are given in Table XXX, together with some theoretical estimates of E_{rot} based on the configurations indicated in the right-hand column of Table XXX.[150-153] As can be seen in Table XXX, the rigid-body estimates of E_{rot} agree reasonably well with the experimental values, as was the case for the hadron resonances discussed above.

We can use the experimental values of E_{rot} in Fig. 10 and Table XXX to extract the corresponding moments of inertia of the rotational bandheads. The resulting moments of inertia I are plotted together in Fig. 11. As can be seen in Fig. 11, the moments of inertia I for hadrons and for very light nuclei extrapolate smoothly into one another, which suggests that the present use of nuclear-physics concepts to treat nonadiabatic rotations in hadrons is a valid procedure.

As one final result, we define an effective radius R_{eff} for these resonances by means of the equation

$$I = \tfrac{2}{5} M R_{\text{eff}}^2 , \tag{36}$$

where I is the experimental moment of inertia and M is the mass of the bandhead. The values for I in Fig. 11 give the values for R_{eff} shown in Fig. 12.

TABLE XXVII. Mapping the kaon resonances. The kaon rotational bands shown here include all of the experimental kaon resonances listed in Table II. Although the mapping of the kaon resonances is somewhat fragmentary as compared to the mapping of the meson resonances, the kaon resonances clearly fit into the same framework that was erected to account for the meson resonances. Tables XXVIII and XXIX give a quantitative evaluation of these kaon rotational bands, and also a comparison to the corresponding meson rotational bands.

Group element	Geometry	Spinless bandhead S_1	Bandheads which contain SS spinor pairs $I=\frac{1}{2}$ $^1S_{10}$	$^1P_{11}$	$^1D_{12}$	$^1F_{13}$	$I=\frac{3}{2}$ $^1S_{30}$	$^1P_{31}$
S_1S_2	$7=34$	$K(494)$						
S_2S_2	$SS1$		$\kappa(725)$					
D_6	SSK		$K_N(1160)$	$C(1242)$	$K_N(1421)$	$K_N(1660)$	$K_A(1175)$	$K_A(1265)$
T_2	$1SS1$		***[a]	$K^*(892)$	...	***[b]		
T_3	πSSK		$Q(1272)$	$Q(1344)$	...	$K_N(1753)$		
T_5	$4SSK$		$K_N(1368)$	$Q(1417)$	...	$K_N(1850)$		
T_7	$33SSK$		...	...	$L(1765)$	...		

[a] Not allowed by rule (14) of Table XII.
[b] Not allowed by rule (6) of Table XII.

TABLE XXVIII. Intercomparison of meson and kaon rotational bands. Masses and widths for meson resonances of Tables XXIII and XXIV and kaon resonances of Table XXVII are shown. These interrelated meson and kaon resonances form characteristic patterns with respect to geometries and widths. The meson and kaon rotational bands are shown in Fig. 7, and also in Fig. 9 where they are combined with the baryon and hyperon rotational bands. From the average widths shown at the bottom of the table the distinction between rotationless S states and rotational $P-F$ states is phenomenologically clean cut: $\Gamma_S \simeq 23$ MeV and $\Gamma_{P-F} \simeq 119$ MeV.

Geometry	Isospin	S	P	D	F
		Low-mass excitations			
33	?	[420] [a]	$\pi\pi(520)\Gamma 70$		
331	$\frac{1}{2}$	$K(494)\Gamma \simeq 0$	...		
33π	0	$\eta(549)\Gamma < 1$	...		
SS	1	[660] [a,b]	$\rho(770)\Gamma 146$		
$SS1$	$\frac{1}{2}$	$\kappa(725)\Gamma 15$	...		
$SS\pi$	0	$\omega(784)\Gamma 10$	...		
		Higher-mass excitations			
$SS\pi$	0	$\omega(784)\Gamma 10$	...	$\eta_N(1076)\Gamma 98$	
$1SS1$	$\frac{1}{2}$	*** [b]	$K^*(892)\Gamma 50$	...	
$3SS4$	0	$M^0(1148)\Gamma 15$	$\epsilon'(1250)\Gamma 300$	$\rho\rho(1410)\Gamma 90$	...
SSK	$\frac{1}{2}$	$K_N(1160)\Gamma \sim 90$	$C(1242)\Gamma 127$	$K_N(1421)\Gamma 100$	$K_N(1660)\Gamma 60$
$3SS4$	1	$X^-(1153)\Gamma 16$	$B(1237)\Gamma 120$	$K_SK_S(1410)\Gamma 100$	$g(1680)\Gamma 160$
SSK	$\frac{3}{2}$	$K_A(1175)\Gamma \sim 25$	$K_A(1265)\Gamma 50$	...	...
$33SS3$	0	$D(1286)\Gamma 21$	...	$f'(1516)\Gamma 40$	...
πSSK	$\frac{1}{2}$	$Q(1272)\Gamma 18$	$Q(1344)\Gamma 60$	...	$K_N(1753)\Gamma 60$
$44SS3$	0	$E(1416)\Gamma 60$	...	$\omega(1648)\Gamma 139$	...
$4SSK$	$\frac{1}{2}$	$K_N(1368)\Gamma 19$	$Q(1417)\Gamma 89$	...	$K_N(1850)\Gamma \sim 300$
$44SS3$	1	$KK(1425)\Gamma \leq 20$	$\pi/\rho(1490)\Gamma 85$	$A_3(1645)\Gamma 129$	$A_4(1829)\Gamma 127$
$33SSK$	$\frac{1}{2}$	[1543] [a]	...	$L(1765)\Gamma 140$	
$33SS34$	1	$F_1(1543)\Gamma 16$	$\rho'(\sim 1600)$		
Average width $\overline{\Gamma}$		$\overline{\Gamma}=23$ MeV	$\overline{\Gamma}=110$ MeV	$\overline{\Gamma}=105$ MeV	$\overline{\Gamma}=141$ MeV

[a] Unobserved S state.
[b] Not allowed by rule (14) of Table XII.

TABLE XXIX. Measured spin values and values of the rotational energy parameter $E_{rot} \equiv \hbar^2/2I$ for the higher-mass meson and kaon resonances of Table XXVIII. The spin values of the meson and kaon levels are complementary, and they give supportive evidence for the rotational assignments shown in Table XXVIII. Experimental E_{rot} values for the P-wave levels characteristically show some scatter, since the rotational energy interval is small as compared to the uncertainties in the positions of the resonance peaks; the E_{rot} values for the D and F levels, on the other hand, show a rather clear and consistent pattern. Figure 10 shows the average value of E_{rot} for each of these meson and kaon rotational bands, together with corresponding values of E_{rot} for the baryon and hyperon rotational bands.

Geometry	Isospin	Measured spin values				Experimental values for E_{rot}			
		S	P	D	F	S	P	D	F
$SS\pi$	0	1	•••	2		•••	•••	49	
$1SS1$	$\frac{1}{2}$	•••	1	•••		•••	54	•••	
$3SS4$	0	?	0	?		•••	~51	44	
SSK	$\frac{1}{2}$	0	1	2	?	•••	41	44	42
$3SS4$	1	?	1	?	3	•••	42	43	44
SSK	$\frac{3}{2}$	?	?			•••	45		
$33SS3$	0	1	•••	2	•••	•••	•••	38	•••
πSSK	$\frac{1}{2}$	?	1	•••	3	•••	36	•••	40
$44SS3$	0	0, 1	•••	?	•••	•••	•••	39	•••
$4SSK$	$\frac{1}{2}$	(0)	1	•••	3	•••	25	•••	40
$44SS3$	1	?	?	2	?	•••	33	37	34
$33SSK$	$\frac{1}{2}$	•••	•••	2		•••	•••	37	
$33SS34$	1	1, 2	1	•••		•••	?	•••	

Starting with the lightest masses in Fig. 12, we see that as the mass of the bandhead *increases*, the effective radius *decreases*. At about the mass of the nucleon, 1 GeV, a minimum value for R_{eff} is reached, $R_{eff} \simeq 1$ fermi, which is roughly the experimental radius of a nucleon. The effective radius stays fairly constant over the range of hadron masses from 1 to 2 GeV, and then in the region of very light nuclei, R_{eff} goes over into something like the $A^{1/3}$ dependence expected on the basis of optical-model considerations. In paper II we establish a geometrical shape for the spinor S, guided in part by the known properties of the nucleon. The results of Fig. 12 suggest that hadron

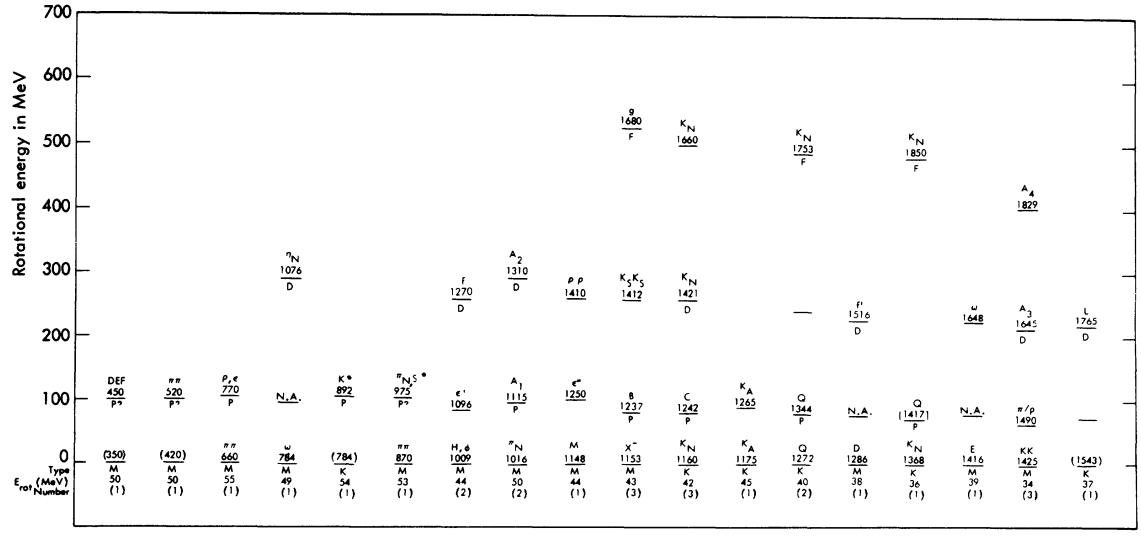

FIG. 7. An energy-level diagram for the meson and kaon rotational bands of Tables XXIV–XXIX. This boson diagram corresponds to the fermion diagram of Fig. 5. S states enclosed in parentheses are unobserved levels, and the P state enclosed in brackets has been shifted graphically to match the E_{rot} value for that rotational band. States labeled N.A. are not allowed by rule (11c) of Table XII except as difficult-to-identify ϵ-type excitations.

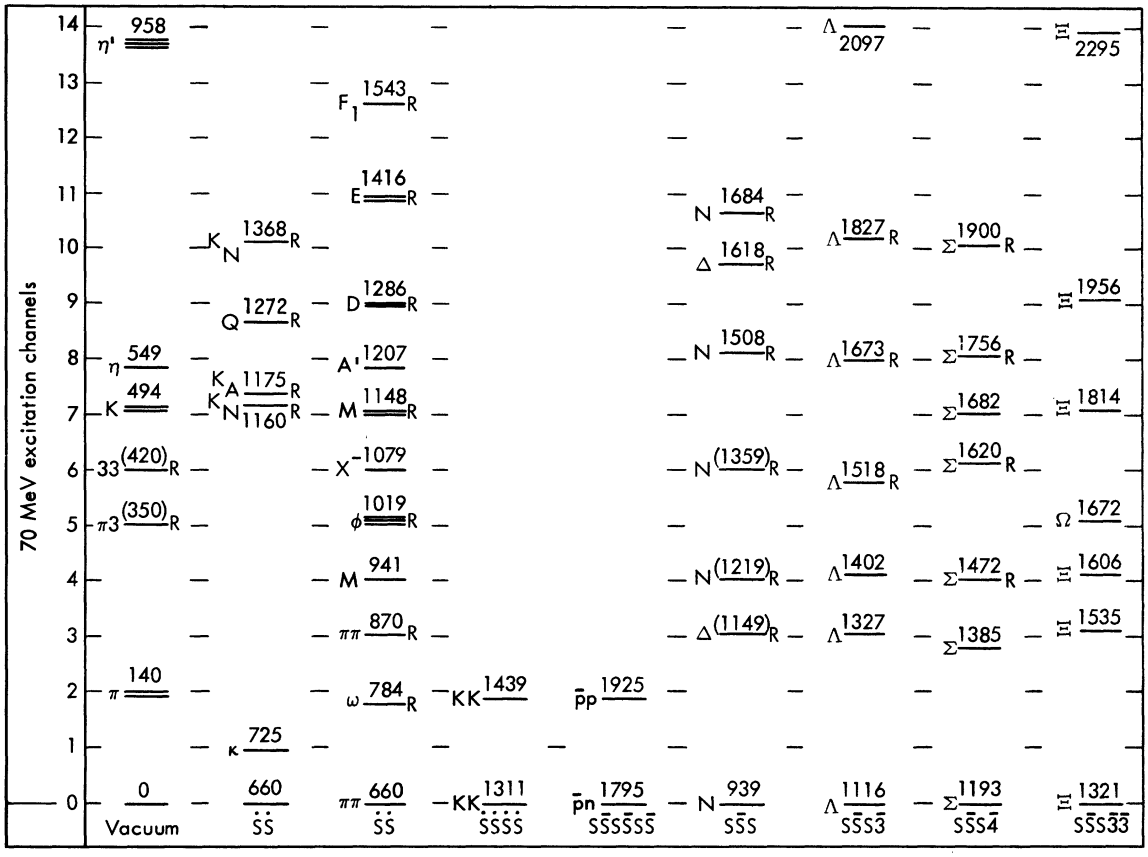

FIG. 8. A plot of the narrow-width and S-state resonances of Tables I–VII. The experimental levels are compared to 70-MeV mass grids erected on the basic "ground states" Vacuum (0), $\dot{S}\dot{\bar{S}}(660)$ (meson and kaon), $\dot{S}\dot{S}\dot{\bar{S}}\dot{\bar{S}}(1311)$, $N\bar{N}(1795)$, $N(939)$ (N and Δ), $\Lambda(1116)$, $\Sigma(1193)$, and $\Xi(1321)$. This figure is essentially a complete mapping of all of the reported low-mass, narrow-width, and S-state boson and fermion resonances. The observed interval spacings and the completeness of the mapping reveal the fundamental 70-MeV mass quantization of these levels, irrespective of any theory of elementary particles. Levels that are labeled with an R serve as bandheads for identified overlying rotational levels, which are shown in Fig. 9. Levels whose mass values are enclosed in parentheses have not been observed directly, but are indicated only by the observed overlying rotational levels. Where levels occur in groups, the mass value of the best known level is quoted. See Ref. 181 for the level $\Lambda(2097)\Gamma 24$, which is not included in Table V.

resonances may in fact have an over-all geometrical scaling that tends to vary inversely with the mass of the resonance. However, for the purposes of the present work we ignore this over-all scaling, and we implicitly assume that the dimensions of the spinor S are the same in all resonances in which it appears.

X. ENERGY AND ANGULAR MOMENTUM DISTRIBUTIONS IN THE ρ MESON

Possibly the strongest motivation for the elementary-particle research of the past two decades has been the hope that the details of elementary-particle structure will reveal the workings of quantum theory on a deeper level than can be reached by studying atomic systems. If we accept the present light-quark results as having physical content, then it appears that this hope has been at least partially realized. With respect to the *quantization of elementary-particle masses*, the present light-quark model has led to the strongest possible quantization condition:

> All particles more massive than the electron can be constructed from a single mass quantum $M = 70$ MeV. (37)

This light-quark model has also furnished an explanation for the *quantization of spin angular momentum* by showing that it follows as a consequence of energy conservation [see results (a)–(d) of Sec. VI A]:

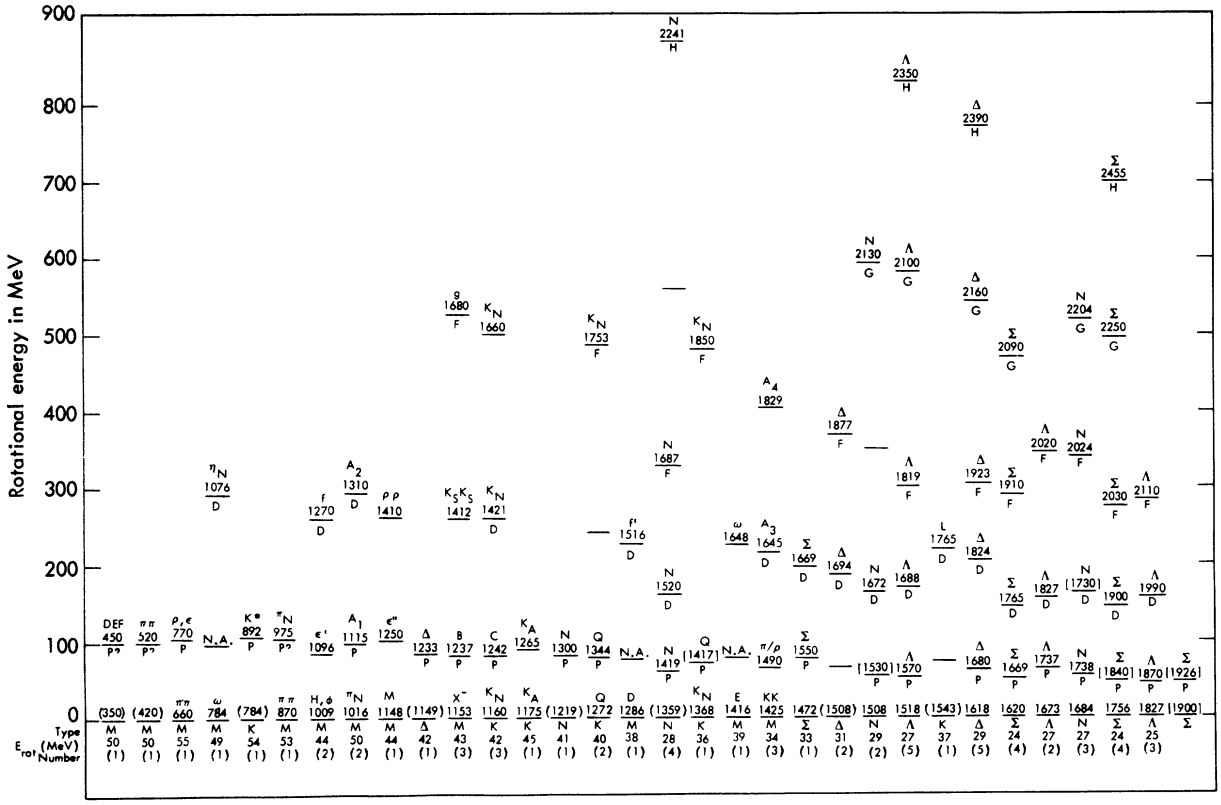

FIG. 9. A plot of the rotational bands for the meson (M), kaon (K), baryon (N and Δ), and hyperon (Λ and Σ) resonances. This energy-level diagram is an intercomparison of the fermion rotational bands of Fig. 5 with the boson rotational bands of Fig. 7. These hadronic rotational bands show a clear $L(L+1)$ interval spacing. The experimentally determined values for $E_{rot} \equiv \hbar^2/2I$ shown at the bottom of each rotational band are plotted in Fig. 10. When mass values for these rotational levels (before any graphical shifting) are compared to mass values calculated from a "universal" E_{rot} curve (the dashed line in Fig. 10), the average mass accuracy for the 74 rotational levels shown is ±1.4% (see Table XXXIV). A visual inspection of Fig. 8 and this figure, which contain essentially all of the experimental resonances listed in Tables I–VII, indicates that the mapping of these resonances is reasonably complete (see Fig. 19).

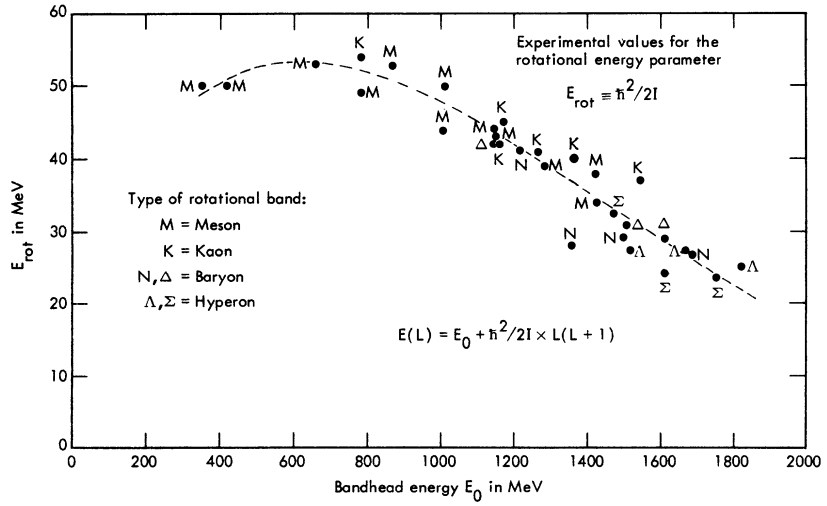

FIG. 10. A graphical plot of experimental values for the rotational energy parameter $E_{rot} \equiv \hbar^2/2I$ as obtained from the rotational bands of Fig. 9. All types of resonance show the same systematic behavior for E_{rot} (and hence for the moment of inertia I) as a function of the bandhead energy. The dashed curve was used to calculate the mass values that are summarized in Table XXXIV.

TABLE XXX. Experimental values of $E_{\rm rot} \equiv \hbar^2/2I$ for energy levels in very light nuclei. A few estimates for $E_{\rm rot}$ based on rigid rotors are also shown.

Nucleus	Observed rotational levels	$E_{\rm rot}$ MeV experimental	$E_{\rm rot}$ (MeV) estimated	Basis for estimate	Footnote
Si^{28}	$0^+2^+4^+$	0.26			
Mg^{24}	$0^+2^+4^+$	0.22			
Ne^{20}	$0^+2^+4^+$	0.24			
O^{18}	$0^+2^+4^+$	0.34			
O^{16}	$0^+2^+4^+6^+$	0.22	0.27	$I=\frac{2}{5}MR^2$, with	
	$1^-3^-5^-7^-$	0.22	0.27	$R=3.5$ fermis	a
C^{12}	$0^+2^+4^+$	0.72	~0.7	3α at 135°	b
Be^8	$0^+2^+4^+$	0.53	0.7	α-α dumbbell	c
Li^5, He^5	1^-	2.5	2.3	α-N dumbbell	c
He^3	1^-	~11.5	~11	$3N$ at 135°	d

[a] See Ref. 150.
[b] See Ref. 151.
[c] See Ref. 152.
[d] See Ref. 153.

$$M = 70 \text{ MeV} \rightarrow M_s = 105 \text{ MeV}, \tag{18'}$$

$$MMM = 210 \text{ MeV} \rightarrow M[M]M \rightarrow M_s M_s = 210 \text{ MeV}, \tag{18''}$$

where $[M]$ denotes the annihilation of a quantum M, with the annihilation energy appearing as rotational energy of the two spinning quanta M_s, which spin at the full relativistic limit (with their equators at the velocity of light). In the present section, we show how the light-quark model illuminates a third aspect of quantization, the *quantization of orbital angular momentum*.

In the preceding sections of the paper, the idea was developed that hadron resonances occur in both rotationless ($L=0$) and rotational ($L>0$) orbital angular momentum modes. From the small

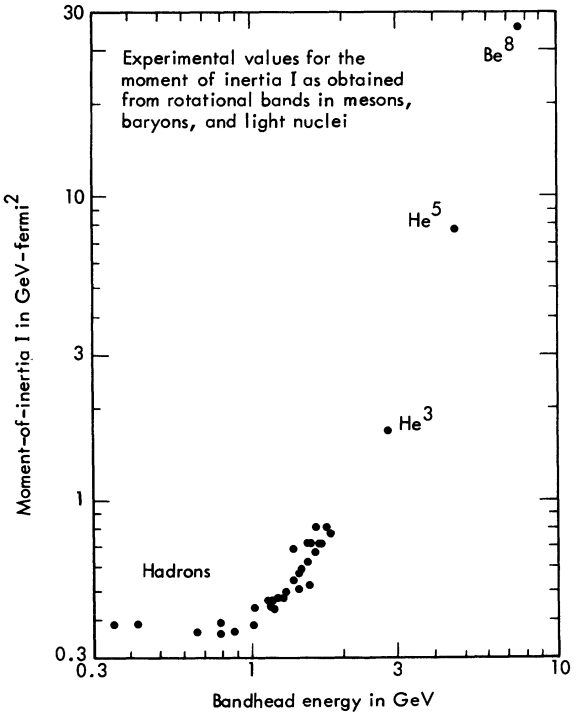

FIG. 11. Experimental values for the bandhead moments of inertia I of hadrons and very light nuclei. These I values were determined from the equation $I = \hbar^2/2E_{\rm rot}$; the hadronic values of $E_{\rm rot}$ were obtained from Fig. 9, and the light-nucleus values of $E_{\rm rot}$ were obtained from Table XXX.

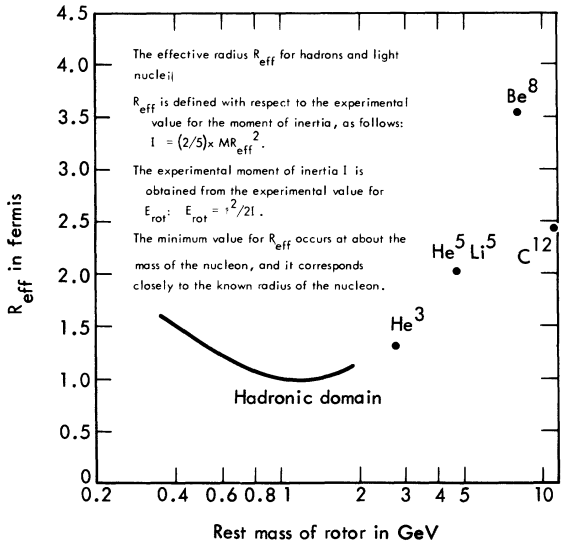

FIG. 12. Experimental values for the effective radii $R_{\rm eff}$ of hadrons and very light nuclei. $R_{\rm eff}$ is defined from the equation $I = \frac{2}{5} MR_{\rm eff}^2$, and the values for I and M are taken from Fig. 11. The nucleon occurs at about the minimum point in the $R_{\rm eff}$ curve, and this minimum value for $R_{\rm eff}$ corresponds approximately to the known radius of the nucleon. In light nuclei, the almost trilinear C^{12} nucleus has a smaller value for $R_{\rm eff}$ than does the dumbbell-shaped Be^8 nucleus (see Table XXX).

moments of inertia possessed by hadron resonances, hadron rotational energies are large [Eqs. (22)–(24)]. With the ρ meson as a specific example of a rotational excitation, a geometric configuration for the $\dot{S}\dot{S}$ bandhead of the ρ was shown in Fig. 4, and Eq. (24) was used to calculate the rotational energy of the ρ as $E(L)=177$ MeV. This energy, when added to the $\dot{S}\dot{S}$ bandhead energy of the ρ, $E_0=660$ MeV, gives a calculated peak energy for the ρ of 777 MeV:

$$\begin{aligned} E_\rho &= E_0 + E(L) \\ &= E_0 + (\hbar^2/2I)L(L+1) \\ &= 660 + 177 = 777 \text{ MeV}. \end{aligned} \tag{38}$$

The world average for the peak energy of the ρ is 770 MeV.[25] The significance of this result with respect to orbital angular momentum quantization lies in the following sequence of observations:

The ρ meson is observed experimentally with energies ranging all the way from about 650 MeV to 900 MeV (Ref. 25). (39a)

The 660-MeV $\dot{S}\dot{S}$ ρ-meson bandhead belongs to a class of meson excitations (Table XXIII) which have natural widths $\Gamma \simeq 10$ MeV. (39b)

From (39b), the 250-MeV spread in ρ-meson energies described in (39a) must be attributed primarily to a spread in rotational energies $E(L)$ and not to a spread in bandhead energies E_0 [Eq. (38)]. (39c)

From (39c) and Eq. (38), we have

$$E_\rho = E_0 + E(L) \text{ and } \Delta E_\rho \simeq \Delta E(L) = E(\Delta L),$$

so that a spread in orbital rotational energies implies a corresponding spread in orbital angular momentum values. (39d)

Thus from (39a)–(39d), we are led unequivocally to the following result:

The spin-1 ρ meson is a pure $L=1$ resonance only at the peak energy E_{res} of the resonance; for $E>E_{\text{res}}$, the ρ has $L>1$, and for $E<E_{\text{res}}$, the ρ has $L<1$. (40)

This result of course applies to the other hadron rotational resonances as well:

We denote a broad-width hadron rotational resonance by its L value, L_{res}, which it has at the peak energy of the resonance, E_{res}; then for $E>E_{\text{res}}$ ($E<E_{\text{res}}$), the resonance has $L>L_{\text{res}}$ ($L<L_{\text{res}}$). (41)

From these results, we can conclude that the broad widths of rotational hadron resonances as compared to the narrow widths of rotationless hadron resonances [Eqs. (16) and (17)] are due to the circumstance that orbital angular momenta for these resonances are less sharply quantized than are spin angular momenta [which are mediated by the transition of Eq. (19)].

In the remainder of the present section, some consequences of Eqs. (40) and (41) are explored, and a number of experimental results are cited which appear to substantiate the rotational systematics of this light-quark model.

As one consequence of Eq. (40), it is possible to use the probability interpretation of the quantum-mechanical ρ-meson scattering amplitudes to determine the mass of the ρ-meson bandhead directly from experiment, without assuming any knowledge of the present light-quark set of basis states. This is accomplished by studying the P-wave phase shifts which have been determined experimentally for the ρ. Since the ρ is a spin-1 resonance, its behavior is characterized by the behavior of the P-wave phase shift δ_1^1, where the notation δ_L^I is used (I = isotopic spin and L = angular momentum). In a recent Berkeley experiment,[154,155] the ρ meson was observed in the reaction $\pi^+ p \to \Delta^{++}\pi^+\pi^- = \Delta^{++}\rho^0$, and a phase-shift analysis was carried out on these data to extract the scattering amplitudes.[155] The invariant-mass spectrum from the Berkeley experiment,[154] which is dominated by the ρ resonance, is shown in Fig. 13. The δ_1^1 energy-dependent P-wave phase shifts from the Berkeley analysis [155] are also shown in Fig. 13, with the phases larger than 90° reflected about 90° to illustrate the resonant nature of the P wave. As can be seen, the shape of the energy-dependent P-wave spectrum accurately follows the shape of the ρ-meson invariant-mass spectrum. In particular, the P waves accurately mirror both the position and the width [full width at half-maximum (FWHM)] of the ρ.

The quantum-mechanical implication of this result is the following. We can relate the energy of the ρ to the angular momentum of the ρ by the equation

$$E_\rho = E_\rho(L) = E_0 + (\hbar^2/2I)L(L+1). \tag{42}$$

As discussed above, this implies that the observed spread in energies of the ρ, ΔE_ρ, is re-

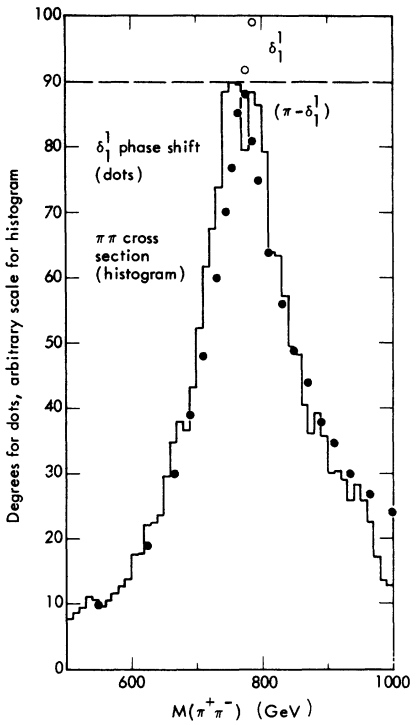

FIG. 13. Comparison of a ρ meson $\pi\pi$ invariant-mass spectrum (Ref. 154) with the corresponding δ_1^1 energy-dependent P-wave phase shifts (Ref. 155; note that the P waves above 90° have been reflected about the 90° axis). The close agreement shows that the behavior of the spin-1 ρ resonance is characterized by the behavior of the P waves, a result which indicates that the ρ is in fact an $L=1$ orbital excitation, and not an $S=1$ spinor-pair excitation.

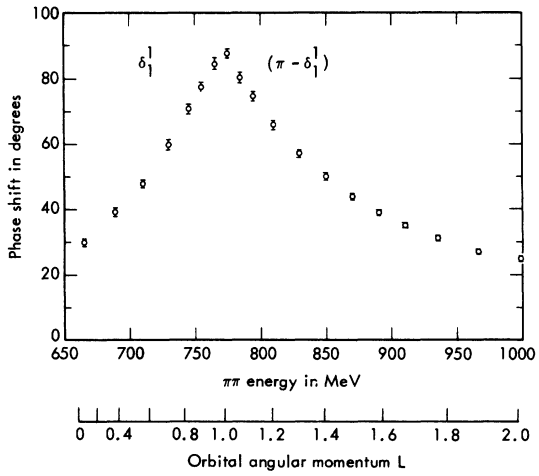

FIG. 14. The δ_1^1 P-wave phase shifts of Fig. 13 and Ref. 155 shown plotted against the conventional energy axis and also against an orbital angular momentum (L) axis. The orbital angular momentum axis was obtained from Eq. (42), with the angular momentum and energy pairs ($L=0$, $E=660$ MeV) and ($L=1$, $E=772$ MeV) chosen so as to reproduce the bandhead energy of the ρ (Fig. 4) and the peak energy of the ρ (Table XXXI), respectively. The value for the moment of inertia I of the ρ in this representation is $I=348$ MeV fermi^2, intermediate between the two values for I calculated in the text.

lated to a corresponding spread in angular momentum values, ΔL. At the peak energy of the ρ, $E_\rho(1)$, the L value is $L=1$ and the relative P-wave amplitude is unity, corresponding to $\delta_1^1=90°$. At the energies where the P-wave phase shifts are $\delta_1^1=45°$ and $\delta_1^1=135°$, the P-wave *amplitude* has fallen to 0.707, and the P-wave *probability* has fallen to 50%. For $\delta_1^1=45°$ $[E_\rho(L)<E_\rho(1)]$, a P-wave probability of 50% can be thought of as half P wave and half S wave, or an L value of $\frac{1}{2}$. Correspondingly, for $\delta_1^1=135°$ $[E_\rho(L)>E_\rho(1)]$, a P-wave probability of 50% can be thought of as half P wave and half D wave, or an L value of $\frac{3}{2}$. In the Berkeley $\pi\pi$ phase-shift analysis,[155] precise values were obtained for the energies at which the 45°, 90°, and 135° δ_1^1 phase shifts occur. These values are shown in Table XXXI. By inserting the 45° and 135° L values, $\frac{1}{2}$ and $\frac{3}{2}$, and the corresponding energies $E_\rho(\frac{1}{2})$ and $E_\rho(\frac{3}{2})$, into Eq. (42), we can determine $\hbar^2/2I$ experimentally:

$$E_\rho(\tfrac{3}{2})-E_\rho(\tfrac{1}{2})=163 \text{ MeV}$$
$$=(\hbar^2/2I)[(\tfrac{3}{2})(\tfrac{5}{2})-(\tfrac{1}{2})(\tfrac{3}{2})],$$

which gives $I=358$ MeV fermi^2, in reasonable agreement with the value $I=333$ MeV fermi^2 calculated from the geometry of Fig. 4. Inserting $E_\rho(1)=772$ MeV (Table XXXI) and $I=358$ MeV fermi^2 into Eq. (42) gives $E_0=663$ MeV as the *calculated* rest mass of the ρ, a result that is independent of any assumptions about the basis set. This is in good agreement with the value $E_0=660$ MeV obtained from Fig. 4. Thus, by invoking the probability interpretation of the experimental ρ-meson scattering amplitudes, we have been able to determine the moment of inertia of the ρ, and hence its bandhead mass, directly from experiment, and this experimental ρ-meson bandhead mass is the same as the bandhead mass that we have previously deduced from light-quark S-state systematics which have nothing to do with the ρ meson.

By using Eq. (42) to relate energies and orbital angular momenta, we can plot the ρ meson on an orbital angular momentum axis as well as on an energy axis. If we set $L=0$ at 660 MeV to match Fig. 4, and $L=1$ at 772 MeV to match the Berkeley value for the peak (Table XXXI), the value for I thus obtained is $I=348$ MeV fermi^2, intermediate between the two values for I quoted above. Figure 14 shows the P-wave phase shifts of Fig. 13 plotted against both energy and angular momentum abscis-

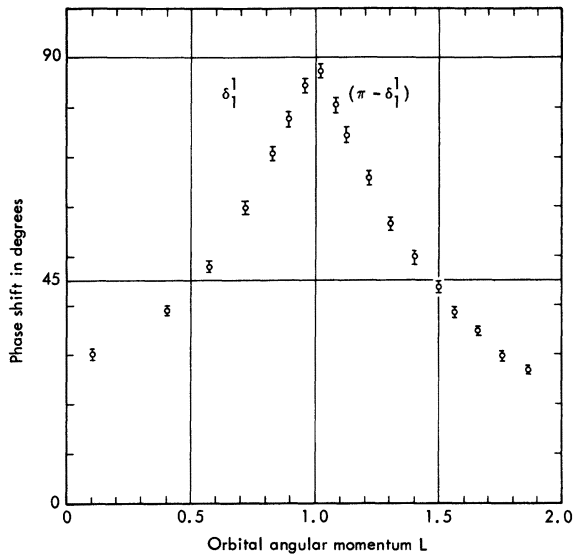

FIG. 15. The P-wave phase shifts of Fig. 14 plotted against the (linearized) orbital angular momentum axis of Fig. 14. In this representation, both the energy-dependent P-wave phase shifts of Fig. 14 and the $\pi\pi$ invariant-mass spectrum of Fig. 13 appear as symmetric bell-shaped distributions.

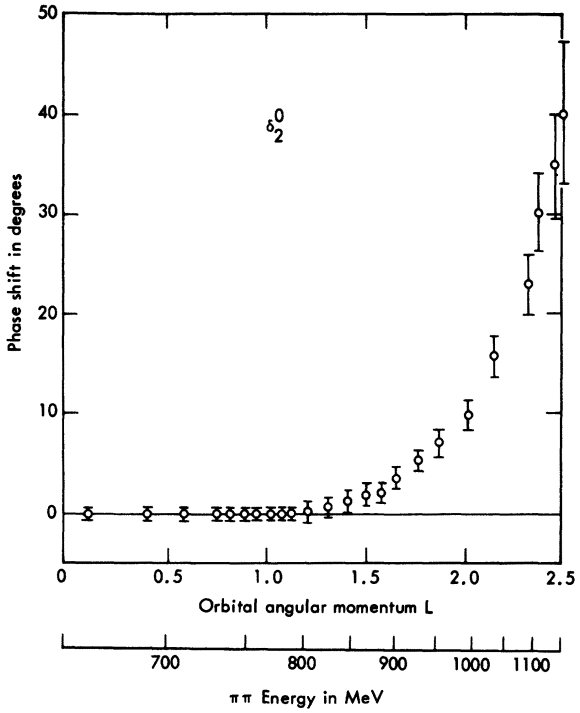

FIG. 16. The δ_2^0 D-wave phase shifts of Ref. 155 plotted against the orbital angular momentum axis of Fig. 14. As can be seen, the D wave starts to rise at just the energy where $L > 1$ for the ρ resonance. The existence of this D-wave component in low-energy $\pi\pi$ scattering has constituted somewhat of a theoretical puzzle, since there are no spin-2 meson resonances in this energy region. The very large D-wave phase-shift values above 1000 MeV are an indication of the presence of the $I = 0$ spin-2 $\eta_N(1076)$ $\pi\pi$ meson resonance, which is shown in Fig. 17.

sas. If Fig. 14 is altered by linearizing the angular momentum abscissa, then the P-wave phase shift curve appears as a symmetric bell-shaped distribution. This plot is shown in Fig. 15.

One of the theoretical puzzles about $\pi\pi$ phase-shift analyses at low energies (below 1 GeV) has been the appearance of a D-wave component in the $\pi\pi$ amplitudes. However, from the present systematics we expect D waves to appear as soon as L becomes greater than 1. Figure 16 shows the D-wave phase shifts δ_2^0 of the Berkeley analysis[155] plotted against the angular momentum abscissa of Fig. 15, with the corresponding energy axis indicated below. As can be seen, the D wave starts to rise at just the energy where L becomes greater than 1. This result tends to substantiate the interpretation given above, in which a ρ-meson L value greater than 1 represents a mixture of P-wave and D-wave components. It also explains the puzzle cited above, namely, the appearance of $\pi\pi$ D waves in an energy region that contains no spin-2 $\pi\pi$ resonances. In a plot[20] similar to that of Fig. 16, the Berkeley δ_3^1 F-wave phase shift[155] starts to rise at just the energy for which L becomes greater than 2.

There are two more experimental puzzles that can be cleared up by the present systematics. These puzzles are: (1) The spin-2, $I = 0$ $\eta_N(1076)$ $\pi\pi$ resonance of Table I is observed to be superimposed on a strong P-wave background[58] of unknown origin; (2) the $\pi\pi$ D-wave phase shifts shown in Fig. 16 have very large values above 1 GeV—values that are too large, according to the Berkeley workers,[155] to be accounted for as coming from the tail of the spin-2, $I = 0$ $f(1270)$ $\pi\pi$ resonance. It turns out that these two puzzles have related explanations, which are as follows. The broad $f(1270)\Gamma 163$ meson, like the broad $\rho(770)\Gamma 146$ meson, is a rotational excitation (see Table XXIV). Hence it must have a range of angular momentum values [Eq. (41)]. Similar results obtain for the broad $\eta_N(1076)\Gamma 98$ meson. The bandheads for these two resonances are given in Table XXIV. Thus we can use Eq. (42) to calculate angular momentum abscissas for these spin-2 resonances, just as for the spin-1 ρ resonance. Figure 17 shows the $\eta_N(1076)$ and $f(1270)$ resonances plotted schematically on a common energy axis, with their respective angular momentum abscissas shown underneath. As can be seen, the η_N sits right on top of the low-energy spin-1 tail of the f, thus explaining the origin of this mysterious

background. This solves puzzle (1). With respect to puzzle (2), we can see in Fig. 17 that the f meson has no $L=2$ component left at an energy as low as 1 GeV; hence the observation of the Berkeley workers[155] that the D waves above 1 GeV in Fig. 16 are too large to be accounted for by the tail of the f takes on added significance. However, the η_N has a substantial $L>1$ component at 1 GeV, and it seems clear that the large D waves above 1 GeV arise from the η_N and not from the f, which solves puzzle (2). We can turn this argument around and assert that the large D-wave values above 1 GeV in Fig. 16 are direct evidence for the existence of the η_N resonance.

The task of establishing the $\eta_N(1076)$ as a *bona fide* resonance[58] is of considerable theoretical importance. This is because the η_N overfills the 2^+ nonet,[25] just as the $M(953)$ overfills the 0^- nonet[65,25] and the $\pi_N(975)$ probably also overfills the 1^- nonet.[49,25] The other SU(3) nonets are underfilled,[156] and experiments have stabilized to the point where it seems probable that they will continue to remain underfilled. An explanation for the overfilling of the 0^-, 1^-, and 2^+ nonets and the underfilling of the 0^+, 1^+, and 2^- nonets can be given in terms of the systematics of the present light-quark model.[157]

Two different calculations in the present paper have indicated that the bandhead mass of the ρ is about 660 MeV: (1) The $\dot{S}\dot{S}$ pair in Fig. 4 has a mass of 660 MeV; (2) the P-wave calculation described in connection with Table XXXI gave a bandhead mass of 663 MeV. This raises the question as to whether any experimental evidence exists for a $\pi\pi$ anomaly at 660 MeV. When the $\pi\pi$ invariant-mass spectrum from the Berkeley experiment[154] is inspected, a small peak can be observed near 660 MeV.[158] After a background subtraction is made,[39] the position of this peak is about 665 MeV, and the width is roughly 15 MeV. Evidence for this peak can also be seen when the data are separated into momentum-transfer components, as is shown in Fig. 18.[159] The anomaly that occurs near 660 MeV in Fig. 18 seems to depend on $|t'|$,

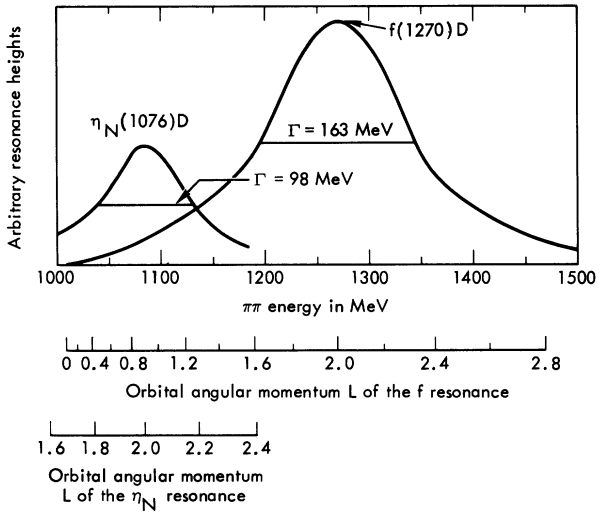

FIG. 17. The spin-2, $I=0$, $\pi\pi$ resonances $\eta_N(1076)\Gamma 98$ and $f(1270)\Gamma 163$, shown schematically on a common energy abscissa. In analogy to Fig. 14, the orbital angular momentum abscissas are also shown for these spin-2 rotational resonances (see text). As can be observed, the low-energy spin-1 tail of the f accounts for the strong P-wave background (Ref. 58) which occurs under the η_N (and which has not otherwise been explained). The D-wave component of the η_N accounts in turn for the very large values of the δ_2^0 D-wave phase shift above 1 GeV noted in Fig. 16.

the momentum transfer. As is shown in the caption to Fig. 18, this $|t'|$ dependence is what one might expect from impact-parameter arguments. Other experimental evidence for a $\pi\pi$ anomaly at 660 MeV is given by Gutay and coworkers,[39] who observed a dip in the $I=0$ $\pi\pi$ S-wave amplitude at 660 MeV, with a width that is commensurate with the Berkeley results.

XI. PREDICTIONS AND FULFILLMENTS

One way to ascertain the physical content of a spectroscopic model is to study the completeness and accuracy of the mapping. Another way is by examining its predictive successes or lack of suc

TABLE XXXI. ρ-meson P-wave shifts as obtained from the Berkeley $\pi\pi$ phase-shift analysis of Ref. 155. By inserting these phase shifts and the associated L values into Eq. (42), as described in the text, we can calculate the bandhead mass of the ρ directly from experiment. The value thus obtained, 663 MeV, agrees well with the value of 660 MeV obtained from Fig. 4 and Table VIII. An experimental indication of the bandhead of the ρ can be observed in Fig. 18. The observed asymmetry shown below for the 45°–90° and 90°–135° interval spacings is characteristic of all measurements of the ρ meson.

P-wave phase shift	45°		90°		135°
$\pi\pi$ invariant mass	703 MeV		772 MeV		866 MeV
L value (see text)	$\frac{1}{2}$		1		$\frac{3}{2}$
Mass interval spacing		69 MeV		94 MeV	

cesses. The present formalism was outlined in some detail several years ago,[2-6] and a number of new resonances have appeared since that time. Thus it is a straightforward matter to determine whether or not these new resonances are in agreement with present expectations. The summary given in Sec. IX has already provided an affirmative answer to this question. However, in order to evaluate the physical content of this light-quark model in more detail, further investigation is warranted. Thus in the present section we discuss the following topics: (a) predictions and verifications, (b) accuracy of mass calculations for rotational resonances, (c) resonances that are predicted but not observed, (d) observed resonances that are not mapped, (e) statistical evidence for the mass quantum $M = 70$ MeV.

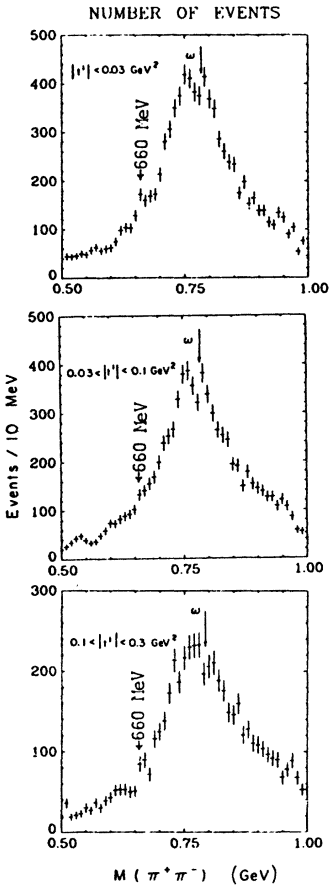

FIG. 18. The $\pi\pi$ cross-section data of Ref. 155 (see Ref. 159) broken down into components of the momentum transfer $|t'|$. As can be seen, an anomaly occurs at 660 MeV which shows a dependence on momentum transfer. From the relationship $|\vec{r}\times\vec{p}| = [L(L+1)]^{1/2}\hbar$, where r = impact parameter ~1 fermi, $\vec{p}$ = linear momentum transfer, and $\hbar = 197$ MeV/c fermi, the value $L \simeq 1$ corresponds to $|\vec{p}| \sim 0.3$ GeV/c. Hence $|t'| \sim |\vec{p}|^2 \sim 0.1$ (GeV/c)^2 sets the scale for the magnitude of $|t'|$ values over which changes in the production of the (spin-1) 660-MeV enhancement should be expected to occur. In the present model, this 660-MeV $\pi\pi$ enhancement is identified with the 660-MeV bandhead shown in Fig. 4.

A. Predictions and verifications

One of the most convincing aspects a theoretical model can possess is a demonstrated ability to predict the results that are obtained by extending and clarifying the experimental data. Two facets of the present light-quark phenomenology that lend themselves to clear-cut spectroscopic predictions are the systematics of the S-state resonances and the systematics of the rotational bands. We summarize here some predictive successes that have been obtained during the past few years from both of these facets.

A number of verified predictions have emerged from the systematics of the meson excitation tower of Fig. 6 and the baryon excitation towers of Fig. 3. The predictions themselves are straightforward: Narrow-width S-state resonances appear at accurate 70-MeV intervals (with some gaps) above the fundamental "ground states" $\dot{S}\dot{S}(658)$, $N(939)$, $\Lambda(1116)$, $\Sigma(1193)$, and $\Xi(1321)$.

Perhaps the most striking predictive successes have occurred in the meson excitation tower of Fig. 6—which is a compilation of narrow-width levels that appear at 70-MeV intervals above the $\dot{S}\dot{S}(658)$ ground state (this ground-state energy is determined experimentally from Fig. 8 in Ref. 14). This meson excitation tower was first published in Table I of Ref. 5. At that time, it contained only eleven of the seventeen levels shown here; the six levels in Fig. 6 which are labeled with double asterisks have appeared subsequent to the publication of Ref. 5. Also, four other levels in Fig. 6 labeled with single asterisks (*a–*d) have had significant additions to the data, as are discussed in the caption to Fig. 6. In fact, the systematics of the meson tower excitations led to the prediction of the existence of the $\dot{S}\dot{S}$ ground state itself[160] prior to the first reliable experimental evidence[39] for such a state, and attention was directed[160] to the relationship between the elusive 658-MeV, spin-1 $\dot{S}\dot{S}$ state and the even more elusive 1310-MeV, spin-2 $\dot{S}\dot{S}\dot{S}\dot{S}$ A_2 dip (for which at least some experimental evidence still persists[40]). In summary, of the seventeen levels shown in Fig. 6, ten levels have either appeared initially or have had significant experimental clarifications subsequent to the time when this meson tower was first published. In assessing the predictive powers of Fig. 6, the nonappearance of any notable counterexamples[161] is as significant as the appearance of the six new double asterisk levels.

TABLE XXXII. Dominant baryon and hyperon rotational bands. A comparison of early (1969–1970) and recent (1974) observed resonances and level assignments. This comparison illustrates a number of predictive successes.

			Observed rotational levels					
Rotat. band	Year	Calc. mass	S	P	D	F	G	H
$N\dot{3}\dot{3}$	1969[a]	1350	···	$N(1470)P$[d]	$N(1520)D$	$N(1690)F$	···	···
	1974[b]	1359	···	$N(1419)P$[d]	$N(1520)D$	$N(1687)F$	···	$N(2241)H$
$N\dot{4}\dot{4}$	1969[a]	1487	···[e]	$N(1470)P$[d]	$N(1680)D$	···	···	···
	1974[b]	1499	$N(1508)S$	$N(1530)P$[d]	$N(1672)D$	···	$N(2130)G$	···
$\Lambda\dot{3}\dot{3}$	1970[c]	1530	$\Lambda(1518)D$	···	$\Lambda(1690)D$	$\Lambda(1865)F$	$\Lambda(2080)G$	$\Lambda(2351)H$
	1974[b]	1536	$\Lambda(1518)D$	$\Lambda(1570)P$	$\Lambda(1688)D$	$\Lambda(1819)F$	$\Lambda(2100)G$	$\Lambda(2350)H$
$\Lambda\dot{4}\dot{4}$	1970[c]	1672	$\Lambda(1673)S$	$\Lambda(\sim1750)P$	$\Lambda(1835)D$	$\Lambda(2020)F$		
	1974[b]	1676	$\Lambda(1673)S$	$\Lambda(\sim1737)P$	$\Lambda(1827)D$	$\Lambda(2020)F$		
$\Sigma\dot{3}\dot{3}$	1970[c]	1601	$\Sigma(1619)$[f]	$\Sigma(1670)$[g]	$\Sigma(1766)D$	$\Sigma(1909)F$	$\Sigma(2120)G$	
	1974[b]	1613	$\Sigma(1620)S$	$\Sigma(1669)P$	$\Sigma(1765)D$	$\Sigma(1910)F$	$\Sigma(2090)G$	
$\Sigma\dot{4}\dot{4}$	1970[c]	1743	$\Sigma(1750)S$	$\Sigma(\sim1880)P$	$\Sigma(1910)D$	$\Sigma(2041)F$	$\Sigma(2253)G$	$\Sigma(2455)H$
	1974[b]	1753	$\Sigma(1756)S$	$\Sigma(\sim1840)P$	$\Sigma(\sim1900)D$	$\Sigma(2030)F$	$\Sigma(2250)G$	$\Sigma(2455)H$

[a] Reference 162.
[b] Present paper.
[c] Reference 163.
[d] For a discussion of the prediction of this split Roper resonance, see Ref. 90.
[e] The existence of an S state was predicted on the basis of an inelastic dip.
[f] This state appeared as a production peak with no spin identification.
[g] This state was predicted to be a P state from the experiment of Aguilar 70, but prior to the confirmation by Kim 71 and Vanhorn 72; see Ref. 111.

In the baryon and hyperon excitation towers of Fig. 3, recent experimental refinements have also been in agreement with the systematics suggested in the figure. Although the $\Delta(1149)$, $N(1219)$, and $N(1359)$ levels that are indicated in brackets in Fig. 3 are unobserved levels, a possible direct indication of the $\Delta(1149)$ level has been reported,[137] an $N(\sim1300)P$ resonance, which clearly corresponds to the unseen $N(1219)$ bandhead, has been identified by several groups,[89] and the lower half of the split Roper resonance, $N(1419)P$ (Ref. 79; see Table XXXII and Refs. 162, 163, 90, and 111), which has been clarified recently as a resonance,[78] corresponds to both the unseen $N(1359)$ bandhead and the peak observed in the dozen production experiments listed in Ref. 79. The systematics of the unobserved S-state baryon bandheads of Fig. 3 and the observed overlying P-state rotational levels is illustrated in the following compilation:

$$\begin{aligned} &\Delta(1149)S \dashrightarrow \Delta(1233)P, \\ &N(1219)S \dashrightarrow N(1300)P, \\ &N(1359)S \dashrightarrow N(1419)P. \end{aligned} \tag{43}$$

In addition to these baryon S-state resonances, the observed $N(1508)S$ resonance, which has been reported with a wide range of both energies and widths,[25] has recently been clarified in several phase-shift analyses (see Table III) as a rather narrow-width resonance centered at about the expected energy from Fig. 3—1499 MeV. Although the predicted $\Lambda(1327)$ resonance shown in Fig. 3 has officially been proclaimed as a "dead" resonance in RPP73 (Ref. 25) because it does not appear in a number of expected channels, the author is nevertheless of the opinion that the original measurements of this resonance[25] will turn out to be reproducible experiments (see Refs. 8, 103, 125); an explanation for the difficulty in observing this resonance is given in Appendix A. Another resonance which has officially been declared "dead" in RPP73, namely, $\Sigma(1440)$, is a resonance that does *not* fit into the systematics of Fig. 3, whereas a neighboring resonance, $\Sigma(1472)$, which does fit Fig. 3 has survived. The $\Sigma(1620)$ resonance, which appeared in the original publication of this hyperon excitation tower (Table II of Ref. 4) with no spin identification (see Table III of Ref. 4), has now been identified[25] as an S-state resonance. The suggested $\Sigma(1682)$ resonance of Fig. 3 has received some support as an S state by a recent analysis of Van Horn[25] (see the discussion in Appendix D). The resonances $\Lambda(1827)S$ and $\Sigma(\sim1900)S$ have appeared recently (Refs. 96 and 115, respectively), although their positions are experimentally very uncertain, and the values for the masses shown

in Fig. 3 are more in the nature of predictions than of verifications (see Appendix D). Finally, the narrow-width $\Xi(1606)$ resonance has appeared quite recently (see Table VII) with the proper mass to complete the $\dot{4}$ excitation row of Fig. 3. In summary, of the 21 excitation levels shown in Fig. 3, nine have appeared or have been experimentally clarified since the first publication[4] of this baryon excitation scheme [although two of these nine levels, $\Lambda(1827)$ and $\Sigma(1900)$, do not as yet add anything of statistical significance to the 70-MeV level spacings of Fig. 3]. As in the case of the meson levels of Fig. 6, no counterexamples to the systematics of Fig. 3 have appeared among the recently identified experimental baryon and hyperon S-state resonances, whose compilation gives us the systematics of Fig. 3.

One of the earliest light-quark predictions [Ref. 2(a)], that of the split Roper resonance,[90] is contained in the systematics of the baryon rotational levels. Table XXXII is a compilation of the dominant $N\dot{3}\dot{3}$, $N\dot{4}\dot{4}$, $\Lambda\dot{3}\dot{3}$, $\Lambda\dot{4}\dot{4}$, $\Sigma\dot{3}\dot{3}$, and $\Sigma\dot{4}\dot{4}$ rotational bands, shown as they appeared in the years 1969 ($N\dot{3}\dot{3}$ and $N\dot{4}\dot{4}$, Ref. 162) and 1970 ($\Lambda\dot{3}\dot{3}$, $\Lambda\dot{4}\dot{4}$, $\Sigma\dot{3}\dot{3}$, and $\Sigma\dot{4}\dot{4}$, Ref. 163), and as they appear in 1974 (the present paper). As can be seen in Table XXXII, the predicted split Roper resonance has now materialized. Also, the states $N(1508)S$, $N(2130)G$, $N(2241)H$, $\Lambda(1570)P$, $\Sigma(1620)S$, and $\Sigma(1669)P$, all of which are required in order to fill out the rotational levels, have subsequently been identified in phase-shift analyses. In addition to the baryon rotational levels shown in Table XXXII, a $\Delta(2160)G_{39}$ resonance has recently been reported[164] which accurately fills out the principal Δ rotational band of Table XIX, and, as mentioned above, the $N(\sim 1300)P$ rotational state has appeared as evidence for the unseen $N\dot{4}(1219)S$ ground state. In the meson rotational bands, the $\epsilon(\sim 800)$ $\Gamma \sim 150$ resonance has now been reported[47] with a mass and width that match those of the $\rho(770)$ $\Gamma 146$ resonance, which suggests that the ϵ meson is a $^3P_0$ counterpart of the $^1P_1$ ρ meson (see Table XXIV). Also, the identification of the $g(1680)$ meson as a spin-3 resonance fits in naturally with the rotational assignments of Table XXIV.

As one final predictive area for the present light-quark systematics, we cite the $\bar{p}n(1795)$ and $\bar{p}p(1925)$ resonances of Table XXIII. Although we have made heuristic use of the existence of the $\bar{p}n$ bound state to "derive" (or at least rationalize) the light-quark binding energies of Secs. IV and V, these binding energies were in fact deduced directly from the systematics of the hadron resonances (see Ref. 14, page 255) prior to the appearance of the $\bar{p}n$ results. Thus the $\bar{p}n$ bound state serves as a confirmation of the present systematics rather than as a necessary cornerstone for the formulation of the systematics; it is in a modest sense the Ω^- state of this light-binding-energy quark model. As Table XXIII shows, the $\bar{p}n(1795)\Gamma 8$ and $\bar{p}p(1925)\Gamma 8$ resonances appear to be related phenomena. The $\bar{p}p(1925)$ resonance was originally reported in RPP71 (Ref. 27) as a narrow-width resonance. After this interpretation was challenged (see the discussion in Ref. 42), the data were rebinned into wider bins in RPP72 (Ref. 26). However, recent experimental results[42] have confirmed the original interpretation of the $\bar{p}p(1925)$ enhancement as a narrow-width S-channel resonance, a result that is in agreement with present expectations.

As an example of a "theoretical" prediction, the spinor mass value $S = 325$ MeV was published (in Ref. 4) prior to the working out of the systematics of Table VIII, and well before the appearance of the $\bar{p}n$ bound-state experiment.

The predictions and verifications discussed above are summarixed in Table XXXIII, along with some predictions that have not yet been verified and some predictions from paper II. As can be seen in Table XXXIII, almost $\frac{1}{4}$ of the experimental resonances of Tables I–VII serve in one way or another as recent predictive examples of the present light-quark hadron spectroscopy. It should be noted that this new experimental information does not seem to add significantly to the successes of either the SU(3) or SU(6) formalisms in accounting for the observed spectrum of hadron resonances.

B. Accuracy of mass calculations for rotational resonances

A uniform set of calculated rotational energies for the meson and baryon rotational resonances can be obtained by the following procedure. The universal $E_{\rm rot}$ curve in Fig. 10 (the dashed line) is used as the definition of the function $E_{\rm rot}^{\rm univ}(E_0)$, where E_0 is the bandhead energy. Then the (S-state) bandhead energies E_0 for the rotational bands are taken from Tables XV, XVI, XVIII, XIX, XXIV, and XXVII and are inserted together with the $E_{\rm rot}^{\rm univ}(E_0)$ values and the resonance L values into the equation

$$E_{\rm res}^{\rm calc}(E_0, L) = E_0 + E_{\rm rot}^{\rm univ}(E_0) L(L+1). \tag{44}$$

These values for $E_{\rm res}^{\rm calc}$ are then compared to the experimental resonance energies. The results of this calculation for all of the rotational levels included in the present paper are summarized in Table XXXIV. As can be seen in Table XXXIV,

TABLE XXXIII. Predictions and fulfillments. Subsequent to the publication of Refs. 3–6, almost $\frac{1}{4}$ of the 130-odd resonances of Tables I–VII have emerged in one form or another as predictive examples of the present light-quark phenomenology. Here we first summarize these predictive achievements (which are discussed in detail in Sec. XIA), and then we list a number of other results that are predicted from the systematics of the present paper and which still await definitive experimental verification.

Fulfillments

10 of 17 S-state meson resonances shown in Fig. 6
9 of 21 S-state baryon resonances shown in Fig. 3.
6 of 24 baryon rotational levels shown in Table XXXII.
The $N(\sim 1300)P$ and $\Delta(2160)G$ baryon rotational levels shown in Table XX.
The $\epsilon(\sim 800)\,^3P_{00}$ and $g(1680)F$ meson rotational levels shown in Table XXIV.
The $\bar{p}n(1795)$ and $\bar{p}p(1925)$ resonances shown in Table XXIII.
Total: 31 resonances.

Predictions

(1). Narrow-width $\pi\pi((660)$ spin-1 and $A_2(1310)$ spin-2 interference effects (dips or peaks) exist as reproducible effects in certain experiments.

(2). The $\pi_N(975)\Gamma 60$ meson exists as a broad-width $J^P = 1^-$ resonance; the DEF, if it has a width $\Gamma > 50$ MeV, is a spin-1 resonance; and the $\delta^-(962)$ possibly exists as a narrow-width ($\Gamma < 5$ MeV) $J^P = 0^-$ resonance.

(3). The $\eta_N(1076)\Gamma 98$, $\rho^0\rho^0(1410)\Gamma 90$, and $K_S K_S(1412)\Gamma 100$ are spin-2 resonances.

(4). The $E(1416)$ resonance will be observed with a narrow width ($\Gamma \sim 20$ MeV).

(5). The $f'(1516)$ has a broad width ($\Gamma \sim 100$ MeV).

(6). The $\Lambda(1327)$ resonance is not "dead."

(7). The $\Sigma(1472)$ is an S-state resonance.

(8). The $I = 1$ resonances $\pi_N(1016)\Gamma \sim 25$ and $X^-(1153)\Gamma 16$ both exist.

(9). The ϕ meson as observed in its $\pi\pi\pi$ decay mode is about 10 MeV lower in energy and has a broader width than the ϕ as observed in its KK decay mode; the $\pi\pi\pi$ decay mode corresponds to the H meson.

(10). The M meson (from its symmetric production mode) is the fundamental ground state of the η' multiplet, and the $M(953)$, $\eta'(958)$, and $\delta^0(963)$ members of the multiplet have accurate 5-MeV energy spacings.

(11). Narrow-width peaks $\Delta(1149)$ and $N(1219)$ will be observable in certain experiments.

(12). The missing levels in the rotational bands of Table XX will appear.

(13). The Roper resonance is split.

(14). The ρ meson has identifiable $L < 1$ and $L > 1$ angular momentum components for energies $E < 770$ MeV and $E > 770$ MeV.

(15). From the calculations of hyperon mass splittings in Paper II, two magnetic-moment conclusions are obtained: (1) The $\Xi^- - \Xi^0$ mass splitting suggests that the Ξ^- and the neutron have similar magnetic moments[a]; (2) the $\Sigma^- - \Sigma^0$ and $\Sigma^0 - \Sigma^+$ mass splittings suggest that these particles all have similar magnetic moments.[b]

[a] This conclusion seems to be in accord with the measurement of Cool *et al.*[165]

[b] In the present model, the most straightforward way to reproduce the $\Sigma^0 - \Sigma^+$ and $\Sigma^- - \Sigma^0$ mass splittings is to assume that the Σ^+, Σ^0, and Σ^- resonances are the configurations $S_\uparrow^+ S_\uparrow^- S_\uparrow^+ 4^0$, $S_\uparrow^+ S_\downarrow^- S_\uparrow^+ 4^-$, and $S_\uparrow^+ S_\downarrow^- S_\downarrow^+ 4^=$, respectively [see Eq. (49); also see Ref. 24]. This leads to the prediction that the Σ^+, Σ^0, and Σ^- all have comparable magnetic moments: $\mu_\Sigma \simeq \mu_p \simeq 2.8\,\mu_N$. Although the Σ^+ fulfills this expectation, the Σ^- has recently been reported [J. Fox *et al.*, Phys. Rev. Lett. 31, 1084 (1973)] with magnetic moment that is in the range $-1.6 < \mu < 0.8\,\mu_N$, and hence is in disagreement with this prediction. However, in the Fox experiment, the use of 34 degrees of freedom to fit one peak gives a χ^2 value of 50, which is statistically unacceptable and obscures the interpretation of their result.

the energies of 74 rotational resonances are calculated in this manner to an average absolute accuracy of ±1.4%, which is within the range of experimental accuracies to which most of these resonances are known. The mass accuracies shown in Table XXXIV indicate that the assumed $L(L+1)$ energy splitting for hadron rotational levels is experimentally correct. They also indicate that all types of resonance—meson, kaon, baryon, and hyperon—have the same geometrical features, since we use one universal moment-of-inertia function $E_{\rm rot}^{\rm univ}(E_0)$ to fit all of these resonances. This is another argument in favor of the universality of the light-quark hadron basis set 1, 3, 4, 7, S.

TABLE XXXIV. Summary of mass calculations for the meson (Fig. 6) and baryon (Fig. 3) S-state excitation towers, and for the meson (Table XXIV), kaon (Table XXVII), baryon (Tables XVIII and XIX), and the hyperon (Tables XV and XVI) rotational levels. The calculated mass values for the excitation towers are simply the 70-MeV mass grids that are erected on the identified $S\bar{S}$, N, Λ, Σ, and Ξ "ground states." The calculated mass values for the rotational levels are obtained from the rotational energy equation, Eq. (44), using experimental S-state energies, and using the dashed-line curve in Fig. 10 for the theoretical moments of inertia. As can be seen, the 34 S-state excitations have average calculated mass accuracies of about 0.5%, and the 74 rotational levels have accuracies of about 1.4%. The last column shows that the observed experimental levels in Figs. 3 and 6 have vanishingly small probabilities of representing random mass distributions (see the calculations in the text). Precision (±0.1%) absolute mass values for the tightly bound hadronic resonances (π, η, η' multiplet, $N, \Lambda, \Sigma, \Xi, \Omega$) are calculated in paper II.

Experimental resonances				Mass accuracy		
Number	Type	Where described	Basis for mass calculation	Absolute	Percent	Random probab.
			Narrow-width S-state resonances			
18	N-W baryons	Fig. 3	70-MeV levels	±8.2 MeV	±0.51%	1×10^{-6}
16	N-W mesons	Fig. 6	70-MeV levels	±6.5 MeV	±0.57%	1×10^{-7}
			Broad-width rotational resonances			
21	Mesons	Table XXIV	Eq. (44)	±10.0 MeV	±0.95%	
10	Kaons	Table XXVII	Eq. (44)	±15.6 MeV	±0.95%	
12	N^* baryons	Table XVIII	Eq. (44)	±51.6 MeV	±2.82%	
8	Δ baryons	Table XIX	Eq. (44)	±25.6 MeV	±1.26%	
11	Λ hyperons	Table XV	Eq. (44)	±31.7 MeV	±1.57%	
12	Σ hyperons	Table XVI	Eq. (44)	±23.6 MeV	±1.19%	
			Summary: 34 S states = ±0.54%; 74 rotational levels = ±1.42%.			

C. Resonances that are predicted but not observed

The main properties of the hadronic basis set 1, 3, 4, 7, S are summarized in Table XXXV, points A–C; the combinations of these basis states that are actually observed experimentally, and also the combinations that are not observed, are listed in Table XXXV, points D–M. As can be seen in D–M, many, but by no means all, of the possible basis-state combinations are identifiable in the experimental data. The task thus becomes one of formulating selection rules to account for the basis-state combinations that are not observed. A set of selection rules for reproducing the observed spectrum of S-state meson resonances is given in Table XXII, and selection rules for mapping the S-state baryon and hyperon resonances are given in Eq. (29). Meson and baryon rotational-level selection rules are listed in Table XII. A production-mechanism selection rule which eliminates the unobserved $S\bar{S}S\,\bar{3}\,\bar{4}$ and $S\bar{S}S\,\bar{4}\,\bar{4}\,\Xi$-type metastable hyperon excitations is discussed in paper II. Since these basis-state selection rules are in general deduced *a posteriori*, it is not an easy task to accurately evaluate their physical content. However, the two main features to be observed in connection with Table XXXV are the following: (1) A common set of basis states—1, 3, 4, 7, S—is relevant for all types of hadron resonance structure; (2) although not all combinations of these basis states actually occur, the phenomenological patterns for those combinations which do occur and for those which do not occur seem to be simple and straightforward.

D. Observed resonances that are not mapped

The experimental resonances that have been accepted by the Particle Data Group for inclusion in RPP73 (Ref. 25) are summarized in Fig. 19, which is reproduced from Ref. 25. Of these resonances, the ones which are not included in the present mapping formalism are shown enclosed in boxes. As is summarized in the caption to Fig. 19, 63 out of the 85 baryon resonances in Fig. 19 are mapped in the present paper, and 44 out of the 55 meson resonances in Fig. 19 are mapped. However, of the 22 baryon resonances and 11 meson resonances that are not mapped, only one baryon resonance, $\Sigma(2070)F_{15}$, and one meson resonance, $B_1(1040)$, are excluded on the basis that they do not fit the present systematics. Essentially all of

TABLE XXXV. Combinations of the basis states $1,3,4,7,S$ which are, and which are not, observed as resonances. A brief definition and summary of the basis states $1,3,4,7,S$ is given. This is followed by a systematic classification of the possible combinations of these states, with statements as to which combinations seem to occur experimentally and which combinations do not seem to occur.

A. The fundamental hadronic basis set

M^0, $\overline{M}^0 = 70.0$ MeV; $M^{\pm} = 74.6$ MeV; $S^{\pm} = 330.6$ MeV [Eq. (10) and paper II];

$1 \equiv M$, $3 \equiv 3M$, $4 \equiv 4M$, $7 \equiv 7M$ $S \equiv (3M)_{\text{spinning}}$.

B. Particle-antiparticle states [Eq. (11)]

$\mathrm{ST} \equiv$ strange—all quanta $M: \rightarrow 1,3,4,S$—strangeness $= +1$;

$\overline{\mathrm{ST}} \equiv$ antistrange—all quanta $\overline{M}: \rightarrow \overline{1},\overline{3},\overline{4},\overline{S}$—strangeness $= -1$;

$\mathrm{NS} \equiv$ nonstrange—mixed quanta M and $\overline{M}: \rightarrow \dot{3},\dot{4},\dot{S}$—strangeness $= 0$;

kaon $= 7 \equiv 3\dot{4}$ or $\dot{3}4$, antikaon $= \overline{7} \equiv \overline{3}\dot{4}$ or $\dot{3}\overline{4}$.

(The *invariant* "strangeness" of the spinors S and $\overline{S}$ is discussed in Sec. V.

C. Hadronic binding energy rules [Eq. (12) and paper II]

$\mathrm{ST} \cdot \mathrm{ST} = \overline{\mathrm{ST}} \cdot \overline{\mathrm{ST}} = 0$—no hadronic binding;

$\mathrm{ST} \cdot \overline{\mathrm{ST}} =$ dominant—~4% hadronic binding;

$\mathrm{NS} \cdot$ all = subdominant—~0% hadronic binding.

D. Basis states observed singly

$(1)_{\text{spinning}}$ (expanded geometry) $= \mu$ meson; $7 =$ kaon;

$3,4,S$ (quark) not observed singly.

E. Basis states observed in pairs

$1\overline{1} = \pi$, $4\overline{4} = \eta$, $7\overline{7} = \eta'$ multiplet [Fig. 1 and Eq. (13)].

$\dot{S}\dot{S} = \pi\pi(660)$, $\dot{S}\dot{S} \cdot \dot{S}\dot{S} = A_2$ dip (Tables I and XXIII).

$3\overline{3}$, $S\overline{S}$, $\dot{1}\dot{1}$, $\dot{3}\dot{3}$, $\dot{4}\dot{4}$, $\dot{7}\dot{7}$ not observed.

F. Basis states observed in triplets

$S\overline{S}S = N$, $\overline{S}S\overline{S} = N$, $S\overline{S}S \cdot \overline{S}S\overline{S} = \overline{p}n$ [Eqs. (5) and (6)]. $\dot{S}\dot{S}\dot{S}$ not observed.

G. Strange baryon excitations

Rule: excitations $= S\overline{S}S$ plus spinless states $\overline{3}$ and $\overline{4}$.

$S\overline{S}S\overline{3} = \Lambda$, $S\overline{S}S\overline{4} = \Sigma$, $S\overline{S}S\overline{33} = \Xi$, $S\overline{S}S\overline{344} = \Omega$ [Eq. (14) and paper II].

$S\overline{S}S\overline{34}$, $S\overline{S}S\overline{44}$, $S\overline{S}S\overline{333}$, $S\overline{S}S\overline{334}$ not observed.

H. Meson excitation tower

Rule: excitations $= \dot{S}\dot{S}$ plus spinless 70-MeV quanta (Fig. 6, Table XXIII).

Figure 16 shows narrow levels for $\dot{S}\dot{S} + N \times 70$, $N = 1$–13.

Levels at $N = 10$ and 12 missing; levels at $N = 1,3,4,6,8$ are weak.

I. Baryon and hyperon excitation towers

Rule: excitations $= N$, Λ, Σ, and Ξ plus spinless states $\dot{3}$ and $\dot{4}$ [Eq. (29)].

Observed levels (Figs. 3 and 8, Table XIV):

$[N\dot{3}]$, $[N\dot{4}]$, $[N\dot{3}\dot{3}]$, $N\dot{4}\dot{4}$, $N\dot{3}\dot{3}\dot{4}$, $N\dot{3}\dot{4}\dot{4}$;

$\Lambda\dot{3}$, $\Lambda\dot{4}$, $\Lambda\dot{3}\dot{3}$, $\Lambda\dot{4}\dot{4}$, $\Lambda\dot{3}\dot{3}\dot{4}$, $\Lambda\dot{3}\dot{3}\dot{4}\dot{4}$; $\Sigma\dot{3}$, $\Sigma\dot{4}$, $\Sigma\dot{3}\dot{3}$, $\Sigma\dot{3}\dot{4}$, $\Sigma\dot{4}\dot{4}$, $\Sigma\dot{3}\dot{3}\dot{4}$; $\Xi\dot{3}$, $\Xi\dot{4}$, $\Xi\dot{3}\dot{4}$, $\Xi\dot{3}\dot{3}\dot{3}$, $\Xi\dot{3}\dot{3}\dot{4}\dot{4}$.

Levels not observed: $N\dot{3}\dot{4}$, $\Lambda\dot{3}\dot{4}$, $N\dot{3}\dot{3}\dot{3}$, $\Lambda\dot{3}\dot{3}\dot{3}$, $\Sigma\dot{3}\dot{3}\dot{3}$, $\Xi\dot{3}\dot{3}$, $\Xi\dot{4}\dot{4}$; $[N\dot{3}]$, $[N\dot{4}]$, $[N\dot{3}\dot{3}]$ are identified only via overlying rotational levels [Fig. 5 and Eq. (43)].

TABLE XXXV *(Continued)*

J. Meson rotational levels

Figure 7 and Tables XXIV–XXIX.

K. Baryon rotational levels

Figure 5 and Tables XV–XX.

L. Mapping the boson resonances

D, E, and H map the observed S-state resonances; missing levels are as noted above.

J maps the observed rotational resonances; missing levels are the following: $\pi\pi(350)S$, $\pi\pi(420)S$, $\epsilon(\sim 900)P$, $\epsilon(1400)P$, $\epsilon(\sim 1500)P$, $Q(\sim 1510)D$, $Q(\sim 1610)D$, $K(\sim 1550)S$, $K(\sim 1625)P$.

M. Mapping the fermion resonances

F, G, and I map the observed S-state resonances; missing levels are as noted above.

K maps the observed rotational resonances; missing levels are the following: $N(1219)S$, $N(1359)S$, $N(1919)G$, $N(1856)F$, $\Delta(1149)S$ (but see Ref. 137), $\Delta(1508)S$, $\Delta(1570)P$.

L, M. Two general rules for mapping boson and fermion resonances

Rule I. The stablest hadron resonances (with the possible exception of the linear kaons) are formed entirely from strange and antistrange basis states; they do not contain nonstrange basis states.

Rule II. Hadron rotational bands are formed only from bandheads which contain nonstrange basis states; the stable resonances of rule I, which do not contain nonstrange basis states, do not have associated rotational levels.

the remaining unmapped resonances are high-energy levels, and most of them lack spin identification. The existence of these high-energy levels is an indication that the S-state excitations and associated rotational levels of Figs. 8 and 9 extend up to higher energies than we have included here. However, the high-energy data are too fragmentary at the present time to permit them to be mapped accurately. In particular, spin identification is essential before any sorting into rotational levels can be carried out. It is this same lack of spin identification that precluded any attempts at sorting the lower-energy Ξ resonances into rotational bands; thus Table VII contains only the narrow-width and therefore rotationless Ξ excitations.

E. Statistical evidence for the mass quantum $M = 70$ MeV

Perhaps the principal conclusion from the present paper is that the mass quantum $M = 70$ MeV is the fundamental building block for all of the hadronic resonances. Since such a quantum has never been observed directly, it is of some interest to summarize the statistical evidence from the present studies which points to the existence of this mass quantum. Phenomenological compilations of experimental data which can be used to pinpoint the M^0 mass right at 70 MeV are summarized in paper II.

Figure 8 is a plot of all of the narrow-width and S-state resonances of Tables I–VII. A visual comparison of the experimental resonance spacings with the 70-MeV tick marks shown in Fig. 8 indicates that these resonances do obey 70-MeV interval spacings. To put this result on a quantitative basis, we can study in detail a portion of Fig. 8, namely the baryon excitation towers shown in Fig. 3 and the meson excitation tower shown in Fig. 6. If the 70-MeV mass intervals are not physically significant, then these resonances should be randomly spaced with respect to the 70-MeV mass grids erected on the N, Λ, Σ, Ξ, and $\pi\pi(658)$ "ground states." A random spacing will give resonances that are, on the average, displaced 17.5 MeV from the 70-MeV grid values. In Fig. 3 the 18 experimental baryon excitation levels have an average displacement of ± 8.2 MeV, and in Fig. 6 the 16 experimental meson excitation levels have an average displacement of ± 6.5 MeV, as is summarized in Table XXXIV. The probabilities for these being random distributions are $(8.2/17.5)^{18} = 1\times 10^{-6}$ and $(6.5/17.5)^{16} = 1\times 10^{-7}$, respectively. Thus, there is no way that the observed level spacings of Figs. 3 and 6 can be regarded as random, especially when the completeness as well as the accuracy of these resonance mappings is taken into consideration.

It might be argued that we have included in Figs. 3 and 6 a number of resonances which are not well established experimentally. However, to

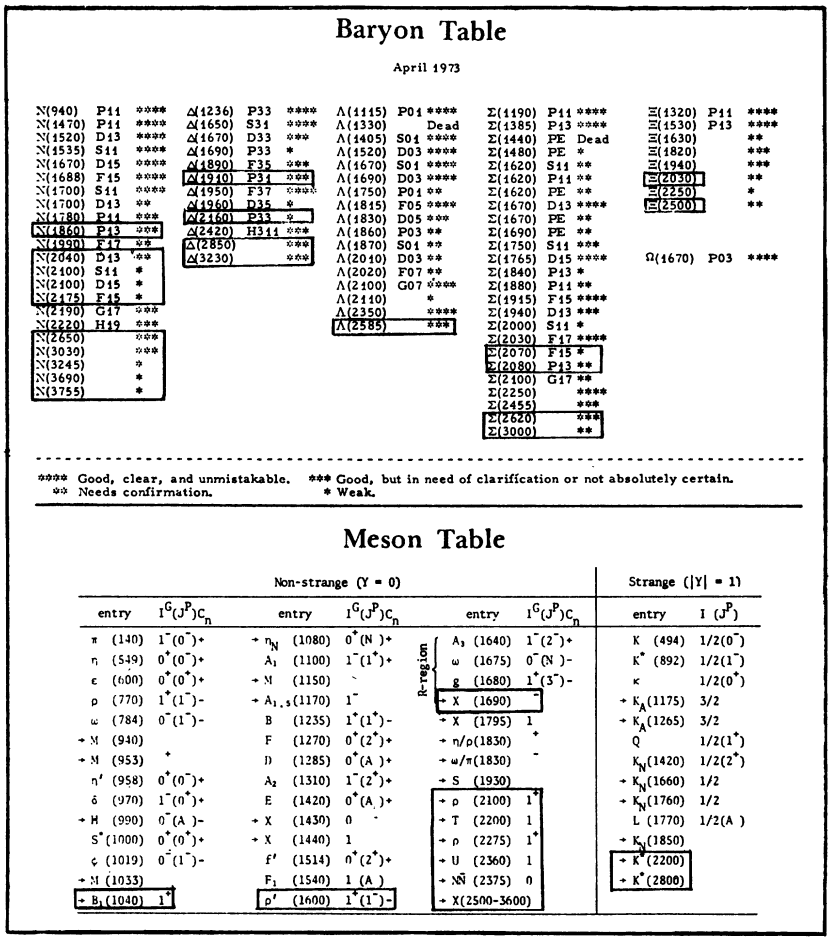

FIG. 19. A mapping summary of the hadron resonances listed in RPP73 (Ref. 25). The baryon and meson tables are reproduced from Ref. 25, and the resonances enclosed in boxes are not included in the present mapping tables. However, only two resonances are excluded on the basis of a poor fit. A summary of the resonances is as follows.

	Baryon	Meson
Total resonances	85	55
Total mapped	63	44
Total not mapped	22	11
Breakdown of the resonances that are not mapped		
High energy, no spin values	12	9
S–F levels, but too high to map accurately	8	
"Dead" resonances	1 Σ(1440)	
Ambiguous resonances (very broad width)		1 $\rho'(1600)\Gamma 350$
Resonances that do not fit the present levels	1 $\Sigma(2070)F_{15}$	1 $B_1(1040)$

take an extreme example, if we were to arbitrarily delete half of the levels from each of these figures, the statistical odds in favor of random spacings would still be no more than 10^{-3} for each of these figures, and the completeness argument would be just as compelling. Moreover, most of the observed deviations from the 70-MeV mass intervals, especially for the higher-mass resonances, are in the downward direction, and thus are indicative of small binding-energy effects. If a correction for these effects were to be inserted, the statistical evidence against random spacings would be even stronger than is shown here.

XII. LIFETIME SYSTEMATICS

The lifetimes of the long-lived ($\tau > 10^{-17}$ sec) elementary particles are of interest here because this totally different aspect of hadron spectroscopy points to the same type of light-quark hadron sub-

structure that we have already deduced from the systematics of Secs. II–XI. The phenomenological characteristics of metastable particle lifetimes were analyzed in detail in Ref. 19, and we summarize here only the salient features of that analysis.

A. Lifetime ratios as factors of 2

Figure 20 shows a logarithmic plot of the lifetimes of the hadron resonances which are in the range $\tau \sim 10^{-8}$ to 10^{-10} sec, with the shortest lifetime, that of the Σ^+, set equal to unity. As can be seen in Fig. 20, the $K^\pm$, $\pi^\pm$, and K_L^0 resonances occur with the accurate lifetime ratios 1:2:4. Guided by this result, we have similarly arranged the K_S^0, Λ, Σ, Ξ, and Ω resonances of Fig. 20, and they also exhibit accurate 1:2 and 1:2:4 lifetime ratios.

From the standpoint of elementary-particle theories, the significant aspect of Fig. 20 is that the $K^\pm$, $\pi^\pm$, and K_L^0 resonances are grouped together into a single lifetime multiplet. These are supposed to be independent particles, and they have radically different decay modes.[19] Hence the observed lifetime ratios of 1:2:4 for these resonances cannot be attributed to factors such as final-state phase-space effects. From a statistical point of view, the occurrence of accurate 1:2:4 lifetime ratios for a set of resonances suggests the existence of 4:2:1 independent decay triggers, or 4:2:1 individual subquanta M which can spontaneously annihilate and initiate the decay process. Thus the lifetime relationships of Fig. 20 lead to the conclusion that these sets of particles possess common substructures. This is a conclusion that is in agreement with the systematics of the present paper, and it is a conclusion that stands independently of any results in the present paper. A suggested identification of specific subquanta M as plausible decay triggers for the $K^\pm$, $\pi^\pm$, K_L^0, and K_S^0 mesons is shown in Ref. 19.

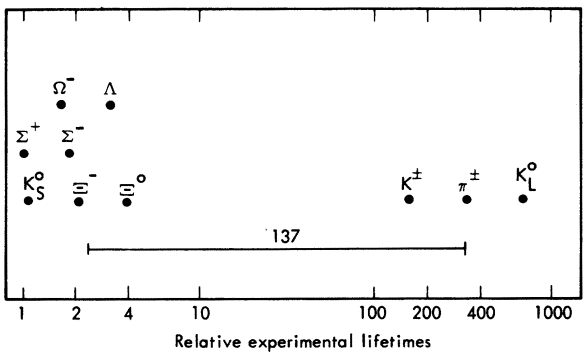

FIG. 20. Relative lifetimes of metastable meson and baryon resonances. The Σ^+ lifetime is set equal to unity. As is evident in this logarithmic representation, these lifetimes occur in accurate ratios of two, with supposedly dissimilar and independent particles grouped together. As discussed in the text, the occurrence of these experimental regularities indicates that the lifetime of a particle is an intrinsic property, and it does not depend, for example, on final-state phase space. It is important to note that there are no experimental counterexamples to the systematics shown here: This figure contains all of the metastable elementary particles that have lifetimes in the range $\tau \sim 10^{-8}$ to 10^{-10} second. As can be seen in the figure, the median values of the two groups of lifetimes are separated by about a factor of $\alpha^{-1} = 137$, where $\alpha = e^2/\hbar c$.

B. Lifetimes ratios as factors of $\alpha = e^2/\hbar c$

In Fig. 20 we have indicated that the two groups of particle lifetimes [$\tau \sim 10^{-8}$ sec $(K^\pm, \pi^\pm, K_L^0)$ and $\tau \sim 10^{-10}$ sec $(K_S^0, \Lambda, \Sigma^+, \Sigma^-, \Xi^0, \Xi^-, \Omega^-)$] are separated by roughly the factor $\alpha^{-1} \simeq 137$. In order to investigate whether or not this result is accidental, we can do two things: (1) Since the observed lifetime ratios of 1:2:4 shown in Fig. 20 are probably extraneous to any over-all scaling in powers of α, we can "medianize" these lifetimes[19] by applying the *ad hoc* correction factors

$$K^\pm \times 2,\ K_L^0 \div 2,\ K_S^0 \times 2,\ \Sigma^+ \times 2,\ \Lambda \div 2,\ \Xi^0 \div 2; \tag{45}$$

(2) we can add the neutron, muon, Σ^0, and π^0 resonances to the resonances of Fig. 20. With the addition of these resonances, we have included all metastable particles with lifetimes $\tau > 10^{-17}$ sec. Also, in going from the π^0 lifetime to the neutron lifetime, we are spanning a range of lifetimes equal to $\tau_{\text{neutron}}/\tau_{\pi^0} \simeq \alpha^{-9} \simeq 10^{19}$—a span of nine decades in α or 19 orders of magnitude. If we now set the neutron lifetime equal to unity, $\tau_n \equiv \tau_0 = 1$, and express the lifetime ratios τ_i/τ_0 in powers of α as

$$\tau_i = \tau_0 \alpha^{x_i}, \tag{46}$$

then an accurate scaling of lifetimes τ_i in powers of α is indicated by the occurrence of integral values for the exponents x_i in Eq. (46). Figure 21 shows the values for x_i that are obtained from Eq. (46) by using both (1) the experimental lifetimes τ_i of these resonances, and (2) the lifetimes as "medianized" in Eq. (45). As can be seen in Fig. 21, the x_i take on almost integral values over the entire span of lifetimes for both the experimental and the medianized data, with the medianization of the lifetimes improving the results only slightly. Since Fig. 21 includes *all* of the known metastable elementary particles, it is evident that there are no counterexamples to this scaling of lifetimes as powers of α, although there are gaps in the spacings.

The lifetime systematics of Figs. 20 and 21, in

which lifetime "multiplets" include supposedly dissimilar and independent particles grouped together, is a direct indication that these particles are in fact not independent of one another. The obvious way of linking these particles together is via a common substructure of quark states. Figure 21, the scaling of lifetimes as powers of $\alpha = e^2/\hbar c$, contains two other features that are of interest here. (1) The μ meson appears to fit in with the hadron resonances as a *bona fide* member of the group; (2) in analogy to the scaling of lifetimes as powers of α, we note the following scaling of particle masses as powers of α:

$$M_e/\alpha = 70.0 \text{ MeV} = M, \tag{47}$$

where M_e is the mass of the electron and M is the 70-MeV mass quantum that can be used to construct all elementary particles more massive than the electron.

ACKNOWLEDGMENT

The author would like to thank R. J. Howerton for his continued interest in this work.

APPENDIX A: SYMMETRY CHARACTERISTICS OF 3-TYPE AND 4-TYPE EXCITATIONS

In the baryon excitation towers of Fig. 3, the excitation basis states $3 \equiv 3M$ and $4 \equiv 4M$ were postulated in order to explain the observed gaps in the level spacings (see the far-left column in Fig. 3). However, these basis states possess a phenomenological significance that goes well beyond the task of just reproducing the levels of Fig. 3. The basis state $3 \equiv 3M$ differs from the basis state $4 \equiv 4M$ in that 3's necessarily have particle-antiparticle asymmetry, whereas 4's can occur symmetrically. When we examine excitations in Fig. 3 which contain 3's—$N3$, $N\dot{3}3$, $\Lambda 3$, $\Lambda\dot{3}3$, $\Sigma 3$, $\Sigma\dot{3}3$, $\Xi 3$—we find that they have quite different characteristics from excitations which contain 4's—$N4$, $N\dot{4}4$, $\Lambda 4$, $\Lambda\dot{4}4$, $\Sigma 4$, $\Sigma\dot{4}4$, $\Xi 4$. Excitations which contain (asymmetric) 3's tend to have one or more of the following characteristics:

(a) They are difficult to observed directly as S states;

(b) they are associated with γ-ray production and/or decay processes;

(c) they are associated with spinor-flip processes (e.g., they appear as narrow-width $J = \frac{3}{2}$ resonances).

Excitations which contain 4's usually do not have these characteristics. For example, the excitations $N\dot{4}\dot{4}$, $\Lambda\dot{4}\dot{4}$, and $\Sigma\dot{4}\dot{4}$ constitute the dominant and easily observed S-state resonances $N(1508)S$, $\Lambda(1673)S$, and $\Sigma(1756)S$. By way of contrast, the excitations $N\dot{3}\dot{3}$, $\Lambda\dot{3}\dot{3}$, and $\Sigma\dot{3}\dot{3}$ constitute the unseen $N(1359)$ bandhead of Table XVIII, the narrow-width $J = \frac{3}{2}$ resonance $\Lambda(1518)$, and the controversial $\Sigma(1620)S$ resonance. Similarly, the $\Lambda 4$ excitation is the dominant $\Lambda(1402)S$ resonance, whereas the $\Lambda\dot{3}$ excitation is the very weak $\Lambda(1327)$ resonance, which has been observed only as a $\Lambda\gamma$ final state. The $\Lambda\gamma$ decay mode of the $\Lambda\dot{3}(1327)$ is in agreement with the systematics of characteristics (a)–(c), as is the decay of the $\Lambda\dot{3}\dot{3}(1518)$, which has decays into both $\Lambda\gamma$ and $\Sigma^0\gamma$. The difficulty in observing the $\Lambda\dot{3}(1327)S$ resonance is paralleled by the difficulty in observing the $N\dot{3}(1149)S$ resonance, which is the unseen[137] bandhead of the $\Delta(1233)P$ resonance; the $\Delta(1233)P$ resonance has both a γ-ray

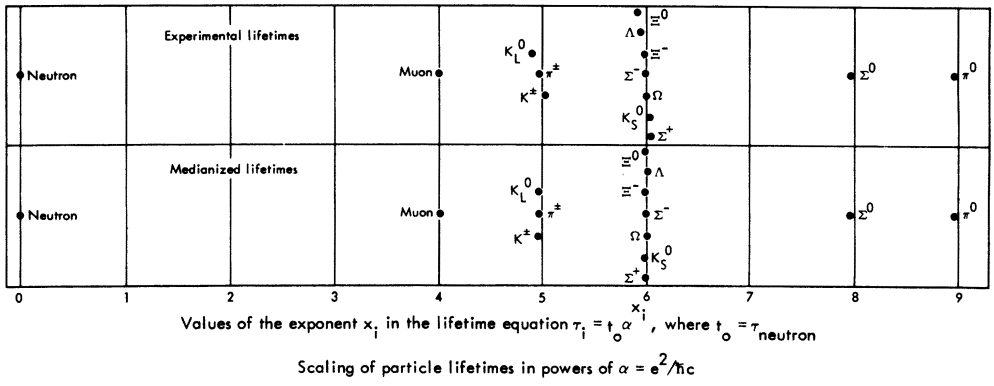

FIG. 21. Values of the exponent x_i for lifetimes expressed as $\tau_i = \tau_0 \alpha^{x_i}$, where τ_0 is the neutron lifetime and $\alpha = e^2/\hbar c$ is the fine-structure constant. Integral values for the x_i indicate that α is a relevant scaling factor for these lifetimes. The experimental lifetimes are from Ref. 1, and the "medianized lifetimes" are obtained by applying factor-of-two "corrections" to the lifetimes of Fig. 20 so as to obtain the median value for each group of lifetimes [see Eq. (45) in the text]. As can be seen, the lifetimes do occur with integral values for the x_i, over a span of 9 decades in α, or 19 orders of magnitude in the lifetime ratios. While there are gaps in the spacings shown, there are no counterexamples: This figure includes all of the reported metastable elementary particles with lifetimes greater than 10^{-17} second.

decay mode and a $J=\frac{3}{2}$ rotational configuration. The $\Lambda(1327)$ has been declared "dead" in RPP73 (Ref. 25) because it was not observed in several expected channels. However, from the above systematics, the difficulty in observing this $\Lambda\dot{3}$ excitation in all reaction channels is not surprising, and, unless the several experiments in which the $\Lambda\dot{3}$ was observed[25] turn out to be irreproducible,[125] the burial of the $\Lambda(1327)$ resonance in RPP73 may have been premature.

The three narrow-width $J=\frac{3}{2}$ hyperon resonances which have been identified experimentally[25] have the following configurations:

$$\begin{aligned}
&\Lambda(1518)=S_{\uparrow}\bar{S}_{\uparrow}S_{\uparrow}\bar{3}\dot{3}\dot{3}\,,\\
&\Xi(1535)=S_{\uparrow}\bar{S}_{\uparrow}S_{\uparrow}\,\bar{3}\dot{3}\dot{3}\,,\\
&\Sigma(1385)=S_{\uparrow}\bar{S}_{\uparrow}S_{\uparrow}\bar{4}\dot{3} \text{ or } S_{\uparrow}\bar{S}_{\uparrow}S_{\uparrow}\bar{3}\dot{4}\,.
\end{aligned} \tag{48}$$

Thus the $\Lambda(1518)$ and $\Xi(1535)$ excitations are both of the general type $SSS333$, and the $\Sigma(1385)$ resonance, whose identification is not phenomenologically as straightforward as that of the other two, contains a single 3 and a single 4. The $\Lambda(1518)$ has a decay mode into $\Sigma(1385)$, and the $\Sigma(1385)$ has a decay mode into $\Lambda\gamma$. The $\Xi(1535)$ has the sequential decay modes $\Xi(1535)\to\Xi+\pi$ and $\Xi\to\Lambda+\pi$, which in the present notation is the sequence $S\bar{S}S\bar{3}\dot{3}\dot{3}\to S\bar{S}S\bar{3}\dot{3}+\pi$, $S\bar{S}S\bar{3}\dot{3}\to S\bar{S}S\bar{3}+\pi$.

The symmetry characteristics of the 3-type and 4-type excitations can also be observed in the metastable baryon resonances. If we construct resonances whose magnetic moments have been determined, we obtain states with the following configurations.

State	Excitation structure	Strangeness	Spin-charge structure	Magnetic moment[165]	Spinor configuration
p	$S\bar{S}S$	$S=0$	$\uparrow\bar{\uparrow}\uparrow$	$\mu\sim+3$	Normal
n	$S\bar{S}S$	$S=0$	$\uparrow\bar{\downarrow}\uparrow$	$\mu\sim-2$	Spinor-flipped
Λ	$S\bar{S}S\bar{3}$	$S=-1$	$\uparrow\bar{\downarrow}\uparrow 3^{-}$	$\mu\sim-1$	Spinor-flipped
Σ^{+}	$S\bar{S}S\bar{4}$	$S=-1$	$\uparrow\bar{\downarrow}\uparrow\bar{4}^{0}$	$\mu\sim+3$	Normal
Ξ^{-}	$S\bar{S}S\bar{3}\bar{3}$	$S=-2$	$\uparrow\bar{\downarrow}\uparrow 3^{-}\bar{3}^{0}$	$\mu\sim-2$	Spinor-flipped

(49)

From the measured magnetic moments shown in (49), and also from the detailed calculations of masses and charge splittings in paper II, we can see that the excitations Λ and Ξ, which contain $\bar{3}$'s, correspond to spinor-flipped configurations, whereas the Σ excitation, which contains a $\bar{4}$, does not. With respect to the decay properties of the resonances shown in (49), we note that the Ξ decays are into Λ resonances and not into Σ resonances.

From the symmetry characteristics of the resonances of Fig. 3, Eq. (48), and Eq. (49), it seems clear that the symmetry differences between 3-type excitations and 4-type excitations extend to both the strange $(3,\bar{3},4,\bar{4})$ and nonstrange $(\dot{3},\dot{4})$ forms of these quanta. This indicates that these symmetry differences must involve quantum numbers such as parities in addition to the obvious particle-antiparticle differences.

APPENDIX B: SPECIAL-RELATIVISTIC EQUATIONS FOR ROTATING SYSTEMS

One of the challenges to elementary-particle spectroscopists is to account for the spin angular momentum of a particle. Conventionally, spin angular momentum is not thought of as arising from the (classical) rotation of an extended mass. However, if we rule out this concept of spin angular momentum, we are left with no quantitative spectroscopic explanation for the spin of a particle. Although the spin of the electron arises naturally as a component in the Dirac equations, these equations give no clue as to the geometry of the rotating electron.

In connection with the above discussion, the following observations about the nucleon and about theories of rotating systems seem relevant.

(a) The *only* elementary particle for which a size has been determined is the nucleon, which has a measured radius $R_{\rm rms}\simeq 0.8$ fermi;

(b) many arguments (for example, those of the quark model) suggest that the nucleon is composed of three nucleon subunits of approximately equal mass;

(c) in order to obtain an over-all nucleon rms radius of 0.8 fermi, spherical nucleon subunits must have radii $R_{\rm ns}\simeq 0.6$ fermi;

(d) from their assumed radii $R_{\rm ns}=0.6$ fermi and from the equation $R_{\rm ns}=\hbar/mc$, nucleon subunits have masses $m\simeq 330$ MeV (also see Table VIII);

(e) if we attribute classical moments of inertia,

$I=\frac{2}{5}mR^2$, to these nucleon subunits, and then spin each subunit until its equator reaches the velocity of light, the calculated angular momenta for these subunits are somewhat less than the assumed angular momentum $J=\frac{1}{2}\hbar$ of a nucleon quark;

(f) textbooks on special relativity indicate that special relativity applies to rotating systems as well as to linearly moving systems;

(g) for the rapidly-rotating nucleon subunits of (e), special-relativistic effects will constitute an important correction;

(h) by inserting a special-relativistic correction into (e), we obtain $J=\frac{1}{2}\hbar$ as a precisely-calculated quantity for these nucleon subunits;

(i) stresses and general-relativistic effects should in principle also be considered, but there are suggestions that these corrections may be of minor importance.

From the spectroscopy of the nucleon and the theory of spinning masses, as summarized in (a)–(i), it seems plausible that the spin angular momentum of a nucleon subunit is in fact associated in a straightforward manner with the rotation of an extended mass. By adding a freely-moving localized electric charge to a spinning nucleon subunit, we obtain an important extension of the above phenomenology:

(j) A unit electric charge e placed on a spinning spherical nucleon subunit of radius $R_{ns}=0.6$ fermi will be forced to the equator of the sphere by the action of the electromagnetic forces, where it will produce a magnetic moment $\mu=2.8$ nuclear magnetons, which is the same magnetic moment as the (intrinsic) magnetic moment that is conventionally assumed for a nucleon quark.[128]

Thus a spherical nucleon subunit that is spinning with its equator at the velocity of light, that has a radius $R=0.6$ fermi and a spinning mass $m=330$ MeV, and that contains an equatorial (unit) charge distribution, is identical to the conventional nucleon quark with respect to its mechanical and electromagnetic properties—mass, radius (range of force), angular momentum, magnetic moment.[166]

Our present interest in special relativity is in connection with the calculation of relativistic masses and relativistic moments of inertia. Before applying special relativity to *rotating* systems, it is of some importance to clarify the concept of the special-relativistic mass increase of a particle as observed in *linearly moving* systems. Although derivations of the relativistic mass equation

$$m=m_0/(1-v^2/c^2)^{1/2} \tag{50}$$

are usually obtained by invoking the Lorentz transformation equations, the relativistic mass of a particle is in fact a straightforward consequence of the proportionality between the total energy E of a particle and its inertial mass m,

$$E=mc^2, \tag{51}$$

and Eq. (50) can be derived directly from Eq. (51), as we now demonstrate.[167] Choosing the electron as a typical massive particle, let v be the linear velocity of the electron as observed in the laboratory frame of reference, and let $m(v)$ be the observed mass[168] of the electron, which depends functionally on the velocity v. Applying a linear impulse Fdx to the electron changes its velocity v, its energy E, and its observed mass $m(v)$:

$$\begin{aligned} dE &= Fdx \\ &= d/dt(mv)dx \\ &= vd/dx(mv)dx \\ &= v^2dm + mvdv \\ &= c^2dm, \end{aligned} \tag{52}$$

which leads to

$$\ln m(v) = -\tfrac{1}{2}\ln(c^2-v^2), \tag{53}$$

and, setting $m(0)\equiv m_0$, to the final result[169]

$$m=m_0/(1-v^2/c^2)^{1/2}. \tag{50}$$

The important point to note here is that Eq. (50) depends only on the energy content of a particle [Eq. (53)] as observed in a particular frame of reference. Although the Lorentz-transformation equations happen to be the correct equations to preserve the form of Eq. (50) in all frames of reference, the essential physical content of Eq. (50) is best understood by working in a single frame of reference.

Now since an increase in *linear* velocity leads to an increase in kinetic energy, and hence to an increase in the observed mass, it seems apparent that an increase in *angular* velocity, which also increases the kinetic energy, will lead to an increase in the observed mass. This conclusion has been verified macroscopically in the sense that an electron obeys the same mass equation, Eq. (50), if it is given a linear acceleration (electron linear accelerator) or if it is given a circular acceleration (betatron or electron synchrotron). This conclusion should also follow microscopically if we associate the spin angular momentum of a particle with the rotation of a mass. Thus it seems incorrect to state, as is sometimes asserted,[170] that no energy is associated with the spin angular momentum of a particle.

The starting point in applying special relativity to rotating masses is the equation for the mass increase of a rotating ring of matter. The general

problem of a ring of matter which initially has rest mass m_0 and radius r, and which is then given an angular velocity ω about the axis of the ring, has been well studied, and relativists are generally agreed[171,172] that it will have a relativistic mass increase given by the equation

$$m = \frac{m_0}{(1-\omega^2 r^2/c^2)^{1/2}}, \tag{54}$$

which is the rotational analog of Eq. (50). Also, since the motion is at right angles to the radial coordinate r, the coordinate r is relativistically unaffected by the rotation.[173] This result is crucial, for it means that spinning rings can be linearly superimposed to form a spinning disk or cylinder or sphere. Although the spinning disk and spinning cylinder have been extensively discussed in the literature,[171,174] the spinning sphere surprisingly does not seem to have been considered. And it is the spinning sphere which yields phenomenologically significant relativistic equations,[3] which we now summarize.

Consider a uniform sphere of matter having radius R and rest mass m_0. Rotate the sphere until the equator attains the velocity of light (or remains infinitesimally below that value). If r is the radial coordinate at right angles to the axis of rotation, the cylindrical mass element $dm_0(r)$ lying between r and dr (which is a relativistic invariant) will have a special-relativistic mass increase, as viewed in the stationary frame of reference, given by the equation

$$dm(r) = \frac{dm_0(r)}{(1-\omega^2 r^2/c^2)^{1/2}}. \tag{55}$$

The integral of (55) over the volume of the sphere is

$$m = (m_0/\tfrac{4}{3}\pi R^2) \times \int_0^R \{2(R^2-r^2)^{1/2}[2\pi r/(1-\omega^2 r^2/c^2)^{1/2}]\}dr, \tag{56}$$

where m_0 is the rest mass of the sphere. The limiting angular velocity is

$$\omega = c/R, \tag{57}$$

where c is the velocity of light. Inserting (57) into (56), we obtain

$$m = 3m_0/R^2 \int_0^R r\,dr = \tfrac{3}{2}m_0; \tag{58}$$

the spinning sphere is relativistically half again as massive as it was at rest. This is a result that is of utmost importance for the present light-quark phenomenology, and in fact the search for a suitable set of light-quark basis states furnished the motivation for the author to investigate[3] this extension of the usual equations of special relativity. Equation (58) establishes an immediate and very direct mass relationship between the unobserved spinless 70-MeV mass quantum M and the readily observed spinning 105-MeV μ meson. While it is true that the quantum M has strong hadronic interactions and the μ meson does not, it is equally true that the μ meson does in fact exist and must somehow be accounted for in the over-all scheme of things. The dominant decay mode $\pi \to \mu + \nu$ indicates that the pion and the muon are in some sense closely related particles.

In the derivation of Eq. (58), three considerations come immediately to mind: (1) Suppose the equator of the spinning sphere does not actually reach the velocity $v = \omega R = c$, but instead remains infinitesimally below that value (as it must). (2) What about problems such as rigidity and stresses? (3) Are general-relativistic considerations important? The answer to (1) is that if the velocity $v = \omega R$ in Eq. (57) is lowered infinitesimally, the change in the integral in Eq. (58) is also infinitesimal; Eq. (58) and the other special-relativistic equations given below do not have divergence difficulties. Question (2), the problem of rigidity and stresses, is one that has been debated in the literature[175] and about which no consensus has been reached. It is important to note, as stated by Arzelies,[176] that no one really knows the environment experienced under rotational motion by a mass point embedded in a matrix of mass points. For example, the non-Euclidean geometry experienced by this mass point may minimize centrifugal effects.[177] By neglecting stresses, we obtain phenomenologically useful results, which is an *a posteriori* indication that, at least for the spherical geometry considered here, stresses are not of crucial importance. Question (3), the importance of general-relativistic effects, can be assessed by examining the components of the Riemann-Christoffel curvature tensor. For the rotating sphere, these components have small values[178] except right at the equator, where $v = \omega R \simeq c$. Since the contribution of the equatorial region to the integrals in Eqs. (56) and (58) is relatively unimportant, it seems reasonable to neglect general-relativistic effects. A uniform sphere of matter which is rotated at the relativistic limit of Eq. (57) has a rather unique relativistic geometry in the sense that all of the calculational difficulties occur right at the equator, and (fortunately) the contribution of this equatorial region to integrals such as those shown in Eqs. (56) and (58) is minimal.

The moment of inertia I of the relativistically spinning sphere about the axis of rotation is obtained by weighting the mass distribution of Eq. (55) by r^2 and repeating the integration over the volume of the sphere. This gives

$$I = 3m_0/R^2 \int_0^R r^3 dr$$
$$= \tfrac{3}{4} m_0 R^2$$
$$= \tfrac{1}{2} m R^2 . \tag{59}$$

The angular momentum of the spinning sphere is, from (57) and (59),

$$J = I\omega = \tfrac{1}{2} mRc . \tag{60}$$

If we specify the ratio between R and m in Eq. (60), we can obtain the spin angular momentum J as a directly calculated quantity. The natural ratio to use is that given by the Compton wavelength,

$$R = \hbar/mc . \tag{61}$$

Inserting (61) into (60) gives

$$J = \tfrac{1}{2}\hbar \tag{62}$$

as the relativistically calculated spin angular momentum of the spinning sphere.

When we apply these relativistic results to hadronic mass quanta (the spinor S), we are led to the consideration of oblate spheroidal geometries. Hence Eqs. (58) and (59) should be generalized to apply to nonspherical (but axially symmetric) geometries. This can be done by defining the radius R as

$$R_A = \text{axial radius},$$
$$R = R_A(1 + \epsilon \sin\theta), \tag{63}$$
$$R_E = \text{equatorial radius}$$
$$= R_A(1 + \epsilon),$$

where

$$\epsilon = (R_E - R_A)/R_A \tag{64}$$

is a deformation parameter, and where θ is the angle with respect to the axis of rotation (which is also the symmetry axis). In terms of (63) and (64), Eqs. (58) and (59) become

$$m = 3m_0 \int_0^{\pi/2} d\theta \frac{(1+\epsilon\sin\theta)^2(1+2\epsilon\sin\theta)\sin\theta\cos^2\theta}{[1-\sin^2\theta(1+\epsilon\sin\theta)^2/(1+\epsilon)^2]^{1/2}} \tag{65}$$

and

$$I = 3m_0 R_A^2 \times \int_0^{\pi/2} d\theta \frac{(1+\epsilon\sin\theta)^4(1+2\epsilon\sin\theta)\sin^3\theta\cos^2\theta}{[1-\sin^2\theta(1+\epsilon\sin\theta)^2/(1+\epsilon)^2]^{1/2}} . \tag{66}$$

Empirically, m in Eq. (65) is a slowly varying function of the deformation parameter ϵ, and I in Eq. (66) is also a slowly varying function of ϵ if R_E in Eq. (63) is held constant. Hence Eqs. (58) and (59) give reasonable approximations for all spheroidal geometries. The spinor S is constructed as an aligned array of three oblate spheroids M, each having $R_{max} \simeq \frac{1}{3}\sqrt{3}$ fermi and $R_{min} \simeq \frac{1}{3}$ fermi ($\epsilon \simeq \sqrt{3} - 1$), where $R_{max} \simeq \hbar/mc$, with $m = 330$ MeV, so that R_{max} for *each subquantum* M in the spinor S reflects the *total mass* of the spinor S. Equations (57) and (66) then give $J = \frac{1}{2}\hbar$ as the calculated spin angular momentum of the spinor S (see paper II).

The relativistically spinning sphere also has phenomenological significance with respect to electromagnetic effects. If we place a localized charge on the spinning sphere and allow it to move freely, it will be forced to the equator of the sphere by the action of the induced magnetic field. An equatorial charge distribution moving at the velocity c gives rise to a magnetic moment

$$\mu = \pi R^2 i = \pi R^2 (e/c)\omega/2\pi = \tfrac{1}{2} eR . \tag{67}$$

Inserting (61) into (67) gives

$$\mu = e\hbar/2mc \tag{68}$$

as the calculated magnetic moment, which is the correct magnetic moment for a Dirac particle. Thus if we represent a μ meson as a spherical quantum with a rest mass of 70 MeV, a radius given by its (spinning) Compton wavelength,[179] and containing a localized charge e that is free to move, we obtain the mass, spin angular momentum, and magnetic moment of the muon as directly calculated quantities. Furthermore, the equatorial ring of charge on the spinning muon gives a contribution to the mass which is of order $e^2/R = (e^2/\hbar c)mc^2 = \alpha mc^2$, which is the same magnitude as the observed first-order correction to the muon magnetic moment. Of course, the equatorial ring of charge also gives rise to an electric quadrupole moment. However, it is shown in paper II that if the standard quantum-mechanical spin and magnetic-moment projection factors are introduced into the above calculations, the electric quadrupole moment vanishes.[180]

APPENDIX C: RULES FOR HADRON ROTATIONAL BANDS

Rules for hadron rotational bands are listed in Table XII. In this section we discuss the manner in which these rules were obtained. It should be noted that experiments are just now arriving at the point where individual resonances are being analyzed in terms of a complete set of spin-space amplitudes. The present rules do not include that complexity of detail, and experiments may well

show that some of the rules given here are either incomplete or incorrect. The rules of Table XII were deduced from the phenomenological requirement that they reproduce the observed spectrum of experimental hadron resonances as given in Tables I–VII (see Fig. 8 and Ref. 181).

Rule (1) in Table XII, the division of resonances into narrow-width S-state bandheads and broad-width rotational levels, is implicit in the phenomenology of the entire paper, and is illustrated by Figs. 8 and 9, by the compilations in Tables XVII, XX, and XXVIII, and by the ρ-meson results of Sec. X.

Rule (2) of Table XII, the $L(L+1)$ interval spacings of the rotational bands, is obtained both from the known systematics of nuclear physics (Ref. 7) and from the present phenomenology [a classification of baryon rotational bands in terms of $J(J+1)$ energy intervals does not seem to be possible]. $L(L+1)$ rotational interval spacings, as given in Eq. (22), constitute a very general result that obtains whenever the specialized conditions that are listed after Eq. 22 do not apply. Hadron rotations, from their small moments of inertia, are highly nonadiabatic, and thus strongly violate these specialized conditions.

Rule (3) of Table XII, the rigid-body-estimates for hadron moments of inertia, is illustrated in Fig. 4 for the ρ meson and in Eqs. (23) and (24) for baryon resonances. The intent of this rule is to show that the observed hadron rotational energies are reasonable. To treat in detail the rotational motion of a quark cluster that includes spinors whose equators are already moving at or near the relativistic limit $v=c$ is a complex problem that is beyond the scope of the present first-pass phenomenology.

Rule (4) of Table XII, the universality of hadron moments of inertia as observed in mesons, kaons, baryons, hyperons, and light nuclei, is a result that follows *theoretically* from the use of a common set of geometric basis states for all of these resonances and *phenomenologically* from the results shown in Figs. 9 through 12 and in Table XXX.

Rule (5) of Table XII, the classification of rotational bands according to isotopic spin, is in line with the classification of experimental resonances given in Tables I–VII.

Rule (6) of Table XII, the limitation on L values imposed by the special-relativistic requirement that the periphery of the rotating structure can not exceed the velocity of light, is a result that is clearly required both theoretically and phenomenologically. The calculation of this effect shown in Eq. (26) is intended only as an order-of-magnitude estimate for evaluating a situation that, in detail, is probably quite complex.

Rule (7) of Table XII, the spectroscopic notation for hadron resonances, is required as soon as the decomposition of the total angular momentum $\vec{J}$ into $\vec{L}$ and $\vec{S}$ components is made. The compilation of hadron spectroscopic assignments given in Table XIII will undoubtedly require some revision as more detailed experimental data become available.

Rule (8) of Table XII, the mapping of baryon and hyperon S states, was obtained from the systematics of Fig. 3.

Rule (9) of Table XII, the L_-, L_+, L_- ordering of baryon resonances, is a phenomenological result that emerged from the baryon and hyperon rotational bands of Tables XV, XVI, XVIII, and XIX.

Rule (10) of Table XII, the mapping of meson S states, was obtained experimentally from Figs. 1 and 6, and is accounted for phenomenologically by the meson excitation systematics of Tables XXII and XXIII.

Rule (11a) of Table XII, the ($S=0$, $I=1$) and ($S=1$, $I=0$) spin and isotopic-spin rule for meson S states, is taken from Eq. (21) in the text.

Rule (11b) of Table XII, the occurrence of $S=0$, $I=1$ bandheads in rotational bands that contain all successive L values, implies that these bandheads have no symmetry contraints such as rotational invariance[10] that would eliminate every other L value [see rule (11c) in this regard].

Rule (11c) of Table XII states that the $S=1$, $I=0$ bandheads are observed only in the following spectroscopic states [in the notation of rule (7)]: ${}^3S_{01}$, ${}^3P_{00}$, ${}^3D_{02}$. This result is due to a combination of several factors: (i) Special relativity precludes $J=L+1$ meson rotational modes, since these would result in the equators of the spinor S moving faster than the velocity of light (if we work entirely in the laboratory frame of reference, velocities add vectorially). (ii) Production mechanisms appear to rule against $J=L-1$ rotational modes, since these involve the creation of resonances with angular momenta in one direction and spins in the other direction. However, a notable exception is the $J=0$ mode, where spins and orbital angular momenta are logically created in opposite directions as an "action-reaction" type of process that does not require the necessity of coupling to external angular momenta. (iii) In nuclear physics, if a rotor has axial and inversion symmetry, and if the projection of the angular momentum on the axis of symmetry is zero, then rotation invariance[10] eliminates every other L value. Although rotation invariance in nuclear physics applies only to spinless rotors, the nonadiabatic decoupling of spins and orbital angular momenta in meson rotations (due to the small

moments of inertia) makes it plausible that rotation invariance might apply to spin-1 meson bandheads. This would affect the $L=J$ rotational levels, and it might explain why the ${}^3P_{01}, {}^3F_{03}, \ldots$ levels seem to be missing (from the point of view of "rotation dynamics," a spin-1 spinor-pair bandhead, which possesses 180° symmetry about the bandhead spin axis, may be more symmetric than a spin-0 spinor-pair bandhead). (iv) With the bandhead masses considered in the present section, the relativistic cutoff $L_{\max}$ [rule (6)] is $L_{\max}=3$. When we combine factors (i)–(iv), the ${}^3S_{01}$, ${}^3P_{00}$, and ${}^3D_{02}$ meson rotational levels emerge as the only surviving $I=0$ rotational levels. The ${}^3P_{00}$ rotational level is of special interest, since it seems to account for the broad $I=0$ $\pi\pi$ ϵ-type resonances listed in Table I.

Rule (12) of Table XII, the G-parity rule that is only weakly established from the results shown in Table XXVI, can be made plausible by the following argument: (a) G parities and ordinary (spatial) parities are usually linked together theoretically. (b) Meson bandheads can have positive or negative "intrinsic" (spatial) parities. (c) Since spatial parities are tied in with spatial orientations, it seems plausible that rotating bandheads, which are not spatially oriented, will appear to have effectively positive intrinsic parities. (d) From (b) and (c), meson rotational bands formed from negative-parity bandheads will have rotational levels whose "intrinsic" parities are opposite in sign to the intrinsic parity of the (negative parity) bandhead. (e) From (a), the change in sign of the intrinsic parity in (d) causes a change in sign of the corresponding G parity. The parity rule given in (c) also leads to the prediction that $J^P=1^-$ and 2^+ meson resonances are plentiful and $J^P=1^+$ and 2^- meson resonances are scarce, as is observed experimentally (see Ref. 157).

Rule (13) of Table XII, the lack of observed rotational bands corresponding to the spinless π, K, η, and η' resonances, is a phenomenological observation. It can be explained by assuming that (a) rotation invariance[10] eliminates $L=1,3,5,\ldots$ rotational levels, and (b) special relativity [rule (6)] eliminates $L=2,3,4,\ldots$ levels.

Rule (14) of Table XII, the nonobservance of ${}^1S_{10}$ configurations for odd-3 excitations, which appears to be phenomenologically correct, follows from the fact that the quark state $3\equiv 3M$ is an asymmetric structure (see Appendix A), so that excitations which contain an odd number of 3's are also asymmetric, and these asymmetric quark configurations cannot couple to symmetric spin-zero S-wave initial or final states. Thus the bandheads of the $I=1$ ρ meson and the $I=\frac{1}{2}$ K^* meson, which are spin-zero configurations [rule (11a)] that contain odd numbers of 3's (Table XXVIII), cannot be observed directly.

Rule (15) of Table XII, the relationship between a spread in hadron rotational energies and a corresponding spread in hadron orbital angular momenta, is discussed in detail in Sec. X.

APPENDIX D: $\bar{K}N$ AND πN SCATTERING AMPLITUDES

Since the baryon and hyperon partial-wave amplitudes, as determined in various phase-shift analyses, still contain ambiguities, each worker who attempts to fit these amplitudes to theory is faced with a number of rather arbitrary decisions. In order to ascertain how these decisions have been reached in the present case, it is useful to discuss the available experimental information as it applies directly to each individual partial-wave amplitude. In the present section we discuss first the hyperon partial wave amplitudes and then the baryon partial-wave amplitudes.

1. Hyperon partial-wave amplitudes

For the purposes of this discussion we use, in addition to the references in RPP73 (Ref. 25), the following abbreviated references: Ch-LBL = Ref. 95, LW = Ref. 97, LOMM = Ref. 99.

S_{01}. The resonances at 1402 MeV and 1673 MeV are well established. Three groups see evidence for a third resonance—Kim 71 at 1780 MeV, LW at 1830 MeV, and Bricman 70 at 1872 MeV. The present systematics would place this state at about 1820 MeV. In Table XIV, the resonance is shown at 1827 MeV, the average position from these three analyses. Ch-LBL do not confirm this state, but LOMM see some evidence for it.

P_{01}. Kim 71 and LW both see two P_{01} resonances, one around 1750 MeV and one about 170 MeV lower. Several other groups have confirmed the 1750-MeV resonance. The lower resonance was predicted on the basis of the present systematics prior to the publication of the Kim 71 and LW results (see Ref. 4, Table III).

P_{03}. Several groups observe a P_{03} resonance at about 1870 MeV. The Kim 71 location for this resonance, 1710 MeV, seems anomalously low.

D_{03}. The very-narrow-width $\Lambda(1518)D_{03}$ $\Gamma 16$ resonance appears to be different in nature from the well-established $\Lambda(1688)D_{03}$ $\Gamma 53$ resonance. From the present systematics, the $\Lambda(1518)$ is a $J=\frac{3}{2}$ spinor excitation [see Eq. (48)], and it forms the bandhead for the dominant Λ rotational band (Table XV). The $\Lambda(1688)$ is the D state in this same rotational band. Two analyses, Galtieri 70 and Brandstetter 72 in Ref. 25, suggest another D_{03} resonance at 1990 MeV, which fits naturally into the present systematics.

D_{05}. The D_{05} amplitude has a well-established resonance at 1827 MeV, and there is some suggestion (Lichtfield 71) of another resonance at 2110 MeV. This latter state is at too high an energy to classify accurately in the present systematics.

F_{05}. The F_{05} amplitude has a well-established resonance at 1819 MeV. Some experiments suggest a second resonance at 2110 MeV, which fits naturally into the present rotational systematics as an example of the L_-, L_+, L_- rule of Table X.

F_{07}. A resonance at about 2020 MeV is suggested in two experiments. This resonance fits naturally into the present systematics, and it follows the L_-, L_+, L_- rule of Table X.

C_{07}. The resonance at 2100 MeV is well established.

G_{09}. No evidence for resonant behavior.

H_{09}. The resonance at 2350 MeV is well established.

S_{11}. The 1756 MeV resonance is well established. The 1620-MeV S_{11} state is clearly required by the present systematics, and it was in fact predicted (Ref. 4, Table III) some time before Kim 71 established the quantum number $L=0$ for this state. LW also confirm the Kim 71 S-state assignment. A narrow production peak at 1620 MeV, which has been seen by several groups, may also correspond to this state. Blumenfeld 69, who see a narrow production peak $\Sigma(1618)$ $\Gamma 30$ that corresponds to the $\Sigma(1620)$ $S\Gamma 40$ resonance, also see a $\Sigma(1682)$ $\Gamma 25$ peak,[113] which suggests another S_{11} state at that energy. Vanhorn 72 furnishes a partial confirmation of this state by reporting a resonance $\Sigma(1697)$ $S\Gamma 66$. LOMM found evidence for a higher S_{11} resonance at somewhere around 1900 MeV, which from the present viewpoint is logically associated with the rather well-established P_{11} resonance observed at 1926 MeV. Vanhorn 72 reports a $\Sigma(2004)$ $S\Gamma 66$ resonance, which may or may not be another manifestation of the LOMM 1900-MeV S state.

P_{11}. It has been known for some time that two Σ resonances appear at 1670 MeV.[25] SU(6) classifiers tend to identify these as both being D_{13} resonances. However, from the present systematics we require both a P state and a D state at 1670 MeV, and a prediction to this effect was made some time ago (Ref. 4, Table III). Aguilar 70 found two experimental $\Sigma(1670)$ peaks, both with the widths we expect for rotational levels ($\Gamma \sim 100$ MeV), and they showed that one peak was much more peripheral than the other (which suggests different L values for the two peaks). Kim 71 subsequently found both a $\Sigma(1670)$ P_{11} resonance and a $\Sigma(1670)$ D_{13} resonance, and Vanhorn 72 confirmed these as $\Sigma(1668)P_{11}$ and $\Sigma(1659)D_{13}$, results that are in agreement with the results of Aguilar 70 and with present expectations, and in disagreement with the SU(6) expectations. The P_{11} state at roughly 1550 MeV observed by Armenteros 70 fits naturally into the present systematics, and we have included it as a resonance in Table VI. However, this may just be another manifestation of the $\Sigma(1670)$ P_{11} resonance just discussed. But LOMM see a low-energy P_{11} resonance which they say agrees with Kim 71 (they constrained the mass to stay about 1620 MeV), and Baillon *et al.*[117] report a P_{11} resonance at 1600 MeV. A P_{11} resonance at about 1926 MeV has been reported by a number of groups.

P_{13}. The $\Sigma(1385)$ $P_{13}\Gamma 36$ resonance, from its narrow width, appears to be a $J=\frac{3}{2}$ spinor excitation [see Eq. (48)]. LW see a P_{13} resonance at 1840 MeV, which fits the present systematics, but Vanhorn 72 reports a P_{13} resonance at 1925 MeV. A $\Sigma(2080)$ P_{13} resonance, which is suggested by two phase-shift analyses, is at too high an energy to classify accurately in the present systematics.

D_{13}. In addition to the well-established resonance at 1669 MeV, Ch-LBL suggest a resonance at around 1750 MeV, which we might phenomenologically relate to the dominant $\Sigma(1765)$ D_{15} level. Several groups see a higher D_{13} resonance—LOMM at 1863 MeV, and several groups in RPP73 at about 1940 MeV. If we place this resonance at about 1900 MeV, which fits the present rotational systematics, it then matches two $\Gamma \sim 55$ MeV cross-section peaks observed at 1905 MeV by Bugg 68 and Bricman 70.

D_{15}. This amplitude has a single dominant resonance at 1765 MeV.

F_{15}. There is a dominant resonance at 1910 MeV plus a possible second resonance at 2070 MeV, which closely resembles the $\Sigma(2030)$ F_{17} resonance. Vanhorn 72 reports an F_{15} resonance at 2250 MeV.

F_{17}. There is a well-established resonance at 2030 MeV.

G_{17}. There is a well-established resonance at 2250 MeV, plus some evidence (Galtieri 70) for a resonance at 2070 MeV. Both of these levels fit naturally into the present rotational systematics.

G_{19}. No evidence for resonant behavior.

H. The quantum numbers of the well-established $\Sigma(2455)$ resonance are not known, but it fits naturally into the present systematics as an $L=5$ H level. It has a width $\Gamma=120$ MeV that indicates a rotational excitation.

2. Baryon partial-wave amplitudes

For the purposes of this discussion we use, in addition to the references in RPP73 (Ref. 25),

the following abbreviated references: AYED = Ref. 78, AL = Ref. 80.

S_{11}. This amplitude resonates at about 1508 MeV, 1684 MeV, and 2184 MeV, with the measured widths $\Gamma = 55$ MeV, 116 MeV, and 240 MeV, respectively. There is no statistically significant evidence for resonances at 1219 MeV or 1359 MeV which are indicated by overlying rotational levels (Table XVIII).

P_{11}. The present rotational systematics have long indicated[90] that the broad 1470-MeV Roper resonance must actually be two resonances, with the lower half of the resonance corresponding to the well-established production peak seen at 1419 MeV.[25] Some early πN phase-shift analyses, Bareyre 68 and Berkeley, showed a double inelastic dip at the position of the Roper resonance, which indicates two resonances, and the recent AYED analysis now shows this splitting directly in the P_{11} phase shift. Several experiments indicate a low-energy P_{11} resonance at about 1300 MeV. The P_{11} amplitude resonates again somewhere above 1700 MeV, where it appears in the AL and AYED analyses as part of the P_{11}, P_{13} criss-cross shown in Table XI.

P_{13}. The only resonance reported for this amplitude occurs as part of the P_{11}, P_{13} P-wave criss-cross shown in Table XI.

D_{13}. The D_{13} amplitude resonates prominently at 1520 MeV, and there are indications for higher resonances at about 1730 MeV and at 2075 MeV. The two lower resonances fit naturally into the present systematics, but the resonance at 2075 MeV is at too high an energy to be included accurately in the classification scheme.

D_{15}. This amplitude has a dominant resonance at 1672 MeV, with a higher resonance indicated at about 2078 MeV. The higher resonance may correspond phenomenologically to the high-energy D_{13} resonance cited above.

F_{15}. This amplitude resonates prominently at 1687 MeV, with indications for a second resonance at about 2088 MeV, in the same energy region as an observed F_{17} resonance.

F_{17}. This amplitude shows a resonance at 2024 MeV which fits naturally into the present systematics.

G_{17}. From the present systematics, we would expect a G_{17} resonance to appear at about 1900 MeV (Table XVIII). However, the only observed G_{17} resonance occurs at about 2200 MeV. In the Λ and Σ resonances, the lowest G-wave resonance appears at about 2100 MeV.

G_{19}. A resonance at about 2130 MeV is reported by AYED, who see G_{17} resonating at 2150 MeV in the same analysis.

H_{19}. This amplitude has a prominent resonance at 2241 MeV.

S_{31}. This amplitude resonates clearly at an energy of about 1618 MeV, and there are very indirect indications[137] for a peak at ~1165 MeV, corresponding to the overlying $\Delta(1233)$ rotational level. There seems to be no indication of an expected S state at 1500 MeV (see Table XIX), although we note that the width of the 1618-MeV resonance, $\Gamma = 147$ MeV, is broader than we expect for an S state.

P_{31}. This resonance appears in the AL and AYED analyses as part of the P_{31}, P_{33} P-wave criss-cross shown in Table XI.

P_{33}. In addition to the dominant resonance at 1233 MeV, this amplitude appears as a part of the P_{31}, P_{33} P-wave criss-cross shown in Table XI. The present rotational systematics favors the lower AL value over the higher AYED value for the position of this resonance.

D_{33}. This amplitude resonates prominently at 1694 MeV.

D_{35}. There is some evidence for a resonance at 1824–1870 MeV. The present systematics favors the low Mehtani[91] value for the position of this resonance.

F_{35}. This amplitude resonates prominently at 1877 MeV.

F_{37}. This amplitude resonates prominently at 1923 MeV.

G_{37}. No evidence for resonant behavior.

G_{39}. A recent analysis, Von Schlippe 72 in RPP73 (Ref. 25), suggests a G_{39} resonance at 2160 MeV. This resonance accurately completes the $\Delta 334$ rotational band in Tables XIX and XX, which is composed entirely of L_+ excitations (Table X).

H_{39}. No evidence for resonant behavior.

$H_{3,11}$. A dominant resonance appears at 2390 MeV.

---

*Work performed under the auspices of the U. S. Atomic Energy Commission.

[1]M. H. Mac Gregor, UCRL Report No. UCRL 71842 (unpublished), Part I; Bull. Am. Phys. Soc. 14, 1178 (1969).

[2]In addition to the published references 3–25 listed below, some of this work has been documented in the following unpublished Lawrence Livermore Laboratory UCRL reports by M. H. Mac Gregor: (a) UCRL Report No. UCRL 71842, revised, 1969 (unpublished), Part II (the first identification of baryon and hyperon rotational bands, and the prediction of a split Roper resonance);

see Bull. Am. Phys. Soc. 14, 1206 (1969). (b) Report No. UCRL 72128, 1969 (unpublished) (the equations for a relativistically spinning sphere, and the identification of the muon mass with the spinless mass quantum $M = 70$ MeV). (c) Report No. UCRL 72187, 1969 (unpublished). (d) Report No. UCRL 72495, 1970 (unpublished) (prediction of the resonance subsequently reported in Ref. 39, and its relationship to the A_2 dip). (e) Report No. UCRL 72736, 1970 (unpublished). (f) Report No. UCRL 73193, 1971 (unpublished). (g) Report No. UCRL 73583, 1971 (unpublished).

[3]M. H. Mac Gregor, Nuovo Cimento Lett. 4, 211 (1970).

[4]M. H. Mac Gregor, Nuovo Cimento Lett. 4, 1043 (1970).

[5]M. H. Mac Gregor, Nuovo Cimento Lett. 4, 1249 (1970).

[6]M. H. Mac Gregor, Nuovo Cimento Lett. 4, 1309 (1970).

[7]M. H. Mac Gregor, Nuovo Cimento Lett. 1, 427 (1971).

[8]M. H. Mac Gregor, Nuovo Cimento Lett. 1, 437 (1971).

[9]M. H. Mac Gregor, Nuovo Cimento Lett. 1, 759 (1971).

[10]M. H. Mac Gregor, Nuovo Cimento Lett. 2, 846 (1971).

[11]M. H. Mac Gregor, Nuovo Cimento Lett. 3, 197 (1972).

[12]M. H. Mac Gregor, Nuovo Cimento Lett. 5, 135 (1972).

[13]M. H. Mac Gregor, in invited papers, Coral Gables Conference on Fundamental Interactions at High energy, 1971.

[14]M. H. Mac Gregor, Nuovo Cimento 8A, 235 (1972).

[15]M. H. Mac Gregor, Particles and Nuclei 1, 473 (1971).

[16]M. H. Mac Gregor, Particles and Nuclei 2, 358 (1971).

[17]M. H. Mac Gregor, Particles and Nuclei 3, 173 (1972).

[18]M. H. Mac Gregor, Particles and Nuclei 5, 69 (1973).

[19]M. H. Mac Gregor, to be published in Nuovo Cimento.

[20]M. H. Mac Gregor, Nuovo Cimento 18A, 169 (1973).

[21]M. H. Mac Gregor, report (unpublished).

[22]M. H. Mac Gregor, essay submitted to the competition of the Gravity Research Foundation (unpublished).

[23]M. H. Mac Gregor, UCRL Report No. UCRL 73328, 1971 (unpublished); the present paper and Ref. 24 constitute a revised version of this paper.

[24]M. H. Mac Gregor, UCRL Report No. UCRL 73328 (unpublished), revision III.

[25]73: Particle Data Group, Rev. Mod. Phys. 45, S1 (1973).

[26]72: Particle Data Group, Phys. Lett. 39B, 1 (1972).

[27]71: Particle Data Group, Rev. Mod. Phys. 43, S1 (1971).

[28]The $\phi(1019)$ is the ϕ meson as measured in its KK decay mode. From its low Q value and spin of 1, kinematic final-state restrictions will shift the mass of the ϕ upwards by $\frac{1}{2}\Gamma$ and lower its natural width (see M. H. Mac Gregor, Ref. 14, end of *Note Added in Proof*).

[29]The $\phi \to \pi^+\pi^-\pi^0$ resonance parameters are from M. Aguilar-Benitez *et al.*, Phys. Rev. D 6, 29 (1971), which indicate a width $\Gamma \sim 20$ MeV. The $\phi \to \pi\pi\pi$ decay-mode resonance parameters roughly match the $H \to \pi^+\pi^-\pi^0$ enhancement reported in Ref. 1, which also appears to be a spin-1 resonance [see G. Goldhaber, in *Proceedings of the Thirteenth International Conference on High Energy Physics*, Berkeley, 1966 (Univ. of California Press, Berkeley, 1967), for the spin value of the H].

[30]This narrow $S^* \to K_S K_S$ enhancement is from J. Duboc *et al.*, Nucl. Phys. B46, 429 (1972).

[31]See the detailed compilation of experimental data listed in RFP 73, Ref. 25.

[32]D. J. Crennell *et al.*, Phys. Rev. Lett. 22, 1327 (1969).

[33]D. L. Cheshire *et al.*, Phys. Rev. Lett. 28, 520 (1972), confirmed by L. Holloway *et al.*, in *Experimental Meson Spectroscopy—1972*, edited by Kwan-Wu Lai and Arthur H. Rosenfeld (Ref. 48), p. 133. There are suggestions that this resonance has a $\pi\pi\pi$ decay mode and thus matches the nearby resonance of Ref. 34.

[34]This is an average of two peaks observed by W. W. M. Allison *et al.*, Phys. Lett. 25B, 618 (1967).

[35]R. W. Jacobel *et al.*, Phys. Rev. Lett. 29, 671 (1972), who note its similarity to the $X^-(1153)$ $\Gamma 16$ peak.

[36]This is a CERN*MMS*$^-$ peak that can be observed on p. S88 of RPP71 (Ref. 27). The quoted mass and width were obtained by fitting a Gaussian curve to the CERN data. This peak, unlike the nearby $X^-(1079)$ peak, which is also seen in the CERN data on p. S88, shows up clearly in various CERN preliminary reports, and it appears to be confirmed by the $M(1148)$ $\Gamma 15$ peak reported by Jacobel *et al.*, in Ref. 35.

[37]A new $A_{1.5}$ measurement by R. Morse *et al.* [Nucl. Phys. B43, 77 (1972)] was averaged with the unweighted average of four older measurements by Cason 67, Ascoli 68, Donald 68, and Junkmann 68, which are listed in RPP73 (Ref. 25).

[38]L. Gray *et al.*, Phys. Rev. Lett. 26, 1491 (1971). The existence of this state was predicted on experimental grounds by W. Chinowsky and G. Kojoian [Nuovo Cimento 43A, 684 (1966); see page 697]. Although the Syracuse experiment of Gray *et al.* has not yet been otherwise confirmed, no experimental reasons have subsequently appeared for questioning the correctness of the Syracuse result (T. Kalogeropoulos, private communication). See T. Kalogeropoulos, CERN Report No. CERN 72-10, 1972 (unpublished), p. 319; also, invited talk presented at the seminar on Interactions of High Energy Particles with Nuclei and New Nuclearlike Systems, Moscow, ITEP, 1973 (unpublished).

[39]This resonance was first reported by L. J. Gutay *et al.* [Nucl. Phys. B27, 486 (1971)], as a dip in the $I = 0$ $\pi\pi$ S-wave amplitude, centered at about 658 MeV (see M. H. Mac Gregor, Ref. 14, Fig. 8). This dip also appears in the isotropic component of the $\pi\pi$ amplitude, which suggests that it arises from the interference of a spin-1 resonance. This resonance also appears as a small peak in the $\pi^+p \to \pi^+\pi^-\Delta^{++}$ measurement of M. Alston-Garnjost *et al.*, Phys. Lett. 36B, 152 (1971), Fig. 1(c) (see Fig. 15 in this paper). A statistical analysis of the data for this peak (which were kindly supplied to the author by S. D. Protopopescu) was carried out by J. I. Karush and N. Smiriga, NMS Technical Memorandum No. 73-2 (unpublished), and it indicated that the peak is centered at about 665 MeV and with a statistical significance (optimistically) of four standard deviations. It should be noted that direct $\pi N \to \pi\pi N$ experiments show no trace of a peak near 660 MeV. But a recent $\gamma p \to \pi^+\pi^- p$ experiment of J. Ballam *et al.* [Phys. Rev. D 7, 3150 (1973), Figs. 2(a) and 2(b)] possibly shows weak indications of a 660–680 MeV enhancement for small momentum transfers. However, a lower-energy experiment by this same group [Phys. Rev. D 5, 545 (1972), Fig. 10], with poorer statistics, does not reveal this enhancement. Theoretically, in the present paper we attribute this 660-MeV anomaly to a pair of 330-MeV spinors (see Sec. X), just as we attribute the 1310-MeV A_2 anomaly to a quartet of 330-MeV spinors, and the two

anomalies from an experimental point of view are equally elusive (see Ref. 40).

[40]Many recent experiments do not show an A_2 dip (see the summary by R. Diebold in Ref. 41). However, a reanalysis of the original CERN data (Ref. 25) by W. Kienzle, report (unpublished), indicates that these data still show a significant dip. Three recent π^+p experiments all show some structure at about 1310 MeV: I. J. Bloodworth *et al.*, Nucl. Phys. B37, 203 (1972); K. W. J. Barnham *et al.*, Phys. Rev. Lett. 26, 1494 (1971); BDNPT Collaboration, Nucl. Phys. B16, 221 (1969). Bloodworth *et al.* comment as follows: "The appearance of some structure in this and in two other experiments (Barnham *et al.* and BDNPT) could clearly be due to statistical fluctuations, although it seems surprising that the effect occurs in the same few bins." These bins are the same bins in which the Kienzle analysis shows a dip. Also, one experiment, D. J. Crennell *et al.*, Phys. Rev. Lett. 20, 1318 (1968), shows a narrow K_SK_S peak, $K_SK_S(1311)$ $\Gamma 21$, at this same location. In the Crennell experiment, the angular distribution of the K_SK_S spectrum changed abruptly at 1311 MeV from an isotropic distribution to a fore-and-aft distribution.

[41]NAL 72: *Proceedings of the XVI International Conference on High Energy Physics, Chicago-Batavia, Ill., 1972,* edited by J. D. Jackson and A. Roberts (NAL, Batavia, Ill., 1973), Vols. 1–4.

[42]The $p\bar{p}(1925)$ $\Gamma 8$ peak reported by Cline 70 in RPP71 (Ref. 27) and the $\bar{p}n(1795)$ $\Gamma 8$ peak of Ref. 38 appear in the present work to be phenomenologically related resonances. The Cline 70 peak was critically challenged by R. Bizzarri *et al.*, Phys. Rev. D 6, 160 (1972), and it did not appear in RPP72 and RPP73 (Refs. 26 and 25) due to a rebinning of the data into wider bins. However, a recent experiment of A. S. Carroll *et al.* [Phys. Rev. Lett. 32, 247 (1974)] has confirmed unambiguously the existence of this peak; these workers obtained a $\bar{p}\bar{p}$ $(1932 \pm 2)\Gamma(9 \pm 4)$ total cross section that was also seen in the $\bar{p}d$ channel, indicating isotopic spin $J=1$.

[43]The $S(1930)$, which is listed as an A-rated resonance in RPP72 (Ref. 26), appears here with a D rating in Table I because of its lack of spin information and because some recent experiments have failed to observe it. However, it fits naturally into the systematics of the present paper as related to the $\bar{p}p(1925)$ peak of Ref. 42, and it seems to be confirmed by the recent measurement of Carroll *et al.* cited in Ref. 42.

[44]The present theoretical systematics indicate that a $\pi\pi$ peak might be expected to appear at about 870 MeV. Some $\pi^+p \to \Delta^{++}\pi^+\pi^+$ experiments show a very slight peaking here [see G. Goldhaber *et al.*, Phys. Rev. Lett. 23, 1351 (1969), Fig. 2(a); M. Alston-Garnjost *et al.*, Phys. Lett. 36B, 152 (1971), Fig. 1(c)]. Also, a $p\bar{p} \to 4\pi$ annihilation experiment of R. A. Donald *et al.* [Nucl. Phys. B11, 551 (1969), Figs. 18 and 19] shows a four-standard-deviation spike, in the $I=0$ channel only, in opposition to the ρ meson (which suggests a spin-1 resonance). However, without theoretical guidance these small experimental effects would not be of much significance, and we assign an E rating for this resonance.

[45]This is a peak that can be observed in the CERN MMS^- spectrum on p. S88 of RPP71 (Ref. 27), although it does not show up clearly in earlier CERN reports. The parameters quoted here were obtained by fitting a Gaussian curve to the peak. A. R. Dzierba *et al.* [Phys. Rev. D 2, 2544 (1970)] also show some evidence for a narrow peak here, and H. W. Atherton *et al.* (Ref. 46) report a $\pi^+\pi^-\pi^\pm$, $J^P=1^+$ peak $M(1076)$ $\Gamma 36$.

[46]H. W. Atherton *et al.*, Phys. Lett. 43B, 249 (1973).

[47]A. Skuja *et al.*, Phys. Rev. Lett. 31, 653 (1973), obtained a $J=0$ $\pi^0\pi^0$ peak with mass and width approximately as quoted here. As other evidence for the ϵ, we note that a plot of the isotropic component of the $\pi\pi$ amplitude (Ref. 48, p. 17, Fig. 8) shows a curve that roughly parallels the shape of the ρ. Also, studies by P. J. Davis *et al.* [Phys. Rev. D 5, 2688 (1972)] suggest that the differences observed in $K^+\pi^-\pi^+$ and $K^0\pi^-\pi^0$ decay distributions can be explained in terms of $\rho(770)$ and $\epsilon(\sim 700)$ enhancements. Similarly, F. Ceradini *et al.*, Phys. Lett. 43B, 341 (1973), discuss evidence for the decay mode $\rho'(1600) \to \rho(760)\Gamma 120 + \epsilon(800)\Gamma 300$. In analogy to the $(I, J) = (1,1)$, $(0,0)$ pair $\rho(770)$, $\epsilon(800)$ in Table I, we also note the similar pairs $\pi_N(975)$, $S^*(980)$, $A_1(1115)$, $\epsilon'(1096)$ and $B(1235)$, $\epsilon''(1250)$.

[48]*Experimental Meson Spectroscopy—1972,* proceedings of the third international conference on experimental meson spectroscopy, Philadelphia, 1972, edited by Kwan-Wu Lai and Arthur H. Rosenfeld (A.I.P., New York, 1972).

[49]The $\pi_N(975)$ is well defined in the experiments of Abolins 70, Barnes 69, Miller 69, and Ammar 70 (Ref. 25) as a broad $\Gamma = 60$ MeV resonance. The measurements of Abolins 70 and Barnes 69 give no spin information. Miller 69 state that the $\pi_N(975)$ is produced peripherally, but decays isotropically (75% confidence level). However, Ammar 70 subsequently find both peripheral production and an anisotropic decay (90% confidence level), which rules out the tentative RPP73 assignment $J^P=0^+$. From the present systematics, the broad width indicates a spin-1 or possibly spin-2 resonance. A. R. Dzierba *et al.*, Phys. Rev. D 2, 2544 (1970), show [Fig. 4(a)] the decay mode $\pi_N(975) \to DEF\,\pi$. From the present systematics, the DEF is a spin-1 resonance. For a further comment on the $\pi_N(975)$ resonance, see Ref. 68. A recent experiment [G. R. Kalbfleisch *et al.*, BNL Report No. 18189, 1973 (unpublished)] gives additional evidence for a broad peak at 976 MeV.

[50]The $S^*(980)$ $\Gamma \sim 50$ mass and width are taken from the $\pi^0\pi^0$ peak shown in Fig. 1(c) of D. M. Binnie *et al.*, Phys. Rev. Lett. 31, 1534 (1973). Also see D. Hyams *et al.*, Nucl. Phys. B64, 134 (1973). For a distinction between the $S^*(980)$ and $\epsilon'(1096)$ resonances of Table I, see Ref. 53. Note the pairs $\rho(770)$, $\epsilon(800)$ and $\pi_N(975)$, $S^*(980)$ which are $J=I=1$ and $J=I=0$ pairings [for the spin of the $\pi_N(975)$, see Ref. 49].

[51]The values quoted here are from the "nondiffractive" measurement of E. W. Anderson *et al.*, Phys. Rev. Lett. 22, 1390 (1969).

[52]We quote the values from RPP71 (Ref. 27) to show the similarity between the A_1 data and some of the S^* data.

[53]Of the six experiments listed in RPP73 (Ref. 25) under $\eta_N(1080)$, two are $p\bar{p}$ experiments, Clayton 70 and Diaz 70. Unlike the πp experiments, which show D-wave $\pi\pi$ enhancements, these experiments indicate an S-wave $\pi\pi$ enhancement, which we denote as $\epsilon'(1096)\Gamma 80$. P. B. Johnson *et al.*, Phys. Rev. 176,

1651 (1968), also report weak experimental evidence for $S^*(1070) \to \pi\pi$.

[54]J. T. Carroll *et al.*, Phys. Rev. Lett. 28, 318 (1972); C. W. Whitehead *et al.*, Nucl. Phys. B48, 365 (1972).

[55]Note that C. W. Whitehead *et al.* (Ref. 54), with two different kinematic constraints, find two different mass values for the f meson, $f(1262 \pm 3)$ and $f(1291 \pm 7)$. The situation is reminiscent of mass shifts observed, for example, in the A_1 meson.

[56]N. Armenise *et al.* [Nuovo Cimento Lett. 4, 201 (1972)] and B. M. Salzberg *et al.* [Nucl. Phys. B41, 397 (1972)] both establish direct 3π decays for this spin-2 resonance.

[57]Unweighted average of five experiments in RPP73 (Ref. 25).

[58]This is a weighted average of Miller 68, Whitehead 68, Oh 69, and Reynolds 70 in RPP73 (see Refs. 25 and 53), with the width taken from Oh 69 and Reynolds 70. The spin of 2 seems well established: Miller 68 conclude $l = 2$; Whitehead 68 concludes $l > 0$; Oh consider several possibilities, but favor a D-state resonance superimposed on a P-wave background, and they cite several reasons for this choice. C. W. Whitehead *et al.* (Ref. 54) report another observation of this enhancement. The large D-wave phase shift observed above 1 GeV by S. D. Protopopescu *et al.*, Phys. Rev. D 7, 1279 (1973), is indirect evidence for the existence of the η_N (see Sec. X of the present paper).

[59]The *DEF* is a broad missing-mass peak at about 450 MeV noted by J. Baniags *et al.*, Nucl. Phys. B28, 509 (1971), and by R. Thun *et al.*, Phys. Rev. Lett. 28, 1215 (1972). N. Cason *et al.* [Phys. Rev. D 1, 851 (1970), Fig. 36 and the discussion on p. 858], found a statistically significant peaking in the $I = 0$ $\pi\pi$ amplitude at about 400 MeV, which was enhanced when placed in opposition to the ρ; this suggests spin 1 for the *DEF*. A. Dzierba *et al.*, Phys. Rev. D 2, 2544 (1970), observed the decay $\pi_N(975) \to DEF\pi$. J. Baniags *et al.*, Phys. Lett. 43B, 535 (1973), give, in their last paragraph, additional evidence for the *DEF* enhancement. Also see J. Baniags *et al.* (unpublished).

[60]The $\rho^0\rho^0$ decay mode possibly suggests spin $J = 2$.

[61]The $\pi/\rho(1490)$ is a $\pi^+ p$ experiment which appears in RPP73 (Ref. 25) grouped together with $p\bar{p}(1540)$ resonances. The CERN MMS$^-$ $\pi^- p$ experiment, Ref. 27, p. S88, also shows some evidence for peaking at about 1490 MeV.

[62]W. C. Harrison *et al.*, Phys. Rev. Lett. 28, 775 (1972); B. M. Salzberg *et al.*, Nucl. Phys. B41, 397 (1972). Also see $\eta/\rho(1830)$ and $\omega/\pi(1830)$ in RPP73 (Ref. 25).

[63]Weak indications for a $\pi\pi$ enhancement at about 520 MeV can be noted in N. P. Samios *et al.*, Phys. Rev. Lett. 9, 139 (1962) (although these data were taken long ago, they are still believed to be correct—N. P. Samios, private communication); G. Goldhaber *et al.*, Phys. Rev. Lett. 23, 1351 (1969) [the existence of this peaking was pointed out to the author by G. Goldhaber—see Fig. 2(a)]; S. D. Protopopescu *et al.*, Phys. Rev. D 7, 1279 (1973), Fig. 18 ($0.03 < |t'| < 0.1$ GeV^2). Also, ABBHHM Collaboration, Phys. Rev. 175, 1669 (1968); Fig. 4, with $E_{\pi^+\pi^-} = E_{CM} - E_p$, shows a peak centered at about 525 MeV. The photoproduction suggests a spin-1 resonance.

[64]Several analyses indicate that the *ABC* may be a threshold effect rather than a resonance. Recent experimental results are given in J. Baniags *et al.*, Phys. Lett. B43, 535 (1973), and in the last paper in Ref. 59.

[65]The values quoted for the M are from M. Aguilar-Benitez *et al.*, Phys. Rev. D 6, 29 (1972). Arguments summarized in Table XIV of that paper appear to clearly separate the M from the η'. $J^P = 0^-$ is favored by the Dalitz plot.

[66]The $\delta^0(963)$ is from D. L. Cheshire *et al.* (Ref. 48, p. 124), with the mass, which was measured relative to that of the η', adjusted here to match the value used in the present paper for the η'. Cheshire measured $\delta^0 - \eta' = 5.4 \pm 1.4$ MeV. A similar peak was observed by L. Holloway *et al.* (Ref. 48, p. 133), who reported its mass as 968 MeV. Also see D. L. Cheshire *et al.*, Phys. Rev. Lett. 28, 520 (1972).

[67]In Phys. Rev. Lett. 28, 520 (1972), D. L. Cheshire *et al.* measured the peak $\delta^0(963.5 \pm 1.7)$ cited in Ref. 66. In Phys. Rev. Lett. 29, 1477 (1972), this same group reported a peak $M^0(1033.6 \pm 2.3)$ (which is adjusted to match the present value used for the η' mass). Thus the M^0-δ^0 mass difference from these two experiments is 70.1 MeV, where the η' was used as a reference mass in both cases. This can be taken as indirect evidence for the existence of the fundamental mass quantum $M = 70$ MeV (see Ref. 24); however, if this is correct, we would expect the resonance to have a much narrower width than reported here.

[68]The $\delta^-(962)$ has been observed directly only in the CERN missing-mass experiment of W. Kienzle *et al.*, Phys. Lett. 19, 438 (1965). However, indirect confirmation of this resonance is supplied by the observation of the $\delta^+(966)$ by J. Oostens *et al.*, Phys. Lett. 22, 708 (1966), and also in recent measurements of C. Defoix *et al.*, Nucl. Phys. B44, 125 (1972), and of H. W. Atherton *et al.*, Ref. 46. Defoix and coworkers confirmed the decay modes $D^0 \to \delta^\pm \pi^\mp \to \eta^0 \pi^+ \pi^-$ and $E^0 \to \delta^\pm \pi^\mp \to \eta^0 \pi^+ \pi^-$. They obtained the masses and widths $D^0(1292 \pm 10)\Gamma 28 \pm 5$ and $\delta^\pm(972 \pm 10)\Gamma 30 \pm 5$. Since Boesebeck 71 in Ref. 25 obtained the values $D^0(1283)\Gamma 10$, we see that Defoix *et al.* are about 10 MeV higher than Boesebeck 71 for the D^0 mass and 10 MeV higher than CERN for the $\delta^\pm$ mass. Thus, their value for the mass of the $\delta^\pm$ is probably consistent with that of CERN and Oostens. The widths that Defoix *et al.* measured for the D^0 and δ are consistent with their experimental resolution, and have not been corrected for resolution effects. Hence Defoix *et al.* find that both the D and $\delta^\pm$ resonances have widths $\Gamma \ll 30$ MeV. Thus, Defoix *et al.* are in agreement with Boesebeck 71 for the D width and with CERN and Oostens for the δ width. It is important to note that Defoix *et al.* are *not* observing the broad $\pi_N(975)$ resonance (Ref. 49), which has a width $\Gamma = 60$ MeV. There is a tendency for SU(3) classifiers to lump the narrow $\delta^-(962)\Gamma < 5$ and the broad $\pi_N(975)\Gamma 60$ together (e.g., see Ref. 25; also see the review by R. Diebold in Ref. 41). Other than the difference in widths, the $\pi_N(975)$ belongs to the natural parity series 0^+, 1^-, 2^+, ..., whereas Atherton *et al.* (Ref. 46) have now demonstrated that the $\delta^-(962)$ has $J^P = 0^-$. As a recent negative result on the $\delta^-(962)$, G. R. Kalbfleisch *et al.* (see Ref. 49) see no narrow structure in the X^- spectrum from 900 to 1020 MeV; they also point out that the experimental result of Oostens is in disagreement with the measurement of Abolins 70 in Ref. 49.

[69]The designations 3-0, 3-1, and 3-2 refer to resonance type No. 3 with 0, 1, and 2 binding-energy defects of 5 MeV, as discussed in Ref. 24. The superscripts denote charge states, and a charged quantum is expected to be 4.6 MeV more massive than a neutral quantum (Ref. 24). The $3\text{-}2^0+$ state denotes a $\delta^0(963)$-type resonance with an additional 70-MeV mass quantum added.

[70]RPP73 (Ref. 25) lists an S-wave resonance somewhere in this region. The values quoted here are from D. J. Crennell *et al.*, Phys. Rev. Lett. 22, 487 (1969). See the following discussions of this resonance region: RPP70, Phys. Lett. 33B, 1 (1970); D. A. Lissauer, UCRL Report No. UCRL-20644, thesis, 1971 (unpublished), p. 32; RPP73, p. S100.

[71]The narrow width of the $K_A(1175)$ is its primary identification feature with respect to the spin of the resonance (see Wangler 64 and Miller 65 in Ref. 25).

[72]A narrow $K\pi$ peak at 1250 MeV has been noted by D. A. Lissauer, Ref. 70, p. 32, consistent with $J^P = 0^+$ or 1^-. Also see W. O. Dodd *et al.*, Phys. Rev. 171, 1991 (1969). However, R. Diebold, ANL Report No. ANL/HEP 7254, Ref. 41, Vol. I, p. 3, summarizes contrary evidence. The values quoted here are from a $K\pi\pi$ peak observed by P. J. Davis *et al.*, Phys. Rev. D 5, 2688 (1972), p. 2707, and by J. Davidson *et al.*, Phys. Rev. D 9, 77 (1974).

[73]W. Frati *et al.*, Phys. Rev. D 6, 2361 (1972), suggest identifying this narrow peak with the $J^P = 0^+$ resonance $K_N(1370)\Gamma < 150$ observed by A. Firestone *et al.*, Phys. Rev. Lett. 26, 1460 (1971). Also see H. Yuta *et al.*, Nucl. Phys. B52, 70 (1973), and see the discussion on page S100 of RPP73 (Ref. 25).

[74]The $\kappa(725)$ values quoted here are from the review of A. R. Erwin *et al.*, Nucl. Phys. B9, 364 (1969). Although no recent experiments have shown this resonance, the earlier experiments which did show a peak do not appear to have been directly repeated.

[75]The relatively broad width and the decay into K^* suggest a spin-1 resonance.

[76]A. F. Garfinkel *et al.*, Phys. Rev. Lett. 26, 1505 (1971); also see D. J. Crennell *et al.*, Phys. Rev. D 6, 1220 (1972).

[77]An average of K. J. Anderson *et al.*, Phys. Rev. D 6, 1823 (1972), and P. J. Davis *et al.*, Phys. Rev. D 5, 2688 (1972).

[78]R. Ayed, P. Bareyre, and Y. Lemoine, unpublished paper presented at NAL 72 (Ref. 41).

[79]AYED (Ref. 78) report $N(1427)P_{11}\Gamma 236$. Twelve production experiments in Ref. 25—Anderson 66, Blair 66, Foley 67, Almeida 67, Bell 68, Lamsa 68, Shapira 68, Tan 68, Rhode 69, Anderson 70, Ballam 71, and Rushbrook 71—give an average value $N(1419)P_{11}\Gamma 148$, in reasonable agreement with AYED. The average value from the production experiments is used in Table III.

[80]S. Almehed and C. Lovelace, Nucl. Phys. B40, 157 (1972).

[81]This is an average of Davies 70 in Ref. 25 (which has the narrow width expected for this resonance), AL (Ref. 80), and AYED (Ref. 78).

[82]A. Barbaro-Galtieri, LBL Report No. LBL-1366, 1972, a review presented at NAL 72 (Ref. 41), Vol. I, p. 159).

[83]This is an average of Orito 69, Schorsch 70, and Wagner 71 in Ref. 25, AL (Ref. 80), and AYED (Ref. 78). See Ref. 84 for a slightly higher average value—1706 MeV.

[84]R. M. Edelstein *et al.*, Phys. Rev. D 5, 1073 (1972).

[85]AL (Ref. 80) and AYED (Ref. 78) disagree on the position of this resonance. Herndon *et al.* (see Ref. 86) agrees with the intermediate value quoted here. This appears to be a P-wave criss-cross ambiguity (see Table XI).

[86]D. J. Herndon *et al.*, Report No. LBL-1065, 1972, paper presented at NAL 72 (Ref. 41) (unpublished).

[87]An average of Anderson 70 and Hull 70 in Ref. 25, AL (Ref. 80), and AYED (Ref. 78).

[88]AL (Ref. 80) and AYED (Ref. 78) disagree by 174 MeV on the location of this resonance.

[89]An $I = \frac{1}{2}$ resonance at about 1300 MeV has been reported by T. W. Morris *et al.*, in *High Energy Physics*, proceedings of the Fifteenth International Conference on High Energy Physics, Kiev, 1970, edited by V. Shelest (Naukova Dumka, Kiev, U.S.S.R., 1972); K. Boesebeck *et al.*, Nucl. Phys. B40, 39 (1972); V. Kistiakowsky *et al.*, Bull. Am. Phys. Soc. 18, 536 (1973); E. Colton and Z. Ma, Nuovo Cimento 11A, 590 (1972); H. Braun *et al.*, Phys. Rev. D 8, 2765 (1973); and D. Lissauer *et al.*, *ibid.* 6, 1852 (1972), who identify it as a P_{11} resonance.

[90]The existence of a split Roper resonance, which now appears in the AYED (Ref. 78) analysis, was predicted several years ago [M. H. Mac Gregor, Ref. 2(a); also Ref. 14, p. 274] on the basis of the systematics in the present paper, and also from the double inelastic dip observed in the analyses of Bareyre 68 (Ref. 25) and others.

[91]U. Mehtani *et al.*, Report No. UCR 34 P107 B-146 (unpublished), presented at NAL 72 (see Ref. 41).

[92]The width is the average of four unbracketed values in RPP73 (Ref. 25).

[93]The width is the average of four values in RPP 73 (Ref. 25).

[94]Unweighted average of Armenteros 68, Bailey 69, Armenteros 70 (low value), Galtieri 70, and Kim 71 (high value) in Ref. 25, and Ch-LBL (Ref. 95).

[95]Chicago-LBL Collaboration, paper presented at NAL 72 (Ref. 41) (unpublished).

[96]Unweighted average of Kim 71, Bricman 70, and Langbein 72 in RPP 73 (Ref. 25).

[97]W. Langbein and F. Wagner, Nucl. Phys. B47, 477 (1972).

[98]Unweighted average of Bricman 70, Conforto 71, and Langbein 72 in RPP 73 (Ref. 25), Ch-LBL (Ref. 95), and LOMM (Ref. 99).

[99]A. T. Lea, G. C. Oades, B. R. Martin, and R. G. Moorhouse, unpublished paper presented at NAL 72 (Ref. 41).

[100]Average of two values in RPP 73 (Ref. 25).

[101]Values from Kim 71 in RPP 73 (Ref. 25); also see Ref. 97.

[102]Values from Berthoni 71 in RPP 73 (Ref. 25); from the present systematics, we require the F_{05} assignment.

[103]Indirect evidence for the existence of this resonance is given in M. H. Mac Gregor, Nuovo Cimento Lett. 1, 437 (1971); see B. A. Shahbazian and A. A. Timonina, Nucl. Phys. B53, 19 (1973). The author is not convinced that this is a "dead" resonance [see RPP 73 (Ref. 25)], even though it does not appear in most production channels (see Ref. 125).

[104]Ch-LBL (Ref. 95) also see a D_{13} resonance at about this same energy (1750 MeV).

[105]Values are as quoted in RPP 72 (Ref. 26).

[106]The width is the average of ten measurements in RPP 73 (Ref. 25).

[107]The width is the average of three unbracketed values in RPP 73 (Ref. 25), and the quantum numbers are from Bricman 71. Vanhorn 72 claims an F_{15} resonance also at this energy, and Lasinski 71 suggests two resonances here. The present systematics require a G_{17} resonance.

[108]The H assignment fits the present systematics.

[109]This is the approximate average of five values in RPP 73 (Ref. 25) plus LOMM (Ref. 99).and Ch-LBL (Ref. 95). While this average value for the position of the peak has considerable uncertainty, it matches cross section peaks seen by Bugg 68, Bricman 70, and Cool 70 in Ref. 25. The very broad width reported for this resonance ($\Gamma \sim 200$ MeV) is another indication of an uncertainty in the position of the peak.

[110]Values from KIM 71 in RPP 73 (Ref. 25); these values correspond closely to the $\Sigma(1619)$ $\Gamma 41$ production peak reported in RPP 73.

[111]The values quoted here are an average of Kim 71 and Vanhorn 72 in RPP 73 (Ref. 25), who both find a P and a D Σ resonance at 1670 MeV, in agreement with present expectations. This state is also confirmed by E. L. Hart *et al.*, Bull. Am. Phys. Soc. 18, 536 (1973). The Vanhorn 72 $\Sigma(1659)D_{13}$ and $\Sigma(1668)P_{11}$ resonances closely match two $\Sigma(1670)$ peaks seen by Aguilar 70, of which one was much more peripheral than the other.

[112]Average of two values measured by Pan 70 in RPP 73 (Ref. 25).

[113]The $\Sigma(1682)$ $\Gamma 25$ peak reported by Blumenthal 69 has the narrow width which is indicative of an S-state resonance, a result that may be confirmed by the Vanhorn 72 observation of a $\Sigma(1697)$ $S\Gamma 66$ phase-shift resonance. Since Blumenthal *et al.* were studying K_L^0+proton, it is interesting to note that $\Sigma^+ + K_L^0$ add up to 1687 MeV, or just the mass of this resonance, so that this peak appears as a $\Sigma^+ + K_L^0$ bound state.

[114]This resonance is quoted as observed by LW (Ref. 97), but Vanhorn 72 in RPP 73 (Ref. 25) sees it at 1925 MeV.

[115]From the present systematics and the existence of the well-established P-state $\Sigma(1926)$, we conclude that there must be an underlying S-state resonance somewhere just below 1900 MeV. LOMM 99 present evidence for such a resonance. However, since another P state appears at an even higher energy, $\Sigma(2080)$, there must be another S state above 1900 MeV. Vanhorn 72 shows an S state at 2004 MeV. We quote an S-state energy of 1900 MeV here with the understanding that it represents a manifestation of one or more S-state resonances which appear in this poorly resolved high-energy region.

[116]Note the similarity between the $\Sigma(2030)$ $F_{17}\Gamma 148$ and $\Sigma(2070)$ $F_{15}\Gamma 140$ levels.

[117]Armenteros 70 suggest this peak, as do the present results. However, it may be another manifestation of the $\Sigma(1670)$ P_{11} peak reported by Kim 71 and Vanhorn 72 (see Ref. 111). P. Baillon *et al.* [CERN Report No. CERN/D. Ph. II/PHYS 73-38 (unpublished)] report a $\Sigma(1600)P_{11}$ $\Gamma 68$ resonance.

[118]M. Bott-Bodenhausen *et al.*, Phys. Lett. 40B, 693 (1972).

[119]S. D. Drell and K. Johnson, Phys. Rev. D 6, 3248 (1973).

[120]For a recent discussion of the ideas with respect to light quarks, see L. W. Jones, Phys. Today, May (1973), p. 30.

[121]M. Gell-Mann, Phys. Lett. 8, 214 (1964); G. Zweig, CERN Reports Nos. TH 401 and TH 412, 1964 (unpublished).

[122]E. Fermi and C. N. Yang, Phys. Rev. 76, 1739 (1949).

[123]It should be mentioned that Y. Nambu [Progr. Theor. Phys. 7, 595 (1952)] long ago pointed out the usefulness of the mass quantum $M = 70$ MeV. However, without the special-relativistic equations relating M and S, and without a theory for binding energies in the Λ hyperon, the universality of the quantum M is not experimentally apparent, and this line of approach was not followed up.

[124]See Ref. 14, page 255.

[125]The crucial test as to whether or not a resonance actually exists is one of reproducibility. If an experiment is repeated exactly and an observed peak does not appear in the second experiment, the observed peak in the first experiment may have been a statistical fluctuation. However, if a somewhat different experiment is performed and an expected peak is not seen, this may be merely an indication that the conditions for the formation of the peak do in fact depend on the experimental factors that were changed. It seems to be experimentally true that many hadron resonances depend quite sensitively on conditions such as momentum transfer. It is also an empirical fact that few high-energy physics experiments are repeated exactly.

[126]See Ref. A22 in Ref. 13.

[127]There is a simple theoretical reason for expecting to find a narrow dip in the A_2 meson at 1310 MeV. If a spin-$\frac{1}{2}$ quark has a mass of 330 MeV, and if these quarks appear pairwise in meson resonances with very small binding energies (Sec. V), then a pair of quarks ($J^P = 1^+$) will produce an effect at 660 MeV (see Fig. 19), and a quartet of quarks ($J^P = 2^+$) will produce an effect at about 1310 MeV. Experimentally, it should be noted that those experiments which do *not* see a split A_2 meson also do *not* see the nearby narrow resonance $X^-(1153)$, which has some independent experimental verification (see Refs. 35 and 36). A deeply split A_2 meson (the dipole shape) seems very unlikely, but a small interference dip in the A_2 continues to be in evidence in a number of experiments, as discussed in Ref. 40.

[128]B. T. Feld, *Models of Elementary Particles* (Blaisdell, Waltham, 1969, p. 339, Eq. (18a′).

[129]For a recent discussion of models of the electron, see F. Rohrlich, invited paper given at the Symposium on the Development of the Physicist's Conception of Nature, Miramare, Trieste, Italy, September, 1972.

[130]J. Franklin, Phys. Rev. 172, 1807 (1968), pages 1811–1812.

[131]B. T. Feld, Ref. 128, Chap. 17, pages 439–440.

[132]P. Vinciarelli, Nuovo Cimento Lett. 4, 905 (1972).

[133]J. Franklin, Ref. 130, p. 1816.

[134]B. T. Feld, Ref. 128, p. 337, Table 15.8, with $\mu_q/\mu_0 = 2.79$.

[135]B. T. Feld, Ref. 128, p. 340, Eq. (18c′).

[136]J. Franklin, Ref. 130, Eq. (9).

[137]In a recent $\gamma + He^4 \rightarrow \Delta^0 + (ppn)$ experiment [P. E. Argen *et al.*, Phys. Rev. Lett. 29, 1191 (1972)], the expected $\Delta(1233)$ curve was obtained together with an unexpected anomalous peak for high momentum transfers to the (ppn) system. This anomalous peak, with a mass of 1165 MeV and a width $\Gamma < 35$ MeV, could be a manifestation of the hitherto unobserved $N\frac{3}{2}$ ground state of the $\Delta(1233)$ rotational band.

[138]However, it should be noted that the 70-MeV mass quantum which appears in the nucleon has a much more compact geometry than the 70-MeV mass quantum which is required to mathematically reproduce the μ meson (see Paper II). Thus whether these should be thought of as two different forms of the same mass quantum or as two different mass quanta is, at this point, an open question. The principal decay mode $\pi \rightarrow \mu + \nu$, which from the present viewpoint is $MM \rightarrow M_s[M] + \nu$, with $[M]$ denoting annihilation of one of the quanta M, relates the spinning quantum M_s at least phenomenologically to the μ meson.

[139]The nucleon is discussed in detail in paper II. The one calculational difficulty with this model is that the calculated magnetic moments, assuming an equatorial charge distribution, are too large by a factor of 3, although magnetic moment ratios are given correctly. Since an equatorial charge distribution gives the largest possible magnetic moment, this deficiency is in principle easy to correct; however, the author has not found a phenomenologically significant basis for altering the assumed charge distribution.

[140]M. Gell-Mann, Phys. Rev. Lett. 14, 77 (1965); B. T. Feld, Ref. 128, Ch. 16.

[141]Y. Dothan *et al.*, Phys. Lett. 17, 148 (1965); L. C. Biedenharn *et al.*, Phys. Lett. 42B, 257 (1972).

[142]O. L. Weaver and L. C. Biedenharn, Phys. Lett. 32B, 326 (1970); Nucl. Phys. A185, 1 (1972).

[143]See Ref. 128, page 362.

[144]L. C. Biedenharn *et al.*, Triangle Universities Nuclear Laboratory Semiannual Report No. 20, 1972 (unpublished); R. Y. Cusson and L. P. Staunton, Nuovo Cimento 17A, 303 (1973). The author would like to thank R. Cusson for communicating the latest results of this work (see Ref. 20).

[145]For recent discussions of R and A results, see P. Johnson *et al.*, Phys. Rev. Lett. 30, 242 (1973); R. C. Miller *et al.*, ANL-ITT report (unpublished). Also see F. A. Berends and S. N. M. Ruijsenaars, Nucl. Phys. B56, 525 (1973). An early discussion of this problem is given by L. D. Roper and D. S. Bailey, Phys. Rev. 155, 1744 (1967). Pion-nucleon R and A experiments are currently being planned for the Los Alamos LAMPF accelerator (R. A. Arndt, private communication).

[146]M. H. Mac Gregor, R. A. Arndt, and R. M. Wright, Phys. Rev. 182, 1714 (1969), and other references cited therein.

[147]R. A. Arndt (private communication); Berends and Ruijsenaars, Ref. 145.

[148]The sorting out of levels above 1600 MeV becomes very difficult because of the many reported peaks (Ref. 25), mostly without spin identification. A 4π spin-1 $I=1$ resonance, $\rho(\sim 1600)$, has been reported by several groups: G. Barbarino *et al.*, Nuovo Cimento Lett. 3, 689 (1972); A. Bramon and M. Greco, *ibid.* 3, 693 (1972); H. H. Bingham *et al.*, Phys. Lett. 41B, 635 (1972); F. Ceradini *et al.*, Frascati Report No. LNF-72/90, 1972 (unpublished), with a broad width, $\Gamma \sim 350$ MeV. B. Hyams *et al.*, Nucl. Phys. B64, 134 (1973), report a $\pi\pi(1590)P\Gamma 180$ peak that seems related. K. W. J. Barnham *et al.* [Phys. Rev. Lett. 24, 1083 (1970)] and R. Holmes *et al.* [Phys. Rev. D 6, 3336 (1972)] report a $\rho'(\sim 1630)\Gamma \sim 125$ peak.

[149]One of the results of the present meson and kaon phenomenology is that the same basic resonance configurations can appear in more than one isotopic-spin mode, as in the $3SS4$ and SSK bandheads discussed here. In Figs. 1 and 2, and in Table I, the column headings $I_z = 0$ and $I_z = 1$ are used. However, it should be noted that if two resonances belong to the same isospin multiplet, such as π^0 and $\pi^\pm$ in Table I, then their production modes are expected to be of comparable magnitudes, with the ratios expressible in terms of Clebsch-Gordan coefficients. For resonances such as η' and δ^- in Fig. 1, whose production amplitudes differ by orders of magnitude, the isospin headings are somewhat misleading. The η' is an $I=0$ resonance, and the δ^-, if it exists (see Ref. 68), is an $I>0$ resonance. In general, the $I_z = 0$ resonances of Table I and Figs. 1 and 2 have much larger production cross sections than the corresponding $I_z = 1$ resonances, so that their relationship is established here because of their basic underlying quark-state similarities (comparable masses and widths), and not because they are true isotopic-spin multiplets. Several of these $I_z = 0$ and $I_z = 1$ pairings appear as examples of the fundamental spin and isotopic-spin selection rule of Eq. (21).

[150]$R = 3.5$ fermis is the "uniform sphere radius" for O^{16} obtained from electron-scattering experiments: H. R. Collard, L. R. B. Elton, and R. Hofstadter, *Nuclear Radii*, Landolt Börnstein: Numerical Data and Functional Relationships in Science and Technology Series (Springer, Berlin, 1967), Group I, Vol. 2, p. 21.

[151]There are arguments which suggest that the C^{12} nucleus can be considered as three α particles arrayed almost in a straight line: H. Friedrich *et al.*, Phys. Lett. 36B, 189 (1971). Also, see R. C. Fuller, Phys. Lett. 43B, 445 (1973). If we give the α particle a radius of 2.11 fermis (Ref. 150), then in order to reproduce the value for E_{rot} shown for C^{12} in Table XXX, the three α's must be oriented with centerlines at an angle of 135°.

[152]The calculations are described in Ref. 2(f), and these resonances are briefly discussed.

[153]The experimental situation with respect to a spin-1 level in He^3 at about 23 MeV is not clear-cut. The original papers reporting this result—A. van der Woude *et al.*, Phys. Rev. Lett. 26, 909 (1971); M. L. Halbert and A. van der Woude *ibid.* 26, 1124 (1971)—were later retracted [M. L. Halbert and A. van der Woude, *ibid.*, 26, 1679 (1971)], because it was discovered that the position of the peak varied from 20 to 26 MeV as the α bombarding energy was varied from 64 to 82 MeV. However, this change in the peak position as a function of momentum transfer is a phenomenon that is frequently observed in hadron rotational excitations (see Ref. 55 for one example). M. L. Halbert, A. van der Woude, and N. M. O'Fallon [ORNL and University of Missouri report (unpublished)] have concluded that at least some of the observed effect is due to a

final-state Li^6 resonance. If we assume that a 23-MeV He^3 resonance effect of some kind exists, then vibrational excitations are ruled out since the binding energy is only 8.7 MeV. The only possible excitation mechanism is rotational excitation, and to (1) minimize centrifugal forces, and (2) obtain a small enough moment of inertia to give a 23-MeV rotational energy, the three nucleons in He^3 must be almost collinear, just as for the C^{12} level discussed in Ref. 162. An orientation angle of 135°, the same as that for C^{12}, gives the value of E_{rot} for He^3 shown in Table XXX.

[154]M. Alston-Garnjost *et al.*, Phys. Lett. 36B, 152 (1971).

[155]S. D. Protopopescu *et al.*, Phys. Rev. D 7, 1279 (1973).

[156]For example, see the review paper by N. P. Samios and F. J. Gilman in Ref. 48.

[157]The very-narrow-width spinless resonances π, K, η, η' all have negative parities, which leads to an abundance of 0^- states. If rotating bandheads all have effectively positive intrinsic parities [as mentioned in connection with the G-parity rule (12) of Table XII], then the abundant $L = J = (1, 2)$ rotational levels will all have $J^P = (1^-, 2^+)$, as observed. When we investigate exceptions to this result, we find that the observed 1^+ D meson is a rotationless spinor-pair excitation (Table XXIII). Also, the $2^- A_3$ meson and the $1^+ A_1$ meson have decays into other rotational final states [Yu. M. Antipov *et al.*, CERN-IHEP Boson Spectrometer Group, in a paper submitted to the Second Aix-en-Provence International Conference on Elementary Particles, 1973 (unpublished), find that A_1 and A_3 resonances have quite different properties than the A_2 resonance], and the $1^+ B, C$, and Q mesons all have decays into spin-1 final-state particles; these complicated decay processes which involve spin-1 or spin-2 final-state particles obscure the parities of the initial rotational states. Finally, there are a number of 0^+ resonances, $\epsilon, \epsilon', \epsilon'', S^*$, which arise from $^3P_0$ rotational configurations, but which do not noticeably follow the mass systematics expected on the basis of SU(3), and whose parities reflect the J quantum number rather than the L quantum number.

[158]Figure 1(c) of Ref. 154. Although the bump is barely visible in the figure, a statistical analysis of the data (see Ref. 39) indicates a statistical significance of possibly four standard deviations.

[159]Figure 18 is taken from Figure 18 of Ref. 155.

[160]See Ref. 2(d) for this prediction and early experimental evidence.

[161]The narrow-width $M^0(1033)$ Γ16 level of Ref. 67, which does not fit the meson tower systematics of Fig. 6, has been grouped in Table I as a part of the η' multiplet for reasons that are discussed in Refs. 67 and 69. The level $B_1(1040)$ Γ55 of DEFOIX 72 in RPP 73 has no spin identification, but its broad width suggests a rotational excitation.

[162]The 1969 values for the rotational levels in Table XXXII are taken from Table II of Ref. 2(a). Some results were contained in Bull. Am. Phys. Soc. 14, 1206 (1969).

[163]The 1970 values for the rotational levels in Table XXXII are taken from Table III of Ref. 4.

[164]W. Von Schlippe, Nuovo Cimento Lett. 4, 767 (1972).

[165]R. L. Cool *et al.*, Phys. Rev. Lett. 29, 1630 (1972), recently measured the magnetic moment of the Ξ^-. Magnetic moments for p, n, Λ, and Σ^+ are given in Ref. 25.

[166]An equatorial charge distribution on the nucleon subunit of Appendix B will give rise to an electric quadrupole moment. It also gives magnetic moments that are too large by a factor of 3. These are probably related difficulties with the present formalism, and they are left here as unresolved difficulties. The same situation occurs in the model for the μ meson, but the quantum-mechanical projection factor in the case of the muon removes the difficulty (see Ref. 180).

[167]The author first obtained this result by using impulse arguments to generate the series expansion of Eq. (50). The much shorter derivation of Eq. (50) given here can be found in H. Arzelies, *Relativistic Point Dynamics* (Pergamon, Oxford, 1972), pages 16 and 17.

[168]The derivation given here is for the inertial mass, but the Eötvös experiment establishes the equivalence of the inertial and gravitational masses.

[169]It should be noted that this derivation of Eq. (50) for massive particles is valid only for $v < c$, and it cannot be mathematically continued to the case where $v > c$. Thus if we accept this derivation as expressing the physical content of Eq. (50) with respect to massive particles, then it does not seem to be correct to think of tachyon theory as being an extension of the theory of special relativity.

[170]L. I. Schiff, *Quantum Mechanics* (McGraw-Hill, New York, 1955), Second Edition, Sec. 44, p. 331.

[171]H. Arzelies, *Relativistic Kinematics* (Pergamon, Oxford, 1966), Ch. IX.

[172]C. Møller, *The Theory of Relativity*, (Pergamon, Oxford, 1952), p. 318, Eq. 42 and the related discussion.

[173]A. Einstein, *The Meaning of Relativity* (Princeton Univ. Press, Princeton, 1956), Fifth Edition, p. 59; C. W. Berenda, Phys. Rev. 62, 280 (1942). There has been considerable discussion of this point in the literature, but the conclusion stated here now seems to be the general consensus arrived at among relativists.

[174]E. L. Hill, Phys. Rev. 69, 488 (1946); N. Rosen, *ibid.* 70, 93 (1946); 71, 54 (1947); B. Kurşunoğlu, Proc. Camb. Philos. Soc. 47, 177 (1951); H. Takeno, Progr. Theor. Phys. 7, 367 (1952); G. H. F. Gardner, Nature 170, 243 (1952); J. L. Synge, *ibid.* 170, 243 (1952); T. E. Phipps, *ibid.* 195, 67 (1962); J. G. Fletcher, *ibid.* 199, 994 (1963); J. L. Anderson, *Principles of Relativity Physics* (Academic, New York, 1967), p. 183; E. L. Hill, Phys. Rev. 71, 318 (1947).

[175]G. Salzman and A. H. Taub, Phys. Rev. 95, 1659 (1954); J. E. Hogarth and W. H. McCrea, Proc. Camb. Philos. Soc. 48, 616 (1952); W. H. McCrea, Proc. Philos. Soc. A206, 562 (1951); G. C. Mc Vittie, *ibid.* A211, 295 (1952); also Ref. 171.

[176]See Arzelies [Ref. 171, Sec. IX, [120], p. 237], who argues that the existence of stresses of a purely special-relativistic origin is by no means obvious. It should be mentioned here that the quantization of masses applies only to *observables* (e.g., particles), and the assumption of a continuous mass distribution *inside a particle* should not be thought of as a *classical* approximation that is in disagreement with the quantum-mechanical guide lines (at least at this level of "observability")

[177]Arzelies, Ref. 176, mentions that the special-relativ-

istic stretching strains may not be real. The present author would like to extend these remarks by noting that centrifugal forces may also be minimal, due to the non-Euclidean geometry experienced by the rotating mass points. If we use the ratio of the radius to the circumference as a measure of the special-relativistic curvature, and hence of the centrifugal forces, then the vanishing of this curvature as the equator is approached may minimize the stresses that originate as centrifugal effects, and it may also minimize equatorial radiative effects.

[178]See C. W. Berenda, in Ref. 173, p. 286.

[179]Conservation of angular momentum appears to require that the relationship $R \sim \hbar/mc$ be maintained for all relativistic values of the mass m of the spinning sphere.

[180]When the quantum-mechanical projection factor $\cos\theta = (\frac{1}{3})^{1/2}$ that projects $J = \frac{1}{2}\sqrt{3}\hbar$ onto $J_z = \frac{1}{2}\hbar$ is inserted into this model for the muon, the z component of the electric dipole moment vanishes identically, and the x and y components average out to zero over one cycle of precessional motion. However, if the muon is moving, and if its longitudinal precessional motion, interpreted as the de Broglie wavelength, satisfies the Bragg condition, the x and y components of the electric dipole moment may produce an observable effect (see the discussion in Paper II).

[181]The $\Lambda(2097)$ $\Gamma 24$ level in Fig. 8 is Bock 65 in RPP 73 (Ref. 25).

[182]The width of the η' is from A. Duane *et al.*, Imperial College (London) Report No. IC/HEP/73/10 (unpublished).